



Theses and Dissertations

2003-06-24

A Self-Retracting Fully-Compliant Bistable Micromechanism

Nathan D. Masters

Brigham Young University - Provo

Follow this and additional works at: <https://scholarsarchive.byu.edu/etd>



Part of the [Mechanical Engineering Commons](#)

BYU ScholarsArchive Citation

Masters, Nathan D., "A Self-Retracting Fully-Compliant Bistable Micromechanism" (2003). *Theses and Dissertations*. 86.

<https://scholarsarchive.byu.edu/etd/86>

This Thesis is brought to you for free and open access by BYU ScholarsArchive. It has been accepted for inclusion in Theses and Dissertations by an authorized administrator of BYU ScholarsArchive. For more information, please contact scholarsarchive@byu.edu, ellen_amatangelo@byu.edu.

A SELF-RETRACTING FULLY-COMPLIANT BISTABLE MICROMECHANISM

by

Nathan D. Masters

A thesis submitted to the faculty of

Brigham Young University

in Partial Fulfillment of the Requirements for the Degree

Master of Science

Department of Mechanical Engineering

Brigham Young University

December 2001

Copyright © 2001 Nathan D. Masters

All Rights Reserved

BRIGHAM YOUNG UNIVERSITY

GRADUATE COMMITTEE APPROVAL

of a thesis submitted by

Nathan D. Masters

This thesis has been read by each member of the following graduate committee and by majority vote has been found to be satisfactory

Date

Larry L. Howell, Committee Chair

Date

Timothy W. McLain

Date

Alan R. Parkinson

BRIGHAM YOUNG UNIVERSITY

As chair of the candidate's committee, I have read the thesis of Nathan D. Masters in its final form and have found that (1) its format, citations, and bibliographical style are consistent and acceptable and fulfill university and department style requirements; (2) its illustrative materials including figures, tables, and charts are in place; and (3) the final manuscript is satisfactory to the graduate committee and is ready for submission to the university library.

Date

Larry L. Howell
Chair, Graduate Committee

Accepted for the Department

Brent L. Adams
Graduate Coordinator

Accepted for the College

Douglas M. Chabries
Dean, College of Engineering and Technology

ABSTRACT

A SELF-RETRACTING FULLY-COMPLIANT BISTABLE MICROMECHANISM

Nathan D. Masters

Department of Mechanical Engineering

Master of Science

The purpose of this research is to present a class of Self-Retracting Fully-compliant Bistable Micromechanisms (SRFBM). Fully-compliant mechanisms are needed to overcome the inherent limitations of microfabricated pin joints, especially in bistable mechanisms. The elimination of the clearances associated with pin joints will allow more efficient bistable mechanisms with smaller travel. Small travel, in a linear path facilitates integration with efficient on-chip actuators. Tensural pivots are developed and used to deal with the compressive loading to which the mechanism is subject. SRFBM are modeled using the Pseudo-Rigid-Body Model and finite element analysis.

Suitable configurations of the SRFBM concept have been identified and fabricated using the MUMPs process. Complete systems, including external actuators and electrical contacts are 1140 μm by 625 μm (individual SRFBM are less than 300 μm by 300 μm). These systems have been tested, demonstrating on-chip actuation of bistable mechanisms. Power requirements for these systems are approximately 150 mW. Testing with manual force testers has also been completed and correlates well with finite element modeling. Actuation force is approximately 500 μN for forward actuation. Return actuation can be achieved either by external actuators or by thermal self-retraction of the mechanism. Thermal self-retraction is more efficient, but can result in damage to the mechanism. Fatigue

testing has been completed on a single device, subjecting it to approximately 2 million duty cycles without failure.

Based on the SRFBM concept a number of improvements and adaptations are presented, including systems with further power and displacement reductions and a G-switch for LIGA fabrication.

ACKNOWLEDGEMENTS

Many people deserve thanks for their contributions to this thesis and my life. I thank the many members of the lab group for their help and friendship. I must especially thank Brian Jensen, on whose work I have built for this thesis and benefited from in the internship at Sandia National Laboratories. Thanks to Scott Lyon, for his amazing knowledge and his willingness to help others. Thanks to Dan Wilcox, who in a short period of time has helped me gather a great deal of data to make this thesis possible.

Thanks to my graduate committee, Dr. Tim McLain and Dr. Alan Parkinson for graciously working with the time constraints I have subjected everyone to. I would also like to thank them for all I have learned from them in and out of classes. Thanks to Dr. John Gardner for helping me fulfill a lifelong dream of peering into the hidden world only an electron microscope can reveal.

I would like to thank my wife for her love, support, and sacrifice as I have pursued (and will continue to pursue) my education. She is a marvelous blessing in my life. Thanks to my son, Riley, whose unstoppable urge to play with the computer mouse finally drove me into a locked room where I was able to finish this thesis. Thanks to him as well for his love and curiosity for which I will be eternally grateful and proud.

My parents deserve a great deal of thanks as well, for loving and supporting me, and for spending time helping me learn. I know that my dad's love of learning and mechanical things, and my mom's willingness to do experiments with a young child have greatly influenced my life.

There are too many to name, but I am forever grateful to the teachers and professors I have had who give so much of themselves to teach and serve. I would like to thank Mrs. Short, who was instrumental in my decision to be a mechanical engineer when I was in the fourth grade.

Special thanks to Dr. Larry Howell, a man I am honored to know as a teacher, an advisor, and a friend. I have learned much more than engineering from him, and feel that I am a much better person for knowing him.

Finally, I would like to thank my Heavenly Father for the talents I have been blessed with and the inspiration to develop the mechanism here presented. I know I owe all to Him, and am grateful for all I have and am.

This work is supported by grants from the National Science Foundation under grant numbers DMI-9624574 and DMI-9980835.

Table of Contents

List of Figures.....	xiii
List of Tables.....	xvii

CHAPTER 1

INTRODUCTION	1
1.1 Importance of the Research	2
1.2 What is the Need?	4
1.3 How the SRFBM Fills the Need	5
1.4 Thesis Outline	5

CHAPTER 2

LITERATURE REVIEW	7
2.1 Compliant Mechanisms	7
2.2 MicroElectroMechanical Systems (MEMS)	7
2.2.1 MEMS fabrication	8
2.2.1.1 Bulk micromachining	9
2.2.1.2 Surface micromachining	9
2.2.1.3 LIGA (Lithographie Galvano-formung Abformung)	12
2.3 Bistable Mechanisms	12
2.3.1 Conventional macro bistable mechanisms	13
2.3.2 Micro-bistable mechanisms	13
2.3.2.1 Buckled beams	13
2.3.2.2 Young mechanism	15
2.3.2.3 Berkeley bistable mechanism	17
2.3.2.4 “Rube Goldberg” system	18
2.3.2.5 Linear Displacement Bistable Mechanism (LDBM)	19
2.3.2.6 Fully Compliant Bistable Micromechanisms (FCBM)	19
2.4 MEMS On-Chip Actuation	20
2.4.1 Electrostatic	20
2.4.1.1 Parallel plate	22
2.4.1.2 Comb drives	23
2.4.1.3 Rotary side drive and wobble motors	24
2.4.2 Thermal	25
2.4.2.1 Comtois or U-beam	26

2.4.2.2 TIM, V-beam, or bent-beam	27
2.4.3 Miscellaneous actuation	28
2.5 MEMS Microswitches	28
2.5.1 Beam switches	29
2.5.2 Cronos	29
2.5.3 Optical switches	29
2.5.3.1 Texas Instruments Digital Micromirror Device™	30
2.5.3.2 Fiber optics switching	30
2.5.4 Miscellaneous	31

CHAPTER 3

BACKGROUND	33
3.1 Mathematics of Bistable Behavior	33
3.2 Pseudo-Rigid-Body Model	36
3.2.1 Beam deflections	36
3.2.2 Large deflection of a cantilever beam: moment load	36
3.2.3 Small deflection of a cantilever beam: vertical end load	38
3.2.4 Large deflection of a cantilever beam	38
3.2.5 Pseudo-Rigid-Body Model	38
3.3 The Principle of Virtual Work	39
3.4 Finite Element Analysis (FEA)	41

CHAPTER 4

DEVELOPMENT OF THE SRFBM	43
4.1 Motivation for Fully Compliant Mechanisms	43
4.2 Design Criteria	47
4.2.1 Double-slider	48
4.2.2 SRFBM Pseudo-Rigid-Body Model	51
4.2.3 Three degree of freedom six-link double-slider PRBM	57
4.2.4 SRFBM FEA	65
4.2.4.1 Beam element model	66
4.2.4.2 Plane element model	67
4.3 Comparison of SRFBM Models	70

CHAPTER 5

FABRICATION AND TESTING	75
5.1 System Layout and Fabrication	75
5.1.1 On-chip actuation	77
5.1.2 Electrical contacts	78
5.1.3 Release	78
5.2 Testing	79

5.2.1 Functionality	79
5.2.2 Reliability	84
CHAPTER 6	
SRFBM APPLICATIONS	87
6.1 Low-Power Electrical Switches	87
6.2 SUMMiT SRFBM	88
6.3 LIGA G-Switch	89
6.4 Amorphous Diamond	91
6.5 Circuit Breaker	92
6.6 Memory and Logic	93
6.7 Optical Switches	93
6.8 Microvalves	93
CHAPTER 7	
CONCLUSIONS AND RECOMMENDATIONS	95
7.1 Conclusions	95
7.2 Recommendations	96
7.2.1 Tensural pivots	96
7.2.2 Model improvement and design optimization	97
7.2.3 Investigation of critical return force	97
7.2.4 Additional applications	97
7.2.5 Fully compliant mechanism design	97
List of References	99
APPENDIX A	
GEAR GENERATION PROGRAM	107
APPENDIX B	
BEAM ELEMENT MODEL FOR THERMAL SELF-RETRACTION	123
APPENDIX C	
SRFBM ANSYS MODEL BATCH FILE	127
C.1 Geometry	127
C.2 ANSYS Plane Element Batch File	127

APPENDIX D

SRFBM AUTOLISP BATCH FILE	137
D.1 Geometry	137
D.2 AutoLISP batch File	137

APPENDIX E

LIGA G-SWITCH ANSYS BATCH FILE	141
E.1 Displacement Loaded batch File	141
E.2 Inertial Loading	148

APPENDIX F

FATIGUE TESTING CIRCUIT	155
F.1 Component List	156
F.1.1 Other components	156

List of Figures

Figure 2-1:	Cross section diagram of a three layer surface micromachining process. Un-released structures (a) show the effects of “print through” due to the conformal layers. “Print through” topography remains in the released structures (b).	10
Figure 2-2:	Ideal etch profiles: isotropic and anisotropic.	11
Figure 2-3:	(a) Ideal buckled beam (Mode 1) subject to residual stress, showing two possible states. (b) Ideal buckled beam subject to a critical force, P , (or displacement, Δ). (c) Ideal (and unlikely) Mode 0 transition (or super-critical buckling) between buckled positions. (d) Mode 2 transition between buckled positions, with rotation of center point. (e) Mode 3 transition is made possible by the addition of multiple beams and central shuttle for symmetry.	14
Figure 2-4:	Bistable snapping microactuator [31].	16
Figure 2-5:	SEM images of Young mechanism bistable microswitch in (a) the initial (or first stable equilibrium) position and (b) the second stable equilibrium position. (Note, these images are not of the same device, but are of devices with the same design.	16
Figure 2-6:	SEM image of the Berkeley bistable switching frame in the (a) open and (b) closed positions. The travel is approximately $17\ \mu\text{m}$ [28].	17
Figure 2-7:	SEM image of the “Rube Goldberg” system. The gear train is composed of partial gears as full revolution is not needed and are not possible with conformal layers of the MUMPs process.	18
Figure 2-8:	(a) Model of double-slider bistable configuration. (b) SEM image of LDBM in both stable equilibrium positions. The image does not show the other set of legs, which provides symmetry for the sliding action. Clips are used to limit out-of-plane deflections.	19
Figure 2-9:	(a) Model of double-slider configuration. (b) SEM image of FCBMs. The mechanism in the upper left of the image has been displaced to its second stable equilibrium position.	20

Figure 2-10:	Illustration of the electrostatic force between charged particles.	21
Figure 2-11:	(a) Diagram and (b) image of comb drive actuators [37]	23
Figure 2-12:	(a) Rotary sidedrive and (b) wobble motors [49]	24
Figure 2-13:	Thermal expansion diagram	25
Figure 2-14:	U-beam diagram	26
Figure 2-15:	SEM image of TIM microactuator	27
Figure 2-16:	TIM model	28
Figure 2-17:	Texas Instruments DMD™: (a) diagram of the components of the DMD™ mechanism [46] and (b) illustration of two micromirrors actuated in opposite directions [47].	30
Figure 2-18:	Bistable optical fiber switch (a) illustration of principle components [21] and (b) top view diagram of an advanced multi-stable version with multiple grooves [20].	31
Figure 3-1:	This figure illustrates the “ball-on-the-hill” analogy. At Positions A and D the ball is in stable equilibrium. At Position B the ball is at an unstable equilibrium. Position C is not an equilibrium position. Position E is neutrally stable.	34
Figure 3-2:	A stop has been added at Position C, making this an externally constrained stable equilibrium.	35
Figure 3-3:	Large deflection path of (a) cantilever beam and (b) its Pseudo-Rigid-Body Model	39
Figure 4-1:	Examples of the effects of pin joint clearances: (a) unreleased pin joint, ideal behavior of released pin joint (b) top view and (c) cross section, (d) in- and out-of-plane misalignment (e) is a top view, (f) angular out-of-plane misalignment.	44
Figure 4-2:	SEM of a Young mechanism experiencing the effects of pin joint clearances, as manifest by the out-of-plane deflection of the mechanism. The reaction force induced by the deflection of the slender beam (on the right) have resulted in the canting of the mechanism (see Fig. 4-1(f)).	45
Figure 4-3:	Fully compliant double-slider PRBM showing the equilibrium positions, torsional springs at pseudo-rigid joints, and linear spring-slider of the coupler.	49

Figure 4-4:	Illustration of the effects of axial loads on bending showing the induced moments due to (a) tension and (b) compression.	49
Figure 4-5:	Rigid-body replacement: (a) Rigid-body link and pin joint, (b) conventional flexural pivot, (c) tensural pivot.	50
Figure 4-6:	SRFBM geometry: (a) overlay of double-slider and geometry resulting from rigid-body replacement with tensural pivots and (b) system geometry with multiple legs for symmetry. Additional features are called-out and hatched areas are anchors. C-beam and slider supports are similar in thickness (in-plane).	51
Figure 4-7:	Coordinate system for SRFBM PRBM. r_4 is the displacement of the slider and is considered the input for the analysis.	52
Figure 4-8:	Diagram of the C-beam.	55
Figure 4-9:	Single degree of freedom PRBM results including actuation force and potential energy. Notice that the zeroes of the actuation force curve correspond to the system equilibria.	56
Figure 4-10:	Pseudo-Rigid-Body Model for the three degree of freedom analysis of SRFBM.	58
Figure 4-11:	Geometry of plane element model.	67
Figure 4-12:	(a) Displaced SRFBM leg near the unstable equilibrium position (6.65 μm displacement) and (b) the second stable position (11.36 μm displacement).	68
Figure 4-13:	Results of finite element analysis including force-deflection and potential (strain) energy.	69
Figure 4-14:	Comparison of SRFBM models: (a) force-deflection and (b) potential energy.	71
Figure 4-15:	Comparison of SRFBM models: (a) force-deflection and (b) potential energy (using modified PRBM parameters $\gamma = 0.65$, $K\Theta = 1.45$).	73
Figure 5-1:	Layout of SRFBM system with (a) SRFBM, (b) forward and (c) return thermal actuators, (d) backlash reducing coupler, (e) electrical contacts, and (f) bond pads for self retraction.	76
Figure 5-2:	SEM of the interdigitated backlash reducing coupler. The forward actuator is out of the image at left.	77

Figure 5-3:	SEMs of SRFBM electrical contacts. Contacts use the interactions of the conformal layers to achieve some degree of gold sidewall coverage, useful for lateral contacts.	78
Figure 5-4:	SEM of TIMs damaged by lift-off process.	79
Figure 5-5:	SEM of SRFBM system	80
Figure 5-6:	SEMs of SRFBM with force testers in (a) undeflected and (b) second stable positions. Compare deflected shape to Figure 4-12(b).	80
Figure 5-7:	SEM of SRFBM and force testers.	82
Figure 5-8:	SEM of an SRFBM and force testers in the second stable equilibrium position. The shuttle and slider support can be observed to have deflected down to where they may be in contact with the substrate, resting on dimples.	82
Figure 5-9:	Comparison of (a) SRFBM to (b) FEA model	83
Figure 5-10:	Images of high-voltage failure of electrical isolation of contacts and bond pads of a SRFBM [17].	84
Figure 6-1:	Comparison of force-deflection curves of reduced power (RP SRFBM) and current (SRFBM) devices.	88
Figure 6-2:	Layout for the LIGA G-switch.	90
Figure 6-3:	Finite element model results for LIGA G-switch.	91
Figure 6-4:	Circuit breaker schemes: (a) Current carrying tensural pivots and (b) external thermal return actuator. The reset actuator on the left side of the SRFBMs is common to both designs.	92
Figure C-1:	Geometry of SRFBM for batch files. Only user specified parameters (and the radii of curvature for use in the PRBMs) are presented.	128
Figure C-2:	SRFBM keypoint numbers and locations	129
Figure F-1:	Schematic of test circuit used for fatigue testing. TIM 1 and TIM 2 correspond to the forward and reverse actuators.	155

List of Tables

Table 4-1:	Sample single degree of freedom PRBM parameters.....	57
Table 4-2:	Partial derivatives of coordinates	60
Table 4-3:	Kinematic coefficients	61
Table 4-4:	Summary of SRFBM selected for fabrication.....	70
Table 5-1:	Force tester results	83
Table F-1:	Resistors	156
Table F-2:	Capacitors	156

CHAPTER 1 *Introduction*

The purpose of this thesis is to present a Self-Retracting Fully-compliant Bistable Micromechanism¹ (SRFBM) with small displacement and linear motion. Included in this presentation will be the development of the mechanism and the theory needed to analyze and synthesize them, plus the description of a number of adaptations for different fabrication processes and applications.

Compliant mechanisms derive some or all of their motion from the deflection of flexible members. Compliant mechanisms can be partially or fully compliant—both being composed of rigid and flexible segments; the former using a combination of traditional kinematic pairs (pin joints, sliders, cams, etc.) and compliant segments to obtain motion, and the latter relying completely on the deflection of flexible segments. In traditional kinematic analysis, compliant mechanisms would be considered to be structures with zero degrees of freedom. As such, alternative methods (including linear and non-linear force-deflection methods, Finite Element Analysis, chain algorithm, etc.) must be used to analyze their motion. The Pseudo-Rigid-Body Model [22, 23], a recent development, allows rigid-body kinematic methods to be used to analyze the path and force-deflection characteristics of compliant mechanisms.

Bistable mechanisms store energy in such a way that they have two stable equilibrium positions within their range of motion. In either stable equilibrium position any small per-

1. I have take some liberties with the usage of hyphenation for the name of the Self-Retracting Fully-compliant Bistable Micromechanism to obtain a manageable acronym.

turbation will result in oscillations about the stable equilibrium, with the system eventually coming to rest at the stable equilibrium. Large perturbations may result in a transition from one stable position to the other. Energy input is not needed to maintain either stable equilibrium position, only to transition the mechanism between the stable equilibria.

The path of the device presented in this thesis is linear. A linear path simplifies the integration of the mechanism with electrical contacts and actuation systems. The small travel of the device allows the use of simple space efficient actuation systems. This is important because of the small displacements available from available microactuators—larger displacements actuators often employ staging, stepping, or reciprocating schemes, which complicate control systems and require more power.

Self-retraction refers to the characteristic of this bistable mechanism to be able to perform the function of the return actuator, eliminating the need for an external return actuator. This can greatly reduce area and power requirements as well as system complexity.

The great strength of surface micromachining fabrication techniques, developed for the production of microelectronics, is the ability to inexpensively produce vast quantities of highly complex integrated circuits. This same technology has recently been adapted for the fabrication of mechanical devices at the micro-scale. MEMS (MicroElectroMechanical Systems) are small mechanical systems, fabricated by various processes, that can be integrated with microelectronics. Applications include microsensors, display technologies, telecommunications devices (RF and fiber optic) and microswitches/microrelays.

Low-power switching refers to the power needed to perform a switching cycle, and not to the power the device is capable of handling. Low-power also refers to the characteristic of bistable mechanisms to be able to maintain a given stable state without additional power input, this is in contrast to solid-state devices, such as transistors, which require constant power input to maintain an “On” state, and have leakage currents even in the “Off” state.

1.1 Importance of the Research

Small, highly reliable, low-power switches are needed for electrical, optical, and fluidic applications that are becoming increasingly small. With this miniaturization come many advantages and challenges. Smaller switches reduce system weight and volume,

which is critical for many applications (from satellites to cellular phones). MEMS switches can also be fabricated using the same processes and on the same substrate as the supporting microelectronics, further reducing size, weight, and production costs.

Power reduction is also very important and miniaturization offers the possibility of further improvements. Bistability can play a key role in power reduction, as power is only applied to transition from “on” to “off” and not to sustain a state (as is the case for semiconductor devices).

Bistable switching mechanisms are extremely simple in concept and yet have posed a difficult design problem in MEMS. Many of the bistable MEMS devices that have been proposed in the past [25, 28, 26, 27] have been partially compliant, using pin joints to reduce force requirements. However, the use of pin joints introduces a number of problems: Microfabricated pin joints have large clearances with respect to the overall geometry of the devices. These clearances require the mechanism to have large displacements in order to insure proper function. Increased mechanism travel requires actuators capable of larger displacement. Pin joint clearances may also result in misalignment, in and out of the plane of motion. Although actuation force may be reduced by introducing revolute joints, the increased displacement and modifications required by the large clearances may result in large energy requirements and complex actuation systems.

Pin joints also require multiple layers and added complexity. Floating pin joints are particularly complex [9]. Fully compliant devices can be made in one layer, removing much of the cost and complexity from fabrication. They are also well suited to LIGA (electroplated techniques) and bulk micromachining fabrication, which require microassembly of non-integral structures.

Several solutions have been attempted in the past to deal with the large deflections needed by bistable mechanisms that use pin joints. An unpublished effort by the author tried to use a gear train to amplify the displacement output of a thermal actuator sufficiently to actuate a bistable mechanism. Any amplification gained was offset by the large clearances in the gear hubs, and the pin joints (including a floating pin joint²) of the mech-

2. Floating pin joints are microfabricated pin joints that are not anchored to ground, i.e., joining to mobile links. In the two layer, conformal process this device was fabricated in, floating pin joints are difficult to design and introduce additional problems in practice.

anism. Baker et al. succeeded in achieving single stroke actuation of a microbistable mechanism by minimizing the displacement of a partially compliant bistable mechanism and coupling it to the actuators through small displacement amplifying levers [2]. All of these systems involve pin joints, and in many cases, floating pin joints. Researchers at the University of Michigan have designed fully compliant displacement multipliers that can be coupled with large-force, small-displacement actuators. However these have not been used in conjunction with bistable mechanisms [35].

The best MEMS pin joints involve isotropic (wet) etches to undercut layers, allowing the joint to be constrained to in-plane rotation. However this adds a number of additional processing steps and associated cost. The Sandia SUMMiT process has such a “pin joint cut.” In other processes pin joints must be designed to work with the conformal layers and anisotropic etches. In either case, floating pin joints still experience friction and wear, have large clearances, and contribute to stiction problems.

1.2 What is the Need?

There is a constant need for smaller more compact electronic systems. Semiconductor based microelectronics have greatly increased the capability and availability of complex industrial and consumer electronics, from supercomputers to personal computers and cellular phones. Many of these applications involve the combination of low voltage control and logic circuitry and high voltage or Radio Frequency (RF) circuits. Solid state devices generally operate at low voltages and attenuate the signal strength of high-frequency signals, making them incompatible with these applications. Another drawback to solid state devices is leakage current, which draws power from the system to maintain a given state.

Micromechanical switches provide good solutions to these problems and are desired for many applications, as they will reduce weight and complexity, and increase capabilities. However, previously proposed solutions do not completely fill the needs of a successful microswitch. These needs are:

1. Design suitable for batch fabrication using the same processes as microcircuitry, preferably without separate die.

2. Reliable and durable mechanisms which will repeatedly perform the task for a large number of duty cycles.
3. Low power requirements, ideally requiring energy only to transition from state to state and positive switching (no leakage current).
4. Low resistance, low attenuation connections.

1.3 How the SRFBM Fills the Need

The device presented in this thesis is compatible with current MEMS fabrication processes, and can be fabricated (including the actuation system) in a single high aspect ratio structural layer.

Reliability and durability are increased by the simple, single layer design (which reduces fabrication errors), the elimination of pin joints increases reliability and reduces friction and wear problems.

Power is reduced by reducing travel, eliminating complex multistage or stepping actuators, tailoring force requirements to better match the force deflection characteristics of actuation systems, minimizing idle travel (due to fabrication clearances), and introducing self-retraction (a more efficient return actuation methods).

Electrical contacts are improved by increased contact forces and the linear travel of the mechanism, which reduces alignment problems common to rotating systems.

Applications for which such a device may be suitable include electrical switching (RF signals, high-power micro-relays, circuit breakers, and low-power switching of micropower sources and devices), non-volatile or state retentive mechanical memory and logic, switching of optical signals (fiber optic networks or optical computers), microvalves for microfluidic applications, and threshold accelerometers.

1.4 Thesis Outline

The balance of this thesis is outlined as follows: Chapter 2 will present the some of the major issues related to this work MEMS, microswitches, compliant mechanism and

microactuators. Chapter 3 briefly introduces some of the techniques that will be useful for the development of the SRFBM. These are applied in Chapter 4 to the development of design criteria, modeling, and design of the SRFBM. Chapter 5 details the fabrication and testing of systems of SRFBM with on-chip actuation. It also presents the results of force testing of the SRFBM and compares this to the models. Chapter 6 extends the development of the SRFBM into other applications and fabrication processes. Chapter 7 contains the summary and conclusions of this thesis.

CHAPTER 2 *Literature Review*

2.1 Compliant Mechanisms

Compliant Mechanism gain some or all of their motion through the bending of flexible segments. Compliant mechanisms may be divided into two main categories: *fully compliant* mechanisms which gain all of their motion from the bending of flexible segments and *partially compliant* mechanisms which contain conventional kinematic pairs (pin joints, sliders, cams, etc.) as well as compliant segments. Compliant mechanisms are very common, however it has only been in the last 50 years that their analysis has been possible, thanks to solution of large-deflection equations, Finite Element Analysis, and other computer techniques and recently, the Pseudo-Rigid-Body Model.

The Pseudo-Rigid-Body Model has contributed greatly to the ability to design and synthesize compliant mechanisms. The Pseudo-Rigid-Body Model will be discussed in greater depth in Section 3.2.

2.2 MicroElectroMechanical Systems (MEMS)

In 1947 the transistor was invented at Bell Laboratories—eventually rendering the vacuum tube obsolete and making a huge advance in the miniaturization and robustness of electronics. In 1958 the first integrated circuit was produced at Texas Instruments, further reducing the size of electronics [48]. Now, more than 40 years since the first integrated circuit, microelectronics are a pervasive technology, used in some form in almost every con-

sumer appliance, vehicle, and even children's toys. Many pocket calculators have computing power far beyond the first room-sized computers. This revolution has been made possible not only by the ability to make electronics smaller and faster, but by the fact that by doing so, they can be made less expensively. The semiconductor industry, based on batch fabrication of microelectronics, achieved \$210 billion in the year 2000 and is expected to reach a yearly revenue of \$316 billion in the year 2004 [5].

Thirty years ago (and fifteen years before the term MicroElectroMechanical Systems—and the accompanying acronym MEMS—was coined at a conference in Salt Lake City, Utah) the first silicon based pressure sensors were fabricated. The subsequent growth of MEMS in research and industry has been impressive,

MEMS leverage the batch fabrication techniques developed for the production of microelectronics to produce micromechanical devices, often integrated with microelectronics. Applications being researched and produced commercially include pressure sensors, chemical sensors, accelerometers, display devices, ink-jet printer heads, synthetic jets, micro-robots and most pertinent to this study, microswitches.

2.2.1 MEMS fabrication

Various processes have been developed for the fabrication of MEMS devices. These processes can be separated into three main technologies: Bulk Micromachining, Surface Micromachining, and LIGA. Each technology has its advantages and limitations. Some of the metrics used to specify the capabilities of a process are defined as follows:

- Minimum linewidth—smallest isolated line that can be reliably patterned.
- Minimum spacing—smallest patternable gap between features.
- Sidewall profile—Degree to which an anisotropic etch deviates from an ideal (vertical) profile.
- Layer thicknesses—thickness of structural and sacrificial layers.
- Aspect ratio—(layer thickness)/(minimum linewidth).
- Number of mechanical and sacrificial layers.

In general, a process that is well suited to mechanical design will have small linewidth and spacing rules, allowing very small complex features to be fabricated. Highly anisotropic, high aspect ratio features are desirable in many applications as this decreases unwanted out-of-plane deflections. Many early surface micromachining processes used highly selective but highly isotropic wet etches in patterning steps. This leads to undercutting of features. Anisotropic etches in polycrystalline materials usually involve high energy reactive ion etching. The number and complexity of mechanical and sacrificial layers is important as more complex structures are possible with more layers.

2.2.1.1 Bulk micromachining

Bulk Micromachining deals with the patterning and etching of single crystal materials, commonly used as the substrates for microelectronics. The most prevalent material for use in bulk micromachining is Single Crystal Silicon (SCS). When exposed to certain etchants single crystals exhibit preferential etch rates along specific crystalline planes (for SCS a common etchant is KOH which etches along the $\langle 111 \rangle$ planes). Normally these processes involve growing or depositing a thin epitaxial layer (often oxides, nitrides, carbides of the bulk material) on the bulk substrate, patterning this new layer and then etching the substrate with the preferential etch, leaving a freestanding, patterned structure in the epitaxial layer.

2.2.1.2 Surface micromachining

Surface micromachining is characterized by the successive deposition, patterning and etching of alternating structural and sacrificial layers, creating one or more mechanical layers. After all of these steps the sacrificial layers are removed by a preferential etch, leaving the structural layers as free standing structures.

A common method of depositing the layers is Chemical Vapor Deposition (CVD), especially Low Pressure Chemical Vapor Deposition (LPCVD). The CVD process uses reactive gases containing the material to be deposited. The gas reacts with the exposed surfaces of the wafers, and is accelerated by high temperatures and *high voltage acceleration*. The nature of this deposition technique results in polycrystalline layers (in contrast to the single crystal materials commonly used as substrates). The deposited layers are conformal, resulting in “print through” of underlying topography. As the accumulation of topog-

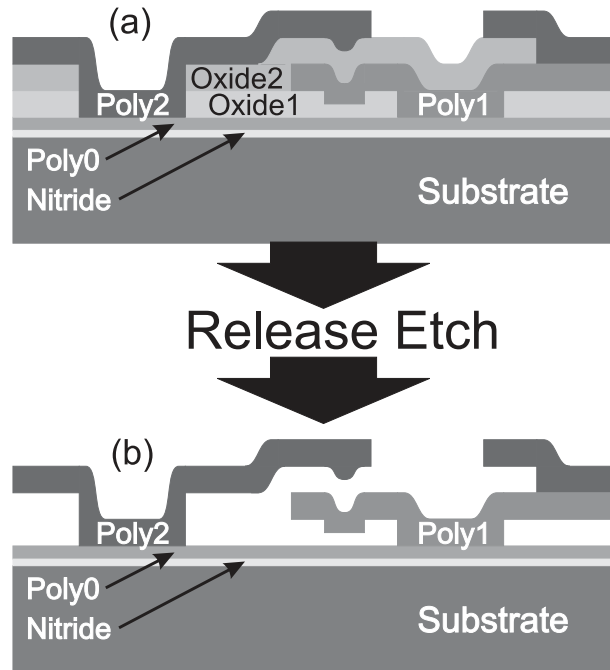


Figure 2-1 Cross section diagram of a three layer surface micromachining process. Unreleased structures (a) show the effects of “print through” due to the conformal layers. “Print through” topography remains in the released structures (b).

raphy affects each successive layer, the number of useful layers that can be deposited is effectively limited to a few layers.

To overcome this limitation Chemical Mechanical Polishing (CMP) has been used to planarize the sacrificial layers, eliminating the conformality of the structural layers and increasing the number of useful layers [19]. This method has been developed by Sandia National Laboratories (Albuquerque, NM) in the SUMMiT V process, which has five structural layers, including two planarized layers, and a set of conformal layers optimized for pin joint and hub fabrication [36, 38].

Thermal annealing and doping steps may also be applied after deposition steps, altering the physical and electrical properties of the layers and relieving residual stresses that may result from the thermal cycles involved in deposition.

Photolithography is used to transfer designs to the layers. Photolithography consists of the deposition of photoresist (a thin layer of light sensitive, etch resistant polymer) that can be selectively exposed to light (for the small features involved in MEMS devices the

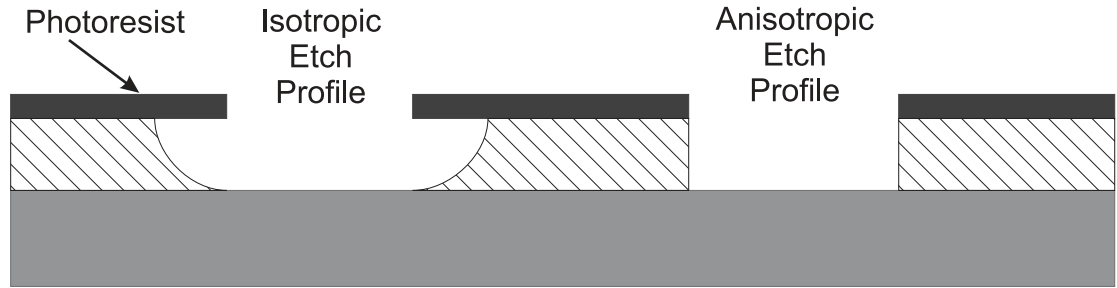


Figure 2-2 Ideal etch profiles: isotropic and anisotropic.

wavelengths are in the UV range of the spectrum). After exposure the patterned areas are rinsed away, exposing or protecting the underlying structural or sacrificial layer to subsequent etch steps.

Patterning steps may involve either isotropic or anisotropic etches, the latter being preferred for its superior linewidth and spacing and capabilities and mechanical behavior. Figure 2-2 contrasts the two etch profiles. Isotropic etches are normally accomplished with wet baths which etch the polycrystalline materials at equal rates in all directions. Anisotropic etches normally use reactive ions (RIE) accelerated by high voltages to etch high aspect ratio features. Because they undercut the photoresist, isotropic etches do not allow for the small feature sizes that are possible with RIE etches. However, wet isotropic etches are more selective, inflicting minimal damage to layers that are not intended to be etched. For this reason wet etch chemistries are used to etch sacrificial layers during release steps. Deep Reactive Ion Etching (DRIE) and Bosch etches use higher accelerating potentials to achieve even better anisotropy. Bosch etching is commonly used as a post processing tool to do backside etching through the thick substrate of the wafers.

One of the major difficulties encountered in MEMS fabrication is post-release stiction. Stiction is a combination of many forces and is exacerbated by the capillary forces during the final rinse and drying following the release etch. Several methods have been developed to minimize stiction including Self Assembling Monolayers (SAM) coatings of organic, hydrophobic chemicals [40, 1, 30], and supercritical carbon dioxide drying. The former eliminates the effects of capillary forces during the drying of the devices, keeping them from being pulled into contact with underlying layers. Supercritical drying removes the

water of the final rinse by a series of miscible rinses until the devices are left submerged in liquid carbon dioxide. At temperature and pressure above the critical point the liquid and vapor phases exist simultaneously and there is no volume change as a result of a change in phase.

2.2.1.3 LIGA (Lithographie Galvano-formung Abformung)

LIGA is the acronym for the German words meaning lithography, electroplating, and molding. This process produces extremely high aspect ratio features, minimum linewidths of 1-10 μm and thicknesses from hundreds of microns to several millimeters [24]. High aspect ratios are obtained by the use of highly columnated synchrotron x-ray radiation. The x-rays are used to pattern a mold (usually polymethyl methacrylate, PMMA). The x-rays break molecular bonds in exposed regions allowing the mold to be developed in a chemical rinse. The developed mold is then electroplated with nickel, copper, or nickel iron. The mold can then be dissolved by other chemicals leaving the electroplated features intact. The metal parts may then be used directly, or as a mold to replicate many parts by additional electroplating, injection molding or hot embossing of plastics [14, 24].

Variations of the LIGA process include using Deep Reactive Ion Etching (DRIE) and laser ablation to make the molds [24].

The high aspect ratios of LIGA make it very attractive for MEMS fabrication, however multiple component LIGA devices must be assembled (usually by hand), which is difficult and time consuming [24].

2.3 Bistable Mechanisms

Bistable mechanisms store energy in some manner (springs, gravitational potential energy, etc.), resulting in two stable equilibrium positions. These stable positions are separated by an unstable equilibrium position that must be overcome to transition between stable states. Bistability is discussed in greater detail in Section 3.1. Jensen has identified and classified many of the simple bistable mechanism configurations [25].

1. Snap-through buckling devices
2. Bistable cam mechanisms

3. Double-slider mechanisms with a pin joint joining the sliders
4. Double-slider mechanism with a link joining the sliders
5. Slider-crank or slider-rocker mechanisms
6. Four-link mechanisms

These classifications will be used where appropriate.

2.3.1 Conventional macro bistable mechanisms

The most familiar macro bistable mechanism is the conventional light switch. Turn it on—it stays on, turn it off—it stays off. This demonstrates the principle benefit of bistability in switching applications, i.e., energy input is only necessary to transition from one state to another, not to maintain a given stable state. Another example of bistability are the caps commonly used on shampoo bottles and other containers.

2.3.2 Micro-bistable mechanisms

Several micro-bistable mechanisms have already been proposed for use in micro-switching. Some of these will be presented and discussed in the following sections.

2.3.2.1 Buckled beams

An ideal fixed-fixed beam, subject to axial compression, may buckle if the critical buckling conditions given in Equation (2.1) (critical compressive stress), Equation (2.2) (critical compressive loading), or Equation (2.3) (critical axial displacement), are exceeded.

$$\sigma_{cr} = \frac{4\pi^2 EI}{AL^2} \quad (2.1)$$

$$P_{cr} = \frac{4\pi^2 EI}{L^2} \quad (2.2)$$

$$\Delta_{cr} = \frac{4\pi^2 I}{AL} \quad (2.3)$$

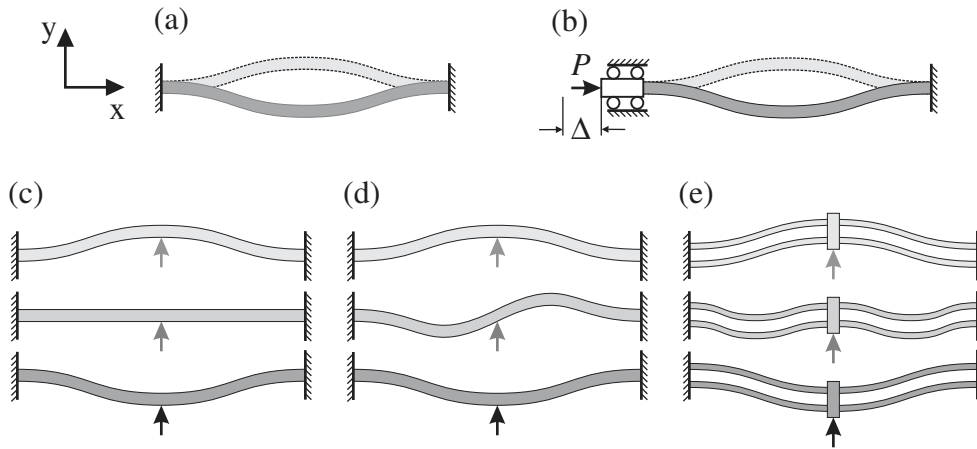


Figure 2-3 (a) Ideal buckled beam (Mode 1) subject to residual stress, showing two possible states. (b) Ideal buckled beam subject to a critical force, P , (or displacement, Δ). (c) Ideal (and unlikely) Mode 0 transition (or supercritical buckling) between buckled positions. (d) Mode 2 transition between buckled positions, with rotation of center point. (e) Mode 3 transition is made possible by the addition of multiple beams and central shuttles for symmetry.

where E is Young's modulus (modulus of elasticity), I is the cross section moment of inertia (in the plane of bending), A is the cross section area, and L is the length of the beam [15]. The plane of buckling will correspond to the smallest moment of inertia (in-plane if $I_{yy} < I_{zz}$ and out-of-plane if $I_{yy} > I_{zz}$, where $I_{yy} = \frac{wt^3}{12}$ (in-plane) and $I_{zz} = \frac{wt^3}{12}$ (out-of-plane) for rectangular cross-sections of out-of-plane thickness t and in-plane width w —using the coordinate system shown in Fig. 2-3 with a the z -axis out-of-plane).

There is a bifurcation in the buckling equations, i.e., the direction of buckling of an ideal beam can be in either direction within the plane of buckling. Thus the beam has two stable equilibria, separated by an unstable equilibrium which corresponds to either a supercritically stressed, unbuckled position or a intermediate elastica. The beam may be actuated from one stable position, through the unstable position, and come to rest in the second stable position. Figure 2-3(a) shows a beam buckled due to super-critical stress (as given in Equation (2.1)). Figure 2-3(b) illustrates a beam subject to a compressive external load (or displacement) that exceeds the critical levels for the beam geometry and properties as given by Equation (2.2) (or Equation (2.3)).

Bistable MEMS based on buckled beams have been proposed utilizing beams buckled by residual stress [51, 50, 18] (a by-product of the fabrication processes), thermally induced stress [8], or by applying external loading by on-chip actuation [42]. Another possible technique is to fabricate the beam in one of the stable positions. Although not buckled in the initial (as fabricated) state, the beam (or beams) can be designed to have a snap-through behavior. They will however remain biased to the initial position.

The stable and transitional shapes of the buckled beams will be classified by modeshapes. The terminology for the modeshapes comes from the number of waveform nodes corresponding to the number of times the beam crosses the y-axis (not including the origin of the beam). The familiar buckled shape (see Fig. 2-3(a)) is Mode 1 buckling. The supercritically stressed transition corresponds to what will be termed Mode 0 buckling, or unbuckled deflection. The mode shape of the intermediate *elastica* is Mode 2 (see Fig. 2-3(d)). This mode is undesirable for bistable switching applications as it introduces rotations that may not be compatible with actuation systems or contacts. This mode does however correspond to the path of lowest potential energy between the stable positions, i.e., the path of least resistance. This is because a Mode 0 is highly unlikely and other modeshapes are always higher energy states. Mode 2 transition can be avoided by using multiple beams and a central shuttle (see Fig. 2-3(e)) to provide stabilizing symmetry. The resulting structure is stiffer than a single beam, due to the additional beam and the Mode 3 transitional modeshape, but will be less prone to rotational deformations.

A variation of bistability based on buckling is found in the bistable snapping microactuator of Matoba, et al. [31], which uses residual stress of a silicon nitride tension band to buckle a fixed-free beam. This results in the out-of-plane deflection of the free end of the beam. The U-shaped buckled cantilever beam (see Fig. 2-4) is fabricated with a layer of silicon oxide sandwiched, above and below, between two layers of polysilicon. The polysilicon layers can be heated individually by Joule heating, which will cause the beam to deflect toward the unheated layer. It can then snap repeatedly from one stable state to another.

2.3.2.2 Young mechanism

Developed at Brigham Young University, the Young mechanism is an in-plane bistable mechanism, classified as a four-link mechanism, when modeled with the Pseudo-Rigid-

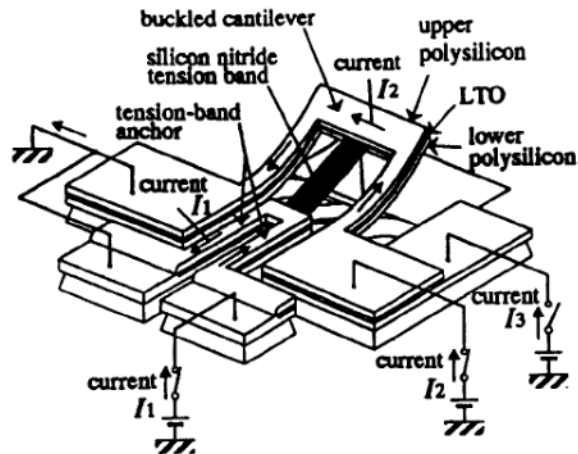


Figure 2-4 Bistable snapping microactuator [31]

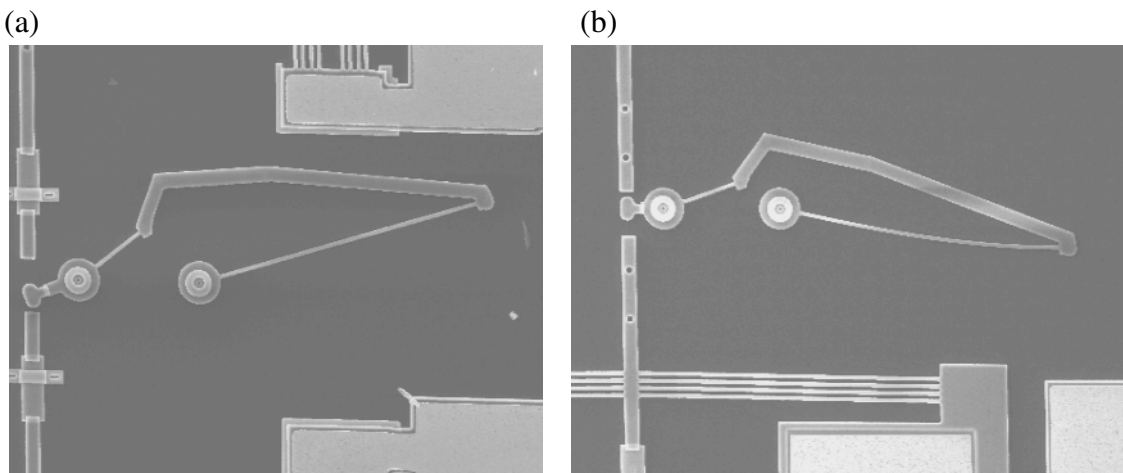


Figure 2-5 SEM images of Young mechanism bistable microswitch in (a) the initial (or first stable equilibrium) position and (b) the second stable equilibrium position. (Note, these images are not of the same device, but are of devices with the same design.)

Body Model (see 3.2—Pseudo-Rigid-Body Model on page 36). This was one of the first complex in-plane bistable micromechanisms. As shown in Fig. 2-5(a) and (b), the Young mechanism is a partially compliant mechanism, normally configured with two flexible segments, joined by a rigid segment and connected to ground by two pin joints. Figure 2-

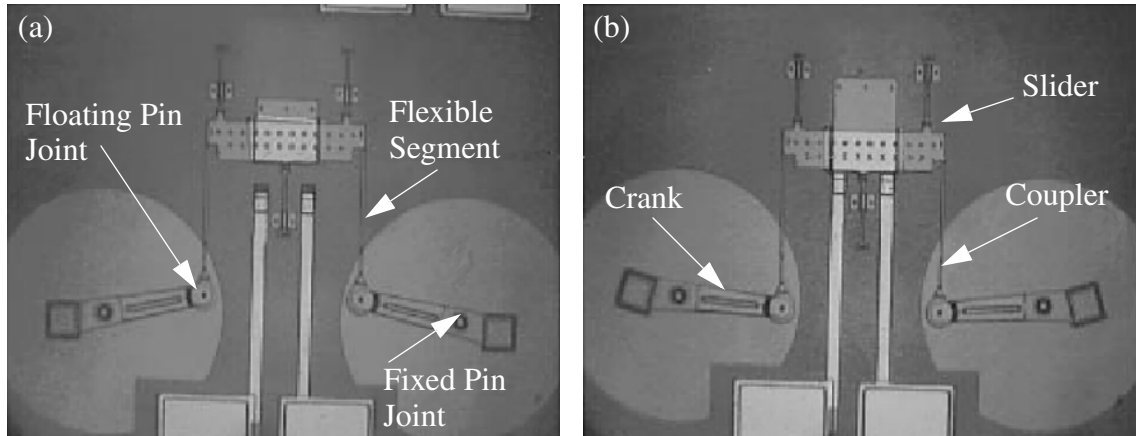


Figure 2-6 SEM image of the Berkeley bistable switching frame in the (a) open and (b) closed positions. The travel is approximately $17\ \mu\text{m}$ [28].

5(a) shows the initial position (or first stable equilibrium) and Fig. 2-5(b) shows the second stable equilibrium position.

In practice, the mechanism is actuated through a small lever attached to one of the flexible segments at the pin joint. This allows a small actuation displacement to produce the relatively large rotational input necessary to switch the device. Figure 2-5 shows the Young mechanism with electrical contacts for switching. It requires actuator displacements of approximately $9.0\ \mu\text{m}$ for the low power versions that have been developed for use with microbattery systems [25, 26, 27].

2.3.2.3 Berkeley bistable mechanism

A bistable mechanism was developed at the University of California, Berkeley at approximately the same time as the Young Mechanism [28]. The mechanism may be modeled as a slider-crank—with the crank pinned to ground and connected to the coupler by a floating pin-joint. The coupler is a flexible segment, the floating pin-joint connecting it to the crank and the compliance of the coupler segment storing energy and performing the function of the other joint to the slider. Linear sliding is achieved by the symmetry of the mechanism.

The travel of the mechanism is reasonable ($\approx 17\ \mu\text{m}$) and thermal actuators are used in a stepping arrangement to achieve the necessary displacement. This device was used to

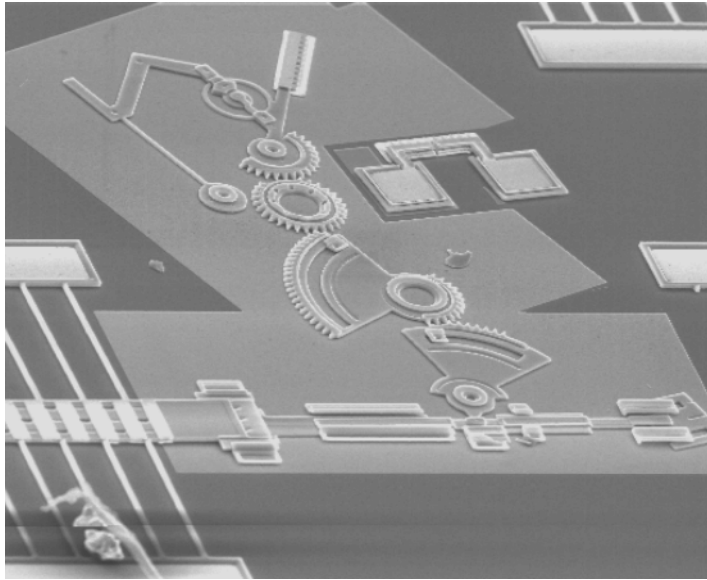


Figure 2-7 SEM image of the “Rube Goldberg” system. The gear train is composed of partial gears as full revolution is not needed and are not possible with conformal layers of the MUMPs process.

evaluate lateral electrical contacts [29]. It is unclear from the literature whether on-chip actuation was achieved.

2.3.2.4 “Rube Goldberg” system

In an unsuccessful attempt to achieve on-chip actuation, a set of gears was used to amplify the displacement of a thermal actuator to drive a bistable four-link mechanism. The bistable mechanism used in this system was first presented by Clements, et al., for evaluating floating micro-pin joints [10]. This system demonstrates the difficulties in designing MEMS devices that use pin joints. As can be seen in Fig. 2-7, a number of pin joints are used for both the mechanism and the gear hubs (three pin joints for the mechanism, including one floating joint). Each joint (and gear tooth interface) requires a minimum of $2.0\ \mu\text{m}$ of spacing on either side (a total of $4.0\ \mu\text{m}$ of clearance) to insure proper fabrication. These clearances add up to the point that any displacement multiplication gained by the gear train is lost in the clearances. Source code for a program developed to generate gears with correct involute tooth profiles is included in APPENDIX A.

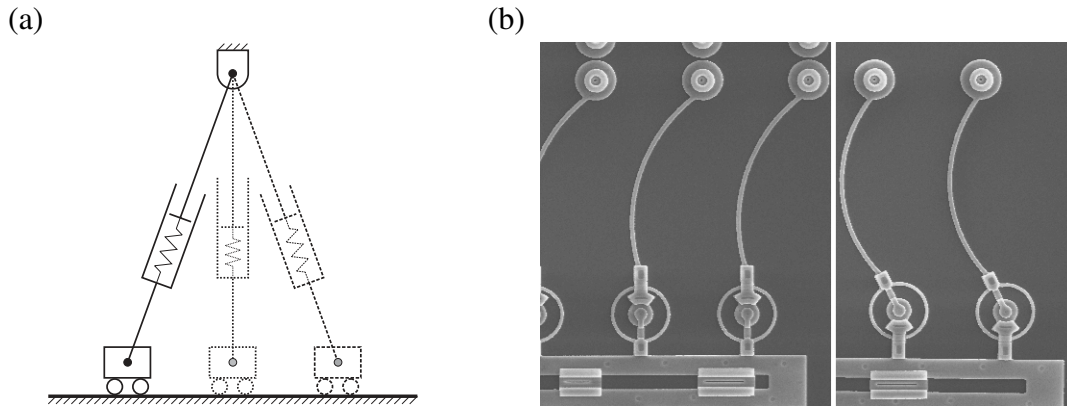


Figure 2-8 (a) Model of double-slider bistable configuration. (b) SEM image of LDBM in both stable equilibrium positions. The image does not show the other set of legs, which provides symmetry for the sliding action. Clips are used to limit out-of-plane deflections.

2.3.2.5 Linear Displacement Bistable Mechanism (LDBM)

The Linear Displacement Bistable Mechanism (LDBM) is another linear bistable micromechanism developed at BYU [3]. This mechanism is classified as a double-slider, with the sliders pinned to each other, as shown in Fig. 2-8(a). The symmetry of the device constrains it to linear sliding. The initially curved functionally binary pinned-pinned segments store energy and perform the function of the second slider.

Due to the relatively large clearances in the pin joints, LDBMs require a large displacement to switch between stable positions. On-chip actuation has been achieved using amplified thermal actuators, but only for the transition from the first stable equilibrium to the second. The return actuation has not functioned correctly due to design errors. Work is continuing to improve this design.

2.3.2.6 Fully Compliant Bistable Micromechanisms (FCBM)

A variation on the double-slider is found in the Fully Compliant Bistable Mechanism (FCBM), which was also developed at Brigham Young University. This alternatively configured double-slider has both sliders connected to ground and joined by a link as shown in Fig. 2-9(a). Linear sliding is again provided by the symmetry of the device. The function of the second slider is performed by the short fixed-fixed beam connections to the substrate. Flexible segments serve as flexural pivots for the links.

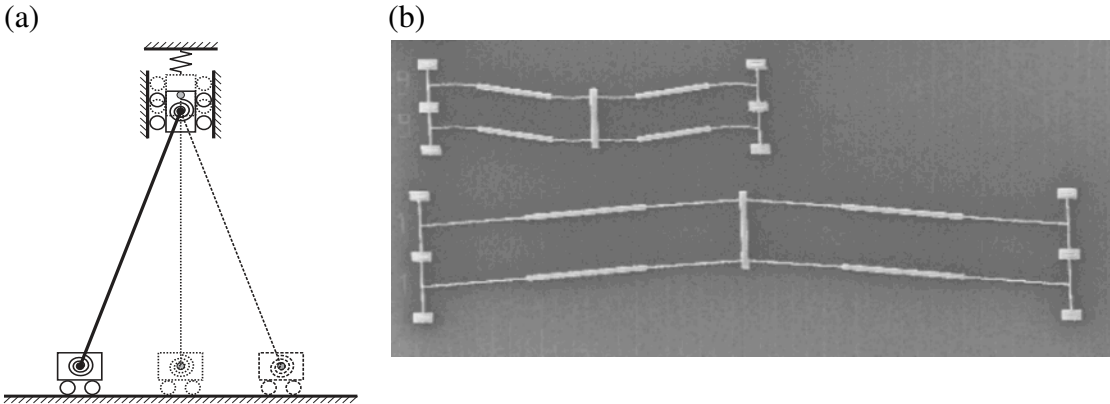


Figure 2-9 (a) Model of double-slider configuration. (b) SEM image of FCBMs. The mechanism in the upper left of the image has been displaced to its second stable equilibrium position.

The flexural pivots are relatively long in order to reduce stresses. However, as the length of these segments increase, the required displacement for bistability increases. This mechanism is also prone to out-of-plane deflections. On-chip actuation has also been demonstrated for these devices using staged thermal actuators.

2.4 MEMS On-Chip Actuation

Micromechanisms are of very little practical value without some method of on-chip actuation. However, integration of bistable mechanisms and microactuators has been an obstacle. One difficulty is that due to fabrication limitations bistable mechanisms often have large travels relative to that of the actuators compatible with the fabrication processes.

At the micron scale, forces that would normally be considered insignificant at the macro-scale can be useful. As a result many novel actuation schemes have been developed for MEMS applications. A few truly novel MEMS actuators are based on more conventional macro techniques.

2.4.1 Electrostatic

Electrostatic attraction is one of the most common actuation technique used for MEMS devices. This force results from the electric field due to a voltage potential. It is

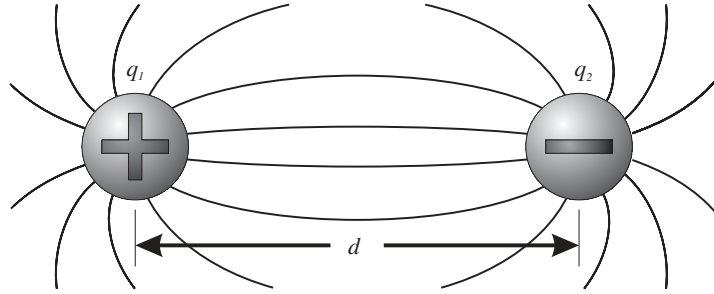


Figure 2-10 Illustration of the electrostatic force between charged particles

only attractive. The attractive force between two charges, q_1 and q_2 (see Fig. 2-10) separated by a distance d , is given by Coulombs law (Equation (2.4)).

$$F = \frac{1}{4\pi\epsilon_0} \frac{q_1 q_2}{d^2} \quad (2.4)$$

where ϵ_0 is the permittivity constant ($\epsilon_0=8.85e^{-12} \text{ C}^2/\text{N}\cdot\text{m}^2$ for free space).

This force is also equivalent to the negative partial derivative of the electrical potential energy, U , with respect to the separation distance, d [14].

$$F = -\frac{\partial U}{\partial d} \quad (2.5)$$

The attractive force of various configurations will be given for parallel plate and comb drive configurations. For point charges the potential energy is given by Equation (2.6)

$$U = \frac{1}{4\pi\epsilon_0} \frac{q_1 q_2}{d} \quad (2.6)$$

In general electrostatic actuators are characterized by high voltage requirements, small deflections and low forces for a given area. However, a major advantage is in power consumption ($P=VI$), as very little current is drawn by electrostatic devices.

2.4.1.1 Parallel plate

The simplest form of electrostatic actuation is that of a set of parallel plates. Depending on the size and proximity of the plates, the forces can be significant. The capacitance, C , of a set of parallel plates is given by

$$C = \frac{\epsilon_0 A}{d} \quad (2.7)$$

where A is the area of each plate. The potential energy of these plates, subject to a potential V , is

$$U = \frac{1}{2} C V^2 \quad (2.8)$$

or by substituting Equation (2.7) for C ,

$$U = \frac{\epsilon A V^2}{2d} \quad (2.9)$$

which by differentiation leads to the attractive force

$$F = -\frac{\partial U}{\partial d} = \frac{\epsilon A V^2}{2d^2} \quad (2.10)$$

As d decreases the attractive force increases, until *pull-in* occur. This may lead to catastrophic failure due to fusing (also referred to as *clamping*) and damage due to spark discharges.

Parallel plate actuation is commonly used for out-of-plane actuation of cantilever and fixed-fixed beam switches [18]. This method has also been used for in-plane actuation by coupling the parallel plates with linkages to multiply the displacements [39].

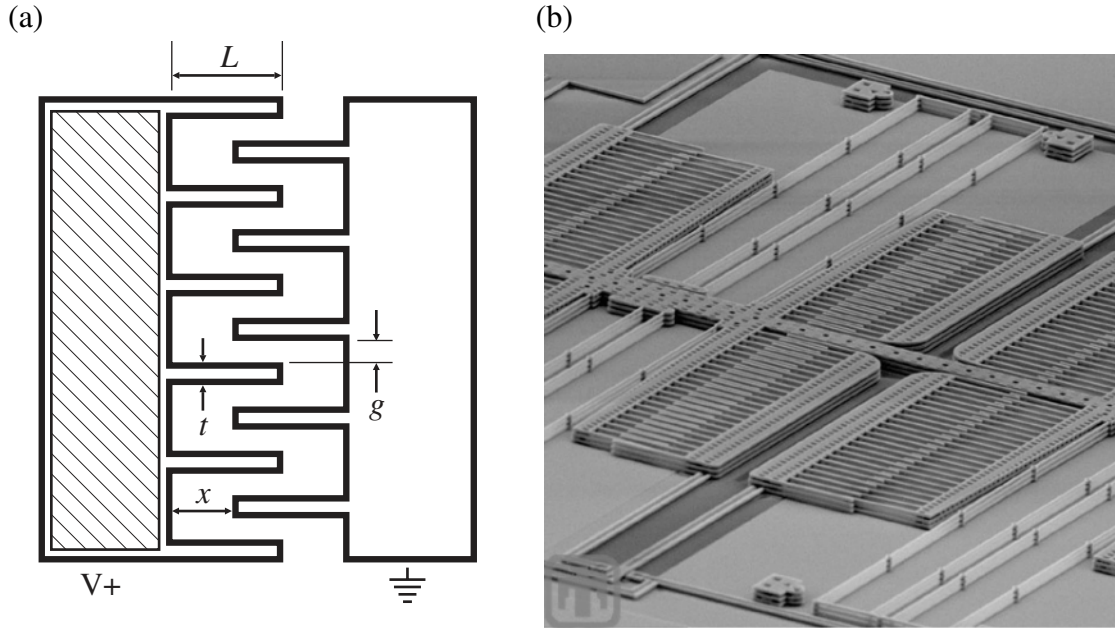


Figure 2-11 (a) Diagram and (b) image of comb drive actuators [37]

2.4.1.2 Comb drives

Comb drives are made of many interdigitated fingers suspended in such a way that they can slide parallel to each other. This allows larger displacements than parallel plate actuators, but the trade-off is reduced force. In comb drives the direct parallel plate attraction is relegated to a passive role. The active attractive force can be considered to come from the change in capacitance (see Equation (2.11)) that results from the movement of the interdigitated fingers.

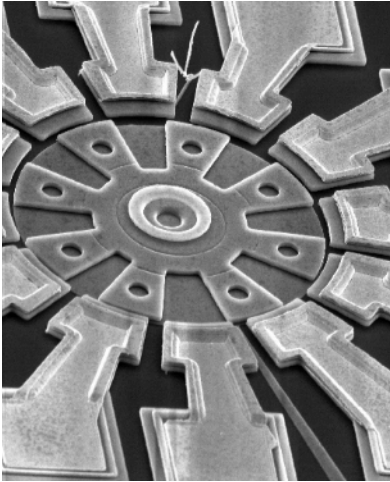
$$C = 2n \frac{\epsilon t(L-x)}{g} \quad (2.11)$$

This leads to the equation for comb drive actuation force of

$$F = n\epsilon \frac{t}{g} V^2 \quad (2.12)$$

where n is the number of comb fingers, t is the out-of-plane thickness of the comb fingers, and g is the gap between comb finger faces [14] (see Fig. 2-11(a)).

(a)



(b)



Figure 2-12 (a) Rotary sidedrive and (b) wobble motors [49]

An advantage of comb drives is that the force is independent of comb position, x , which eliminates the potential of pull-in. However, this also results in much smaller actuation forces. Parallel plate forces must still be considered during design as the fingers can deflect towards each other, which may lead to failure. Total actuation force is increased by using multiple comb fingers (the n in Equation (2.12)) to provide reasonable actuation forces and displacements.

Modifications have been made to comb drives to optimize finger shape [52] and to hybridize comb and parallel plates. Further improvements have recently been made by increasing comb finger density, and decreasing actuator travel, the resulting small displacement, large force low voltage electrostatic actuator is then coupled with a compliant displacement multiplier to achieve a balanced actuator design [35].

2.4.1.3 Rotary side drive and wobble motors

Rotary side drive, or salient pole micromotors (see Fig. 2-12(a)) have demonstrated very high rotational speeds, but are not very useful due to the insignificant (even for a MEMS device) torque output. An additional obstacle is the difficulty of extracting torque from the rotor. They operate by applying a voltage to sets of stator poles, attracting the

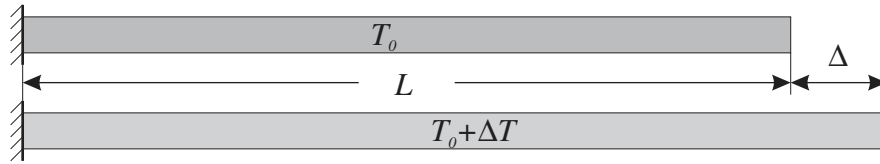


Figure 2-13 Thermal expansion diagram

nearby rotor arms. As the rotor rotates, the stator pole fields must be rotated in the opposite direction as that of the rotor.

Although similar in appearance to rotary side drive motors, wobble motors (see Fig. 2-12(b)) operate by not spinning on a central hub, but by wobbling about it, as the rotor is pulled around by a succession of electrostatically charged stator poles. The torque output of the wobble motor is larger than rotary side drive, but is still quite small, and equally difficult to extract. These devices are not particularly useful and are only mentioned for thoroughness.

2.4.2 Thermal

Another popular family of actuation techniques uses the thermal expansion of the structural material and amplifies these small displacements by the geometry of the mechanism. Figure 2-13 illustrates the amount of thermal expansion as given by Equation (2.13):

$$\Delta = \alpha L \Delta T \quad (2.13)$$

where α is the coefficient of thermal expansion, L is the length of the expanding member, and ΔT is the change in temperature, with respect to the initial temperature, T_0 , (or that of the unheated, undeflected surrounding structure). The high temperature, $(T_0 + \Delta T)$, must be lower than the melting point of the material. It is also preferable to remain below the annealing temperature, where stress relaxation will occur, reducing the effectiveness of the actuator. This results in a maximum ΔT for polysilicon of approximately 600°C . The coefficient of thermal expansion is normally quite small (2.3×10^{-6} for polysilicon). The combination of a relatively small ΔT and α means that the total expansion will be very small for

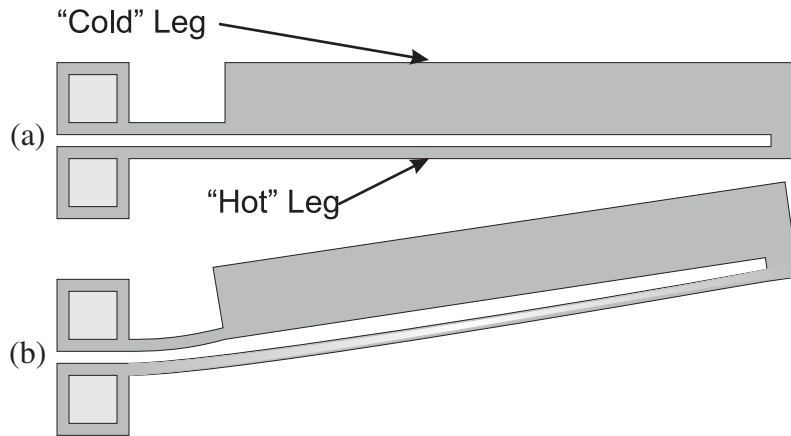


Figure 2-14 U-beam diagram

reasonable lengths. It is for this reason that thermal actuation schemes use mechanical amplification to increase the displacement.

Many thermal actuation schemes are explicitly electrothermal: resistive (or Joule) heating due to an electrical current applied to the expanding members. External heating is also used, such as heating element embedded in the substrate [7], and laser illumination. In most cases the force of the return stroke is greater than the forward stroke. This phenomenon, sometimes referred to as “back-bending,” is the result of the stored mechanical potential energy. During heating energy is used to induce deflections. If an external load is being moved by the actuator this will require additional energy for a given displacement of the actuator. When the actuator cools the energy stored in strain energy can be used to perform work.

2.4.2.1 Comtois or U-beam

The principle of U-Beam actuators is similar to a bimetallic strip. Two legs of dissimilar cross sections are connected at their free ends. As illustrated in Fig. 2-14(a), the lower leg is long and thin and the upper leg has two cross sections: a short narrow segment that serves as a flexural pivot and a wider rigid segment. As an electrical current is passed through the device the narrow lower beam which has a higher resistance experiences a larger temperature increase, resulting in greater thermal expansion than the wider (and

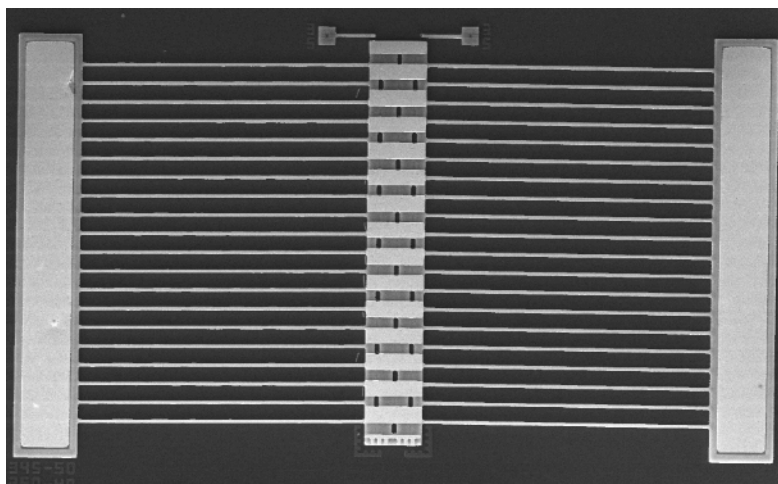


Figure 2-15 SEM image of TIM microactuator

thus cooler) upper beam. The result is an induced moment that causes the actuator to bend towards the “cold” beam as shown in Fig. 2-14(b) [11].

A single device does not produce much force, so these devices are often arranged in parallel to provide greater output force while maintaining the same displacement. Output force from a single 200 μm long device has been reported as approximately 13 μN at 5 mA and 14 V with a displacement of 16 μm [11].

2.4.2.2 TIM, V-beam, or bent-beam

The Thermal In-plane Microactuator, or TIM, is composed of one or more sets of beams anchored to the substrate at the ends and joined together at a shallow angle, forming a *chevron*, often with a central shuttle [13, 12] (see Fig. 2-15). As the beams heat, their expansion is constrained and results in a transverse displacement. The behavior is similar to the buckling of a beam with an initial bias, or imperfection. This action may also be modeled using the PRBM (see Fig. 2-16).

TIMs are scalable in force by adding more legs (at the cost of higher current requirements). Longer legs provide larger displacements, but this is limited by buckling of the legs if they are too long. These actuators provide large forces and considerable displacements and require modest amounts of area and low actuation voltages. (Typically, hundreds of μN and more than 10 μm of displacement are available from devices with 200 μm

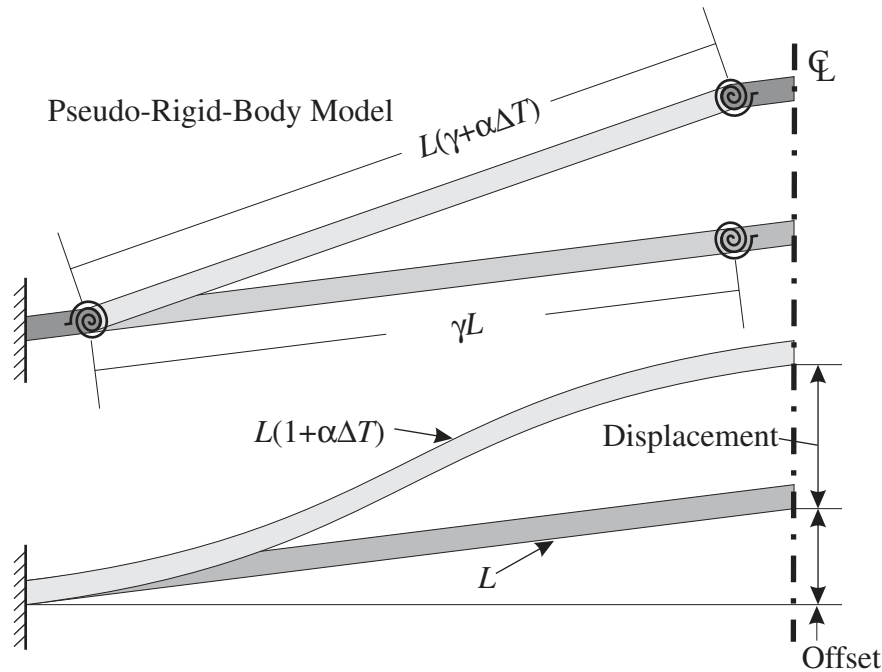


Figure 2-16 TIM model

legs). Current draw is much higher than electrostatic devices and may be the primary concern in their implementation.

2.4.3 Miscellaneous actuation

There are other actuation techniques that have been proposed. The most interesting aspect of these microactuation systems is that they are often the closest to macroscopic actuation schemes. Due to the effects of scaling, these methods—that work so well at the macro-scale—are only of marginal usefulness at the micro-scale. These include magnetic, steam and internal combustion. Magnetic is perhaps the most promising of these, providing large actuation forces. However, external magnetic sources (not fabricated on-chip), are generally used, greatly increasing the size of the overall system.

2.5 MEMS Microswitches

Other microswitches and microrelays have been proposed that are not bistable, or that are intended to switch non-electrical signals. Monostable switches require constant power

input to maintain an “on” state (or “off” for a normally on switch). There are two main families: direct contact and capacitive. From a mechanism standpoint there is little difference between the two families; only the means of electrical contact is different. Direct contact switches allow current to pass through electrodes that are brought into direct physical contact by the motion of the mechanism. Capacitive switches rely on the reduced capacitance of the switch (achieved by decreasing the separation distance between capacitive plates) to be detected externally or allow high-frequency signals to be transmitted. Capacitive switches are developed primarily for use in Radio Frequency (RF) systems.

2.5.1 Beam switches

Some of the first MEMS microswitches were composed of a cantilever beam actuated electrostatically toward the substrate, where it contacts a semiconducting region to close a circuit [14]. Variations include metallic contacts and capacitive transmission. Although these devices are very simple, special care must be taken in their design to avoid stiction and pull-in. Obviously such switches are not bistable, and require continuous actuation to maintain the “on” state.

A variation is to use fixed-fixed (or bridge-type) beams. Fixed-fixed beams have greater mechanical restoring force, increasing their resistance to pull-in and stiction.

These switches are also used as *shunt* switches, shunting the transmission lines of a signal to an electrical ground, ending the transmission.

2.5.2 Cronos

Cronos (formerly MCNC) has developed a thermally actuated microrelay with lateral contacts using a combination of surface micromachining and LIGA [7]. This is of interest because this system is currently available commercially for microrelay applications but is not, however, bistable.

2.5.3 Optical switches

Another area of interest for microswitching involves switching of light. This may involve redirecting a free beam of light or the displacement of a light carrier (optical fiber).

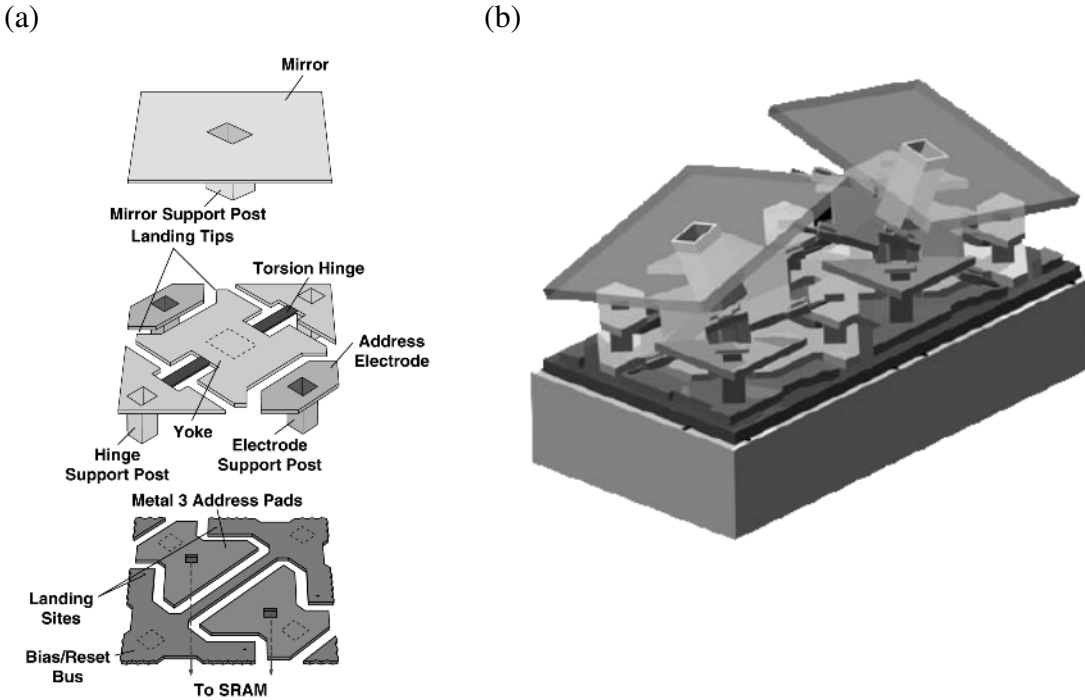


Figure 2-17 Texas Instruments DMD™: (a) diagram of the components of the DMD™ mechanism [46] and (b) illustration of two micromirrors actuated in opposite directions [47].

2.5.3.1 Texas Instruments Digital Micromirror Device™

The Digital Micromirror Device (DMD)™ was developed by Texas instruments for video projection displays. The display unit, or Digital Light Processor (DLP)™, is composed of millions of electrostatically actuated DMDs™, which are the pixels of the display. The DMD™ is described by Texas Instruments as “bistable,” however, this definition is inconsistent with the definition of bistability used in this thesis. The mirrors can be left in the “as-fabricated” position or switched $\pm 10^\circ$. When the actuation potential that holds the mirrors in either switched state is released the mirrors return to the undeflected position. This has been a very successful MEMS based product that is indicative of the promising future of MEMS.

2.5.3.2 Fiber optics switching

A bistable fiber optic switch has been proposed by Hoffmann, et al. [20], that works on the cam principle. Input fibers are held by clamps, the upper half of which is fixed, the

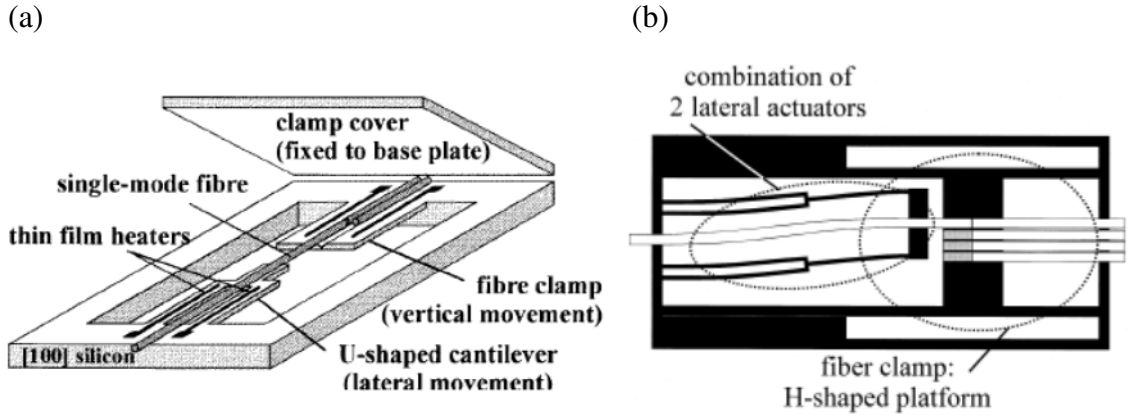


Figure 2-18 Bistable optical fiber switch (a) illustration of principle components [21] and (b) top view diagram of an advanced multi-stable version with multiple grooves [20].

lower half divided between lateral and vertical thermal actuators. When it is desired to switch the fiber, the vertical clamp is actuated, releasing the fiber on the output side. The lateral actuators can then switch the fiber to a different groove (thus acting as a cam) where the fiber will remain, being clamped in place by the release of the vertical clamp actuator. Each groove corresponds to a different output fiber.

2.5.4 Miscellaneous

Other MEMS switching applications applicable to this study are microvalves (especially bistable microvalves [16, 34, 6]) and accelerometers as these may be additional applications for the device developed in this thesis.

CHAPTER 3 *Background*

Before proceeding with the development of the SRFBM, a discussion of the mathematics of system stability, as well as some of the techniques used in the design of compliant bistable mechanisms, must be presented. The Pseudo-Rigid-Body Model allows rigid-body mechanism synthesis techniques to be applied to compliant mechanism design. The principle of virtual work, an energy based method, is used to evaluate the force-displacement characteristics of mechanisms. The basics of finite element analysis, used to refine the final design of compliant mechanisms, are also presented.

3.1 Mathematics of Bistable Behavior

The definition of stability used in this thesis is based on the work of Jensen [25]. Equilibrium refers to a state at which a system has no acceleration. If the response of a system in equilibrium to a small perturbation is to oscillate about (and eventually come to rest at) the point of equilibrium, then this equilibrium is said to be *stable*. If the system remains stable at a continuum of adjacent positions then the system is said to be *neutrally* stable. The response of such a system to a disturbance (that does not remove it from the region of neutral equilibrium) is to remain in the disturbed position. If the system responds to a disturbance by diverging from the point of equilibrium (and the disturbed state), then this equilibrium is said to be *unstable*.

Bistability may be compared to the classic “ball-on-the-hill” example, as illustrated in Fig. 3-1. Consider the ball at position A, a stable equilibrium. If the ball is disturbed a

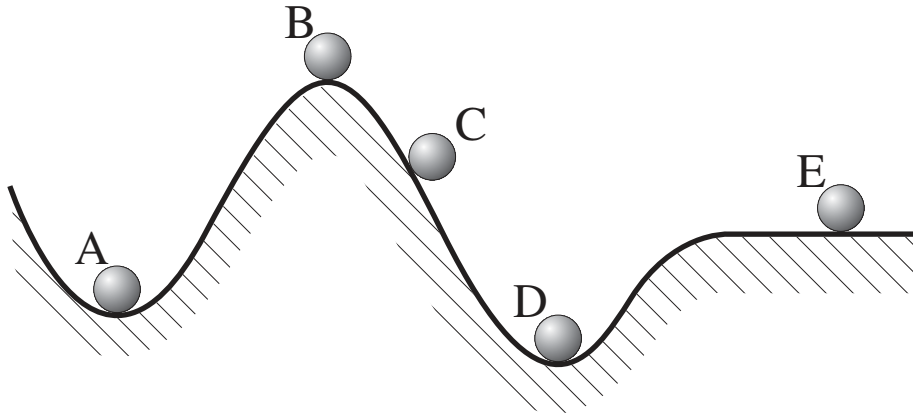


Figure 3-1 This figure illustrates the “ball-on-the-hill” analogy. At Positions A and D the ball is in stable equilibrium. At Position B the ball is at an unstable equilibrium. Position C is not an equilibrium position. Position E is neutrally stable.

small amount it will oscillate about position A, and if friction or damping are present in the system it will return to this position. Position B is an unstable equilibrium, the ball may remain at this point if it is placed precisely at the top of the hill. However, any small perturbation will result in the ball rolling to either position A or D (depending on the direction of the perturbation). Position C is not in equilibrium and the ball cannot rest at this position. Position D is also a stable equilibrium position, like position A. Position E is neutrally stable, and the ball can remain stably at many locations at this same potential.

Figure 3-2 demonstrates how a new stable equilibrium may be created by placing a stop at position C. This could be a physical stop, or appropriate external forces that hold the system in equilibrium. This type of equilibrium will be referred to as an externally constrained stable equilibrium.

Consistent with this analogy is the characteristic that stable equilibria are local minima of the potential energy of the system. Unstable equilibria are local maxima of the system’s potential energy. Two local minima will always enclose a local maximum, thus a bistable mechanism must have at least one unstable equilibrium.

This can be proved by considering that the potential energy (PE) of the system is equal to the work (W) put into the system: $PE=W$. The derivative of the potential energy at equi-

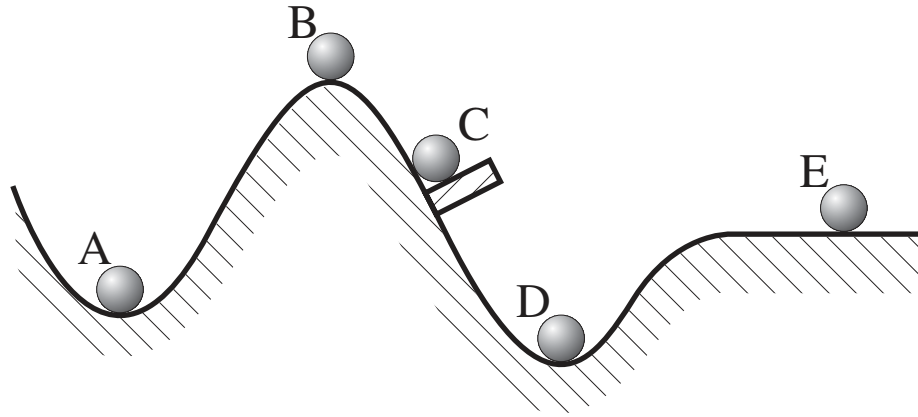


Figure 3-2 A stop has been added at Position C, making this an externally constrained stable equilibrium.

librium positions is zero. The work put into the system for a linear displacement, x , may be represented as

$$W = \int_{x_0}^x F dx \quad (3.1)$$

and for a rotational input, θ , as

$$W = \int_{\theta_0}^{\theta} T d\theta \quad (3.2)$$

The derivatives of these equations with respect to the inputs are

$$\frac{dW}{dx} = F \quad (3.3)$$

and

$$\frac{dW}{d\theta} = T \quad (3.4)$$

Thus the applied loads are equal to the first derivatives of the potential energy of the system, with respect to the input displacement variable. Therefore the zeros of the input force (or torque) correspond to the equilibria of the system, and the sign of the second derivative of the system's potential energy (or first derivative of the input force) indicates whether the zeroes correspond to stable or unstable equilibria (a positive second derivative indicates a stable equilibrium).

3.2 Pseudo-Rigid-Body Model

The Pseudo-Rigid-Body Model (PRBM) is a recent development in compliant mechanism design and analysis. The PRBM allows flexible links of compliant mechanisms to be modeled with rigid links and torsional springs of appropriate sizes. The link lengths and spring rates are based on curve fits of the elliptic integral solutions of the deflection of flexible members. This technique greatly simplifies the analysis, and especially the synthesis, of compliant mechanisms.

3.2.1 Beam deflections

To better appreciate the Pseudo-Rigid-Body Model, some of the theory of large deflection elastic bending of flexible beams will be presented. The deflection of any beam may be expressed by the Bernoulli-Euler equation which states that the curvature of the beam, κ , is proportional to the bending moment, or mathematically

$$\frac{M}{EI} = \frac{d\theta}{ds} \equiv \kappa \quad (3.5)$$

where at any location s along the beam θ is the beam angle, M is the bending moment at that location, E is the Young's Modulus of beam, and I is the moment of inertia for the cross section at location s .

3.2.2 Large deflection of a cantilever beam: moment load

The deflection of a beam of uniform cross section (I and A) and material properties (E and ν) subject to a pure moment load, M_0 , can be evaluated as follows:

$$\int_0^{\theta_0} d\theta = \int_0^L \frac{M_0}{EI} ds \Rightarrow \theta_0 = \frac{M_0 L}{EI} \quad (3.6)$$

where θ_0 is the slope of the beam at its end point.

$$\frac{d\theta}{ds} = \frac{d\theta dy}{dy ds} = \frac{d\theta}{dy} \sin \theta = \frac{M_0}{EI} \quad (3.7)$$

$$\int_0^b dy = \int_0^{\theta_0} \frac{EI \sin \theta}{M_0} d\theta = \frac{EI}{M_0} (-\cos \theta) \Big|_0^{\theta_0} = \frac{EI}{M_0} (1 - \cos \theta_0) \quad (3.8)$$

$$b = \frac{1 - \cos \frac{M_0 L}{EI}}{\frac{M_0}{EI}} \quad (3.9)$$

$$\frac{d\theta}{ds} = \frac{d\theta dx}{dx ds} = \frac{d\theta}{dx} \cos \theta = \frac{M_0}{EI} \quad (3.10)$$

$$\int_0^a dx = \int_0^{\theta_0} \frac{EI \cos \theta}{M_0} d\theta = \frac{EI}{M_0} \sin \theta \Big|_0^{\theta_0} = \frac{EI}{M_0} \sin \theta_0 \quad (3.11)$$

$$a = \frac{\sin \frac{M_0 L}{EI}}{\frac{M_0}{EI}} \quad (3.12)$$

Thus for these conditions there are exact, closed form solutions that are easily evaluated.

3.2.3 Small deflection of a cantilever beam: vertical end load

The Bernoulli-Euler equation, given in Equation (3.5) may be modified to produce Equation (3.13):

$$\frac{d\theta}{ds} = \frac{\frac{d^2y}{dx^2}}{\left(1 + \left(\frac{dy}{dx}\right)^2\right)^{3/2}} = \kappa(s) \quad (3.13)$$

where $\kappa(s)$ is the curvature of the beam at any point s . This equation is simplified for small deflections by assuming that the square of the slope of the beam, $\left(\frac{dy}{dx}\right)^2$ (in the denominator of Equation (3.13)), is much smaller than unity. This leads to the common form of the Bernoulli-Euler equation found in many texts:

$$M = EI \frac{d^2y}{dx^2} \quad (3.14)$$

3.2.4 Large deflection of a cantilever beam

The small angle approximation used to arrive at Equation (3.14) assumes that the slope of the beam at any point is small. For beams with larger deflections (and consequently large slopes) the assumption used to obtain Equation (3.14) is no longer valid. In order to accurately calculate the deflections, Equation (3.5) must be evaluated without small angle approximations. The solution to these equations for a vertical end load using elliptic integrals was presented by Bisshopp and Drucker in 1945 [4]. Solutions for other loading conditions (non-vertical end and combined end and moment loads) have also been found. Solutions are only possible for a few specific cases of loading and geometry.

3.2.5 Pseudo-Rigid-Body Model

The elliptic integral equations are cumbersome and difficult to implement in the analysis of mechanisms. The Pseudo-Rigid-Body Model was developed from observations of the solution to these equations (which give the location and angle of the beam at its endpoint). The path of the endpoint was observed to approach a circular arc. This leads to a

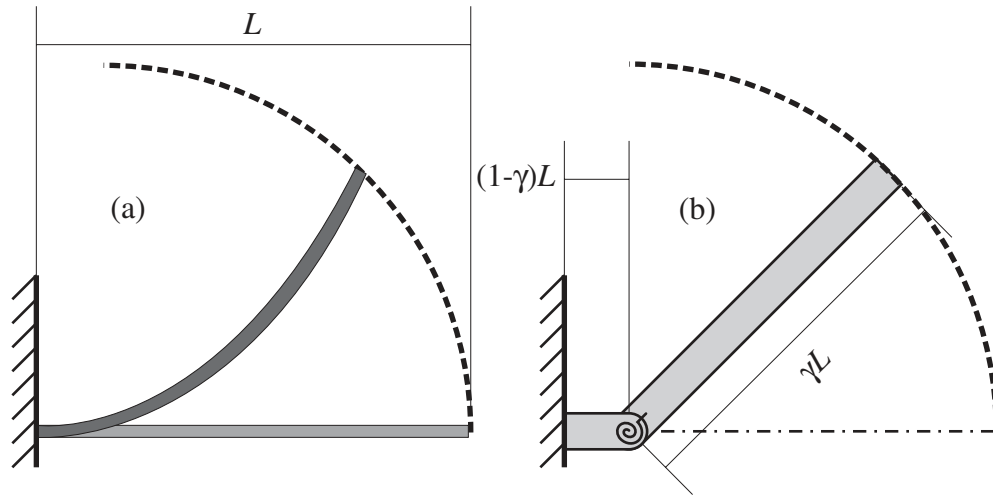


Figure 3-3 Large deflection path of (a) cantilever beam and (b) its Pseudo-Rigid-Body Model

model which treats the flexible beam as appropriately sized rigid links connected by pin joints and suitable torsional springs. The sizes of the links are calculated as γL and $(1-\gamma)L$, for the link and anchor respectively as shown in Fig. 3-3(b). The parameter γ , or *characteristic radius factor*—as well as the *stiffness coefficient*, K_{Θ} , a parameter used to calculate the spring constant of the torsional spring placed at the pseudo-rigid-body joint—depend on the beam geometry and loading conditions. There are additional PRBM for other loading conditions.

3.3 The Principle of Virtual Work

The Principle of Virtual Work is very useful for evaluating the motion and force-displacement characteristics of compliant mechanisms. This is an energy based method that greatly reduces the complexity of the resulting models in comparison to Newtonian methods. The principle of virtual work can be stated as:

If an ideal mechanical system is in equilibrium, the net virtual work of all the active forces is zero for every set of virtual displacements [33, 22].

Howell has proposed a system for utilizing the Principle of Virtual Work to evaluate the behavior of kinematic linkages with resistance elements (springs, etc.), specifying a step-by-step method [22].

- Step 1. Express the applied forces in vector form.
- Step 2. For each force identified in Step 1, express its placement (with respect to the origin) in vector form.
- Step 3. Choose the generalized (or Lagrangian) coordinate(s), q .
- Step 4. Determine the virtual displacements of the applied forces by differentiating the position vectors (from Step 2) with respect to the generalized coordinate(s).
- Step 5. Calculate the virtual work, δW , due to the applied forces by taking the dot product of the force vector(s) (Step 1) and the virtual displacement(s) (Step 4).
- Step 6. Express the applied moments in vector form.
- Step 7. Determine the angles the moments (from Step 6) act through, and express in vector form, $\vec{\Phi}$.
- Step 8. Find the virtual angular displacements, $\delta\vec{\Phi}$, by differentiating the angular displacements (Step 7) with respect to the generalized coordinate(s).
- Step 9. Calculate the virtual work, δW , due to moments by taking the dot product of the moment vector (Step 6) and the virtual angular displacement (Step 8).
- Step 10. Find sources of potential energy that have not been accounted for in previous steps.

Step 11. Find the virtual work from potential energy (Step 10) by differentiating the potential energy with respect to the generalized coordinate(s) and multiplying by $-\delta q$ (for each generalized coordinate)

Step 12. Calculate the total virtual work by summing the virtual work terms in Steps 5, 9, and 11.

Step 13. Apply the principle of virtual work: if in equilibrium then the virtual work is equal to zero ($\delta W=0$)

Step 14. Solve the equation(s) from step 13 for the unknown(s).

For all systems the number of generalized coordinates is equal to the number of degrees of freedom. Thus for multi-degree of freedom systems there will be multiple generalized coordinates. The virtual displacements, linear and angular, and the potential energy must be differentiated by each generalized coordinate (and the potential energy derivatives then multiplied by the corresponding $-\delta q$). Generalized coordinates are independent of each other, thus $\frac{\partial q_m}{\partial q_n} \equiv 0$ for all $m \neq n$ (and $\frac{\partial q_m}{\partial q_m} \equiv 1$). For multi-degree of freedom systems, the number of equations in Step 13 is equal to the number of generalized coordinates (and the degrees of freedom). Section 4.2.3 presents a thorough derivation of a three degree of freedom model of the SRFBM.

3.4 Finite Element Analysis (FEA)

Finite Element Analysis (FEA) is a useful tool in the analysis of compliant mechanisms. FEA divides the continuum of a model into discrete elements, each element having a set of equations governing its reaction to loading conditions. Elements can be one-, two-, or three-dimensional, and include numerous loading conditions such as linear and rotational displacement, force, moment, thermal, electrical, and pressure loads. Adjacent elements are connected to each other by coupled degrees of freedom. The equations for the elements are then gathered to form a stiffness (or flexibility) matrix. Loading conditions

are then applied and the system of linear equations can be solved for all degrees of freedom of the system. Due to the complexity and required analysis time, the principal role of FEA in the design of compliant mechanism is the analysis and verification of designs, after such designs have been synthesized by other techniques.

CHAPTER 4 *Development of the SRFBM*

4.1 Motivation for Fully Compliant Mechanisms

There is a need for efficient micromechanical switching systems, especially for low-power applications. Bistability can be used to improve the efficiency of a system by eliminating power consumption during steady state conditions. The ability to maintain state may also be used for non-volatile memory. Many of the bistable micromechanisms that have been proposed have depended either on residual stresses (for buckling) or are partially compliant. This research is primarily interested in identifying mechanism which are kinematically bistable. As such, no further consideration will be given to mechanisms that rely on residual stress.

Some of the limitations of traditional kinematic joints in MEMS have been presented by Clements [9], as well as some of the difficulties of designing compliant MEMS. Rigid-body and partially compliant mechanism are adversely affected by the limitations of micro-fabrication technology—specifically the linespacing, which is the minimum resolvable spacing between adjacent features as determined by the patterning process. Features spaced closer than this limit will merge. Current MEMS fabrication technology provides linespacing and linewidth (minimum resolvable isolated feature size) of roughly the same size. When pin joints are made, the hub and annulus must be separated on all sides by the minimum linespace, resulting in a total clearance of twice the specified linespacing. These clearances are quite large in comparison to the overall system dimensions. Furthermore,

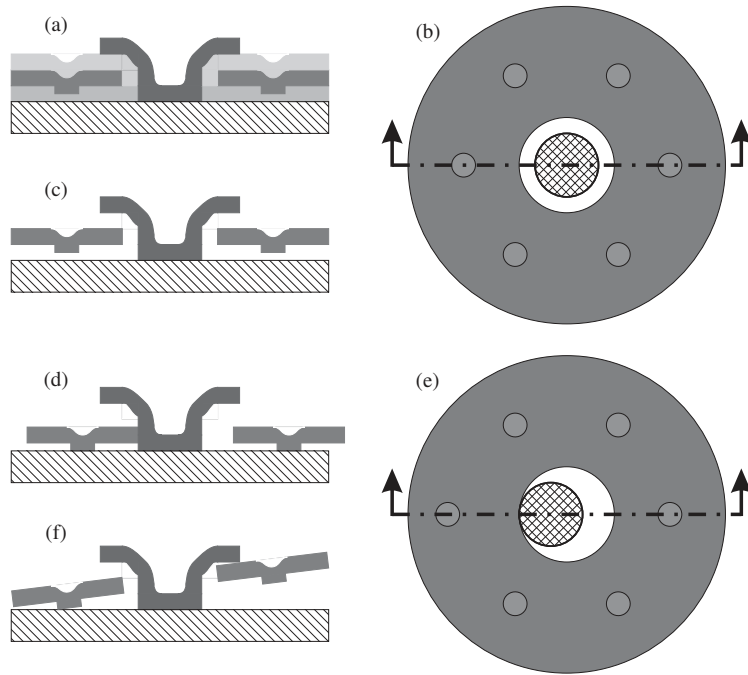


Figure 4-1 Examples of the effects of pin joint clearances: (a) unreleased pin joint, ideal behavior of released pin joint (b) top view and (c) cross section, (d) in- and out-of-plane misalignment (e) is a top view, (f) angular out-of-plane misalignment

out-of-plane clearances are introduced by the sacrificial layers, allowing linear and angular misalignment orthogonal to the plane of fabrication.

Figure 4-1 illustrates the effects of clearances on pin joints¹. The cross section of the unreleased pin joint is depicted in Fig. 4-1(a), showing the structural (darker shades of grey) and sacrificial (lighter shades) layers (substrate is hatched). Figure 4-1(b) and (c) represents the ideal behavior of the joint following the etching of sacrificial layers.

The unconstrained system is unlikely to be so well behaved. The removal of the sacrificial layers allows the unsupported pin joint to drop to the substrate, where it will rest on dimples (see Fig. 4-1(d)). This brings the rest of the structure much closer to the substrate, making it more susceptible to stiction. Lateral misalignment (also depicted in Fig. 4-2(d)

1. This example uses a representative, but fictitious process, with 2.0 μm thick conformal sacrificial and structural layers, 2.0 μm linewidth and linespacing rules and 0.5 μm deep dimples.



Figure 4-2 SEM of a Young mechanism experiencing the effects of pin joint clearances, as manifest by the out-of-plane deflection of the mechanism. The reaction force induced by the deflection of the slender beam (on the right) have resulted in the canting of the mechanism (see Fig. 4-1(f))

and (e)) leads to friction between the annulus and the hub. This friction, although small can be a significant source of failure due to wear [44, 43, 45].

Lateral clearance also affects the function of the mechanism of which the pin joints are constituent. This may reduce, or eliminate, the bistable behavior of partially compliant bistable mechanisms, as the displacement of the system is used to take up the clearance, and not stored as strain energy. A secondary effect is the loss of precision as the stable equilibrium positions will deviate from the ideal.

Angular misalignment (see Fig. 4-1(f)) also increases friction and leads to significant out-of-plane deflection of the mechanism. This may interfere with the ability of the mechanism to interface properly with other structures, such as actuators or contacts. Figure 4-2 shows the effects of pin joint clearance on a Young mechanism. The mechanism is in its second bistable position and reaction forces have induced out-of-plane deflections. The pin joints are canted, allowing the long flexible segment on the right to contact the substrate, and the rigid segments (left) are approximately 20 μm out-of-plane. Lateral misalignment, not visible in this image, also affects the function of the mechanism.

The effect of pin joint clearances must be dealt with during the design phase by increasing the displacement of the mechanism. This provides sufficient energy storage

after the clearances are overcome. The designer must also account for any effect on the path or alignment (in- and out-of-plane) of the mechanism with other structures.

In summary, pin joints are ill-suited for bistable micromechanisms and MEMS in general. The primary advantage of traditional joints in micromechanical systems is their familiarity to designers. The disadvantages include in- and out-of-plane misalignment, increased friction and wear, stiction (due to unsupported or canted members touching underlying layers), and deviation from intended mechanism path or function.

Although special processes can be developed to optimize pin joints, the ideal solution is to eliminate them entirely. The positive consequences of utilizing fully compliant mechanisms is particularly important for systems requiring precise location, mechanical energy storage, or which are subject to a large number of duty cycles.

An additional—and significant—benefit of fully compliant systems is greater fabrication freedom. Fully compliant systems require fewer mechanical layers, and thus fewer processing steps. In some cases complete systems may be fabricated from a single mechanical layer, which also facilitates integration with on-chip electronics.

Fully compliant alternatives can be developed for most applications not requiring complete rotation of any member. Designing fully compliant mechanisms should involve not only the mechanism design, but the system function, i.e., the designer needs to be allowed to eliminate any need for traditional joints. This requires additional design work, but results in increased reliability, improved functionality, and greater flexibility in design and fabrication.

There are drawbacks to fully compliant mechanisms, particularly the difficulty of design. The Pseudo-Rigid-Body Model can facilitate design, but it is necessary to carefully evaluate the motion of the mechanism and stresses in flexible segments. Fully compliant mechanisms also tend to require higher actuation forces—directly impacting the stated goal of power reduction. When revolute joints are functioning properly, their frictional resistance to the motion of a system is generally much less than that of flexural joints. With careful design, the actuation forces (or moments) can be reduced to acceptable levels. For bistable mechanisms the additional energy storage (compared to a partially compliant equivalent) is beneficial. Fully compliant systems are more conservative, as

energy is stored in strain energy and not lost in friction. This stored energy is available to be used by the system to return to the initial, undeflected state.

4.2 Design Criteria

The impetus for the SRFBM (or Self-Retracting Fully-compliant Bistable Micromechanism) was to develop a bistable MEMS suitable for low-power switching applications. Small displacement, linear motion is desired to integrate with linear thermal actuators [13] [12] and reduce the displacement component of the potential energy function². Furthermore, the force-deflection characteristics of the mechanism need to be compatible with the actuators.

Bistability will be evaluated in terms of potential energy, critical force, equilibrium separation, and stress. Equation (4.1) gives the relationship for the Bistability Ratio, *BSR*.

$$BSR = \frac{(PE_{USP} - PE_{SSP})}{PE_{USP}} \quad (4.1)$$

where PE_{USP} and PE_{SSP} are the potential energy at the unstable and second stable equilibrium positions respectively (with respect to the PE of the first stable equilibrium position).

The critical force refers to the minimum force necessary to transition from one stable state to another. This is equal to the maximum of the first derivative of the potential energy function.

As this mechanism may be used for switching applications where a contact force is needed, the mechanism will be configured with electrical contacts that stops the travel prior to the natural stable equilibrium (see Fig. 3-2 on page 35), ideally at the point corresponding to the critical force. The result is considerable contact force and a further reduction in the travel for the return actuation.

2. The potential energy function of a conservative system is equivalent to the work put in to the

system $PE = W = \int_0^{\dot{S}} \vec{F} \cdot d\vec{s}$. In principle, the system power requirements can be reduced by

reducing PE , which may be reduced by decreasing the displacement, \dot{S} .

The separation of the equilibrium positions—stable-to-stable and unstable-to-stable—is useful for evaluating the suitability of a configuration to the available actuator displacement, and to provide adequate electrical isolation. The locations of equilibria correspond to the zeroes of the first derivative of the potential energy function (with respect to the displacement), and are distinguished by the sign of the second derivative (positive indicative of stable equilibria).

The final criteria requires that the mechanism not fail due to the results of stress. In the case of brittle materials, e.g., polysilicon, high stresses can result in fracture. Ductile materials, such as the nickel alloys used in LIGA, will yield. A further constraint is that these devices are intended to experience a large number of duty cycles, making fatigue a concern. Initial designs were made for polysilicon with material properties of modulus of elasticity, E , of 165 GPa and fracture strength, S_f of 2 GPa.

4.2.1 Double-slider

As an initial concept, the double-slider was selected. The double-slider is one of the simplest mechanisms that can be configured for bistability [25]. The PRBM and equilibrium positions of a fully compliant double-slider are presented in Fig. 4-3. The coupler of this double-slider is a compliant member with motion that can be modeled as a slider. In this configuration it is subject to compression as shown in Fig. 4-3 (b).

A common practice in compliant mechanism design is the use of *flexural pivots*—small slender segments that perform the function of pin joints. Howell [23, 22] has presented a PRBM for small-length flexural pivots (SLFP) that allows the pseudo-rigid-body pivot to be placed at the mid-point of the SLFP. Conventional rigid-body replacement could then be used to develop a fully compliant mechanism. However, this approach would result in compressive loading of the SLFP, leading to increased stress and possible buckling in- and out-of-plane. It is important to consider the effects of compression on compliant mechanisms. Stress stiffening, a common phenomenon in compliant mechanisms, occurs when axial forces are applied to flexible segments subject to bending loads and moments.

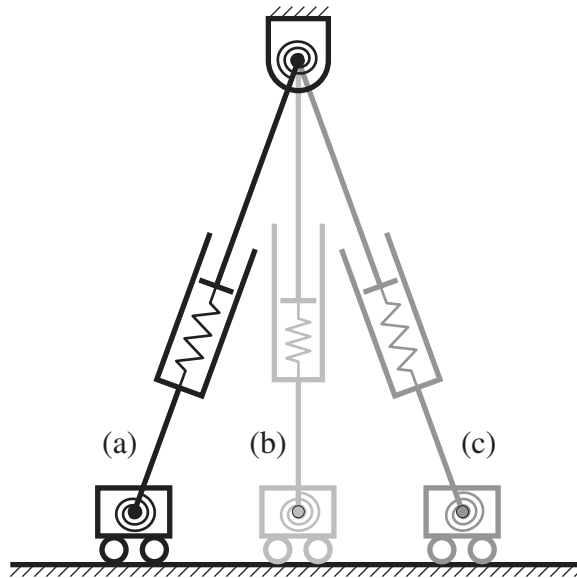


Figure 4-3 Fully compliant double-slider PRBM showing the equilibrium positions, torsional springs at pseudo-rigid joints, and linear spring-slider of the coupler.

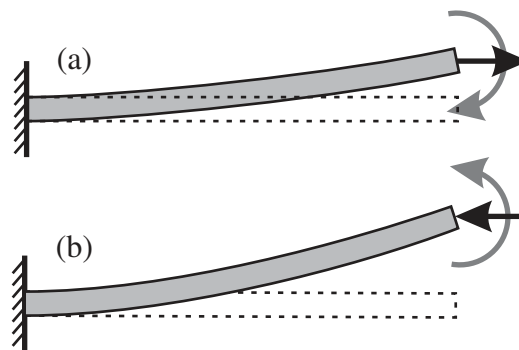


Figure 4-4 Illustration of the effects of axial loads on bending showing the induced moments due to (a) tension and (b) compression.

The result of a tensile load (see Fig. 4-4(a)) is the stiffening of the member because it induces a moment opposing the deflection of the member. Compression (see Fig. 4-4(b)) results in a moment that contributes to the bending deflection of the member.

In most cases, the effect of compression on compliance is much greater than that of tensile loads and can lead to buckling, which may degrade the function of the compliant

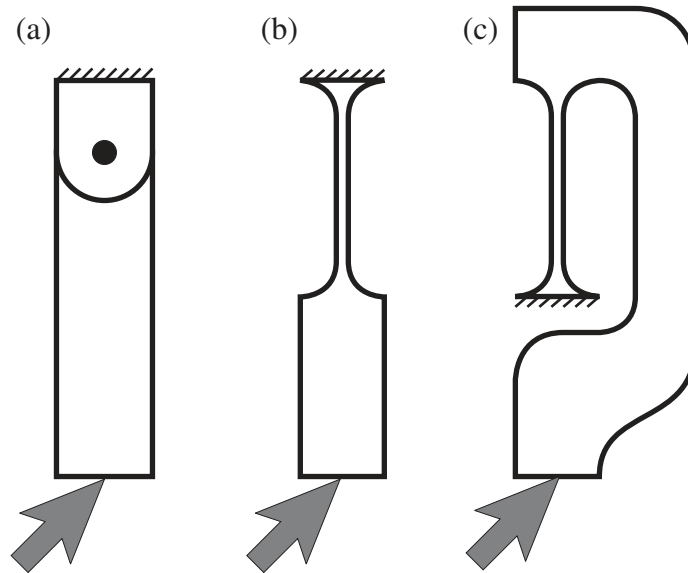


Figure 4-5 Rigid-body replacement: (a) Rigid-body link and pin joint, (b) conventional flexural pivot, (c) tensural pivot.

segments. With this in mind, special care should be taken when designing with compression.

A technique for dealing with compression in compliant mechanisms is to use *tensural pivots*. Tensural (tensile flexural) pivots are flexural pivots integrated into the overall design of a mechanism in such a way that they are subject primarily to bending and tension. Compression in the flexural pivots is completely avoided, improving the behavior of the mechanism. Segments adjacent to the tensural pivots are modified to carry the compressive loads to which they are subject. Figure 4-5(a) shows a rigid-body link subject to compressive bending loads. The result of rigid-body replacement using conventional small-length flexural pivots is shown in Fig. 4-5(b) and using a tensural pivot in Fig. 4-5(c). The compressive segments used in the SRFBM will be referred to as C-beams (due to both their “C” shape and compressive loading).

The result of integrating tensural pivots in the design of a fully compliant double-slider by rigid-body replacement is shown in Fig. 4-6(a) (the rigid offsets added to the double-slider for clarity do not affect the motion of the mechanism). The tensural pivots are situated to experience tension and bending as the slider moves to the right, compressing the C-

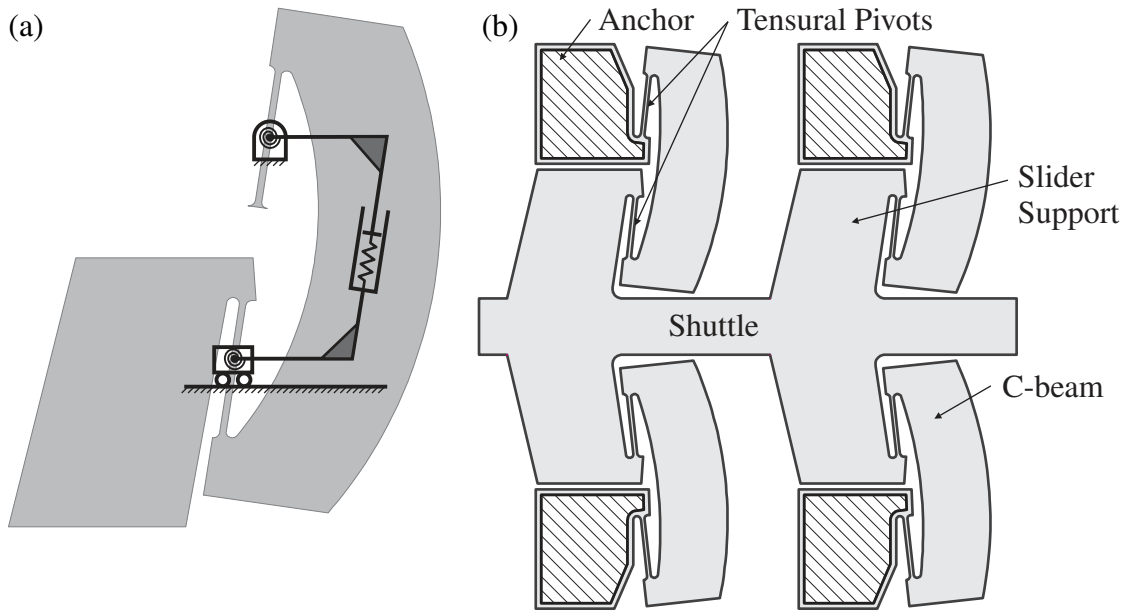


Figure 4-6 SRFBM geometry: (a) overlay of double-slider and geometry resulting from rigid-body replacement with tensural pivots and (b) system geometry with multiple legs for symmetry. Additional features are called-out and hatched areas are anchors. C-beam and slider supports are similar in thickness (in-plane).

beam and Slider Support. Fig. 4-6(b) shows how the legs are arranged for symmetry to provide correct sliding motion and redundancy. The basic geometry presented in Fig. 4-6(b) is used for all subsequent modeling and design.

4.2.2 SRFBM Pseudo-Rigid-Body Model

With the mechanism topology identified and the design modifications for tensural pivots implemented, the single degree of freedom Pseudo-Rigid-Body Model of Figure 4-3 was adapted to reflect the preliminary geometry. (The complete PRBM is presented in Fig. 4-7). This model was used to identify suitable bistable configurations of the double-slider concept.

The force-deflection relationship and potential energy can be obtained for the Pseudo-Rigid-Body Model by applying the principle of virtual work [22, 33]. The resulting force-deflection relationship is given in Equation (4.2), with r_4 as the independent variable or input.

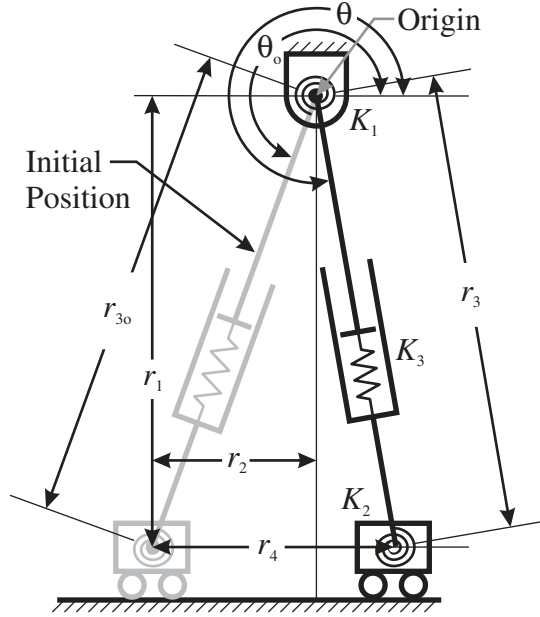


Figure 4-7 Coordinate system for SRFBM PRBM. r_4 is the displacement of the slider and is considered the input for the analysis.

$$F = (K_1 + K_2)(\theta - \theta_o) \frac{d\theta}{dr_4} + K_3(r_3 - r_{3o}) \frac{dr_3}{dr_4} \quad (4.2)$$

r_1 and r_2 are constants, r_3 is the (variable) length of the spring-slider and is calculated as

$$r_3 = \sqrt{r_1^2 + (r_4 - r_2)^2} \quad (4.3)$$

The coupler angle, θ , is given by the following equations:

for $(r_4 - r_2) < 0$,

$$\theta = \pi + \text{atan}\left(\frac{-r_1}{(r_4 - r_2)}\right) \quad (4.4)$$

for $(r_4 - r_2) > 0$,

$$\theta = 2\pi + \text{atan}\left(\frac{-r_1}{(r_4 - r_2)}\right) \quad (4.5)$$

and for $(r_4 - r_2) = 0$

$$\theta = \frac{3\pi}{2} \quad (4.6)$$

The kinematic coefficients, $\frac{d\theta}{dr_4}$ and $\frac{dr_3}{dr_4}$ are given by

$$\frac{d\theta}{dr_4} = \frac{r_1}{(r_4 - r_2)^2 + r_1^2} \quad (4.7)$$

$$\frac{dr_3}{dr_4} = \frac{r_4 - r_2}{\sqrt{r_1^2 + (r_4 - r_2)^2}} \quad (4.8)$$

The spring constants, K_1 and K_2 are obtained from the PRBM torsional spring formula for fixed-pinned segments:

$$K = \gamma K_{\Theta} \frac{EI_{TP}}{L_{TP}} \quad (4.9)$$

where γ is the characteristic radius factor (which specifies the size of the pseudo-rigid-body link, see Section 3.2.5). At this point in modeling, the approximate value of $\gamma \approx 0.75$ is used. K_{Θ} is the pseudo-rigid-body model stiffness coefficient, which will be approximated as 2.65. These values are used for design purposes, as tensural pivots have not been fully characterized. These do, however, recognize that the tensural pivots are loaded in a fixed-fixed manner. As such, values for γ and K_{Θ} are based on the model for fixed-fixed segments which in turn uses values for initially curved beams (because of the induced moments experienced by fixed-fixed segments can be equated to an initial curvature). Fur-

ther work needs to be done to characterize the PRBM of tensural pivots. E is the modulus of elasticity of the material (for polysilicon $E \approx 165$ GPa). I_{TP} is the area moment of inertia of the tensural pivots, $I_{TP} = (w^3t)/12$, where w is the in-plane width and t is the material thickness. L_{TP} is the length of the tensural pivots. For this design the tensural pivots have the same dimensions, so $K_1=K_2$.

K_3 is the spring constant of the C-beam. Because this segment is subject to small deflections, Castigliano's theorem can be used to analytically evaluate the spring constant of this curved member. The effect of axial elongation of the tensural pivots is lumped into this spring constant.

$$K_3 = \frac{1}{2(C_1 + C_2 + C_3 + C_4)} \quad (4.10)$$

where the factors C_1 , C_2 , C_3 , and C_4 are the components of the spring constant due to axial compression of the C-beam, axial elongation of the tensural pivots³, bending of the C-beam, and transverse shear of the C-beam, respectively. These factors are calculated as:

$$C_1 = \frac{R}{EA_C} \left(\frac{\phi_o}{2} + \frac{1}{4} \sin 2\phi_o \right) \quad (4.11)$$

$$C_2 = \frac{L_{TP}}{EA_{TP}} \quad (4.12)$$

$$C_3 = \frac{R^3}{EI_C} \left(\phi_o \left(\frac{1}{2} + \cos^2 \phi_o \right) + \frac{1}{4} \sin 2\phi_o - 2 \cos \phi_o \sin \phi_o \right) \quad (4.13)$$

$$C_4 = \frac{6R}{5GA_C} \left(\frac{\phi_o}{2} - \frac{1}{4} \sin 2\phi_o \right) \quad (4.14)$$

3. The contribution of C_2 and C_3 are of roughly the same order of magnitude and are an order of magnitude greater than the contributions of C_1 and C_4 . This means that the principal energy storage modes of the C-beam are axial elongation of the tensural pivots and bending of the C-beam.

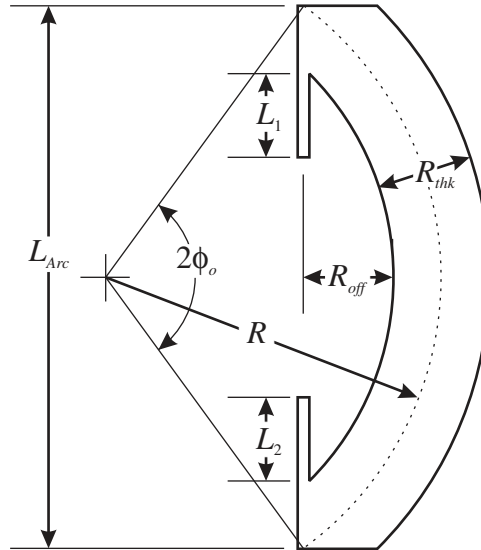


Figure 4-8 Diagram of the C-beam.

Some of these parameters are illustrated in Fig. 4-8 and explained as follows:

- R : Radius of curvature of the neutral axis

$$R = R_C - R_{thk} \left(\frac{R_C}{R_{thk}} - \frac{2}{\ln\left(\frac{R_C/R_{thk} + 1}{R_C/R_{thk} - 1}\right)} \right) \quad (4.15)$$

- R_C is the average radius of curvature of the beam $((R_o - R_i)/2)$
- R_{thk} is the width (in-plane) of the C-beam.
- ϕ_o : One half of the arc angle of the C-beam $(\phi_o = \sin^{-1}(L_{Arc}/2R))$
- A_C : Cross section area of the C-beam $(A_C = R_{thk} \cdot \text{Layer Thickness})$
- I_C : Moment area of inertia of the C-beam $(I_C = R_{thk}^3 \cdot \text{Layer Thickness}/12)$

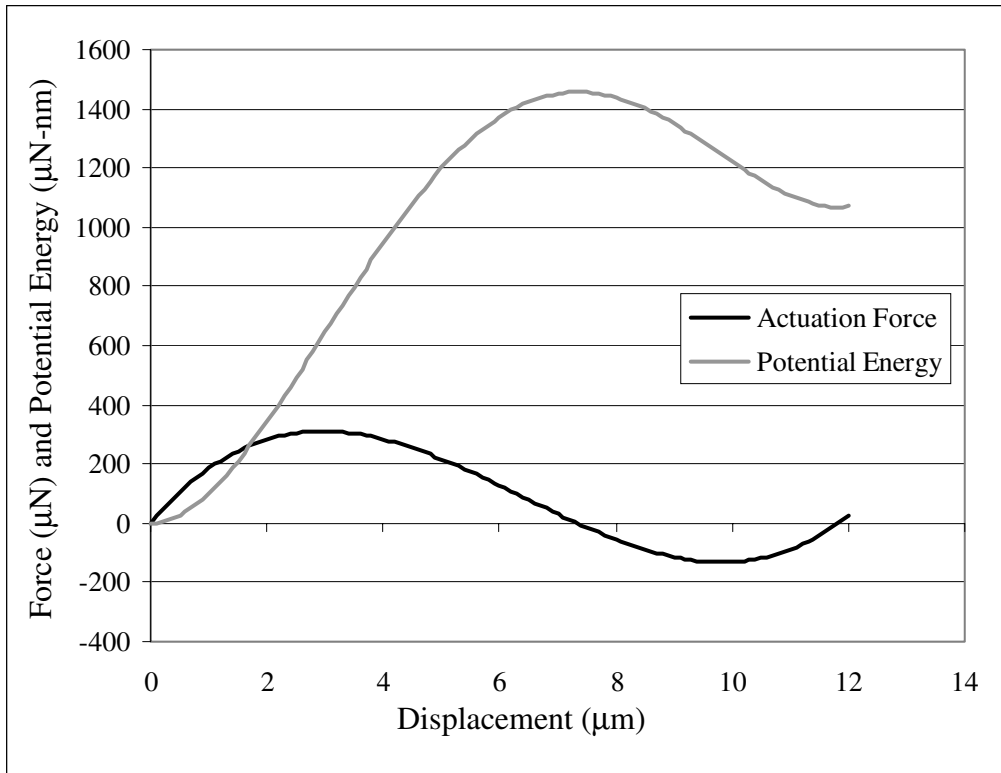


Figure 4-9 Single degree of freedom PRBM results including actuation force and potential energy. Notice that the zeroes of the actuation force curve correspond to the system equilibria.

- G is the modulus of rigidity for the material (67 GPa for polysilicon).

The potential energy of the system is the sum of the stored energy of the system.

$$PE = \frac{1}{2}(K_1 + K_2)(\theta_3 - \theta_{3o})^2 + \frac{1}{2}K_3(r_3 - r_{3o})^2 \quad (4.16)$$

Using this model, the various geometric parameters (link lengths, widths of flexible segments, etc.) can be varied to find preliminary configurations based on the design criteria. Sample results from this model are presented in Fig. 4-9. The parameters for this model are found in Table 4-1.

This configuration appears to be bistable, with the unstable and stable equilibria occurring at displacements of 7.4 μm and 11.8 μm , respectively with corresponding potential

Table 4-1 Sample single degree of freedom PRBM parameters

r_1 μm	r_2 μm	K_1 $\mu\text{N}\cdot\mu\text{m}/\text{rad}$	K_2 $\mu\text{N}\cdot\mu\text{m}/\text{rad}$	K_3 $\mu\text{N}/\mu\text{m}$
49.9	5.7	25506	25506	17049

energy of 1455 $\mu\text{N}\cdot\text{nm}$ and 1067 $\mu\text{N}\cdot\text{nm}$. Thus the Bistability Ratio of this system is 0.27 (see Equation (4.1)). Critical forces are approximately 311 μN (forward) and 130 μN return. Approximate stress may be calculated for the PRBM by treating the moment produced by the torsional spring as the bending moment and combining this with the axial stress (see Equation (4.17)). The maximum predicted stress for this configuration is 2290 MPa. This will need to be accurately evaluated and reduced in later design steps to avoid failure of the mechanism.

$$\sigma = \frac{Tw_{TP}}{2I_{TP}} - \frac{F_s}{A_{TP}} = \frac{K_1(\theta - \theta_o)w_{TP}}{2I_{TP}} - \frac{K_3(r_3 - r_{3o})}{A_{TP}} \quad (4.17)$$

4.2.3 Three degree of freedom six-link double-slider PRBM

Tensural pivots, as implemented in the SRFBM, are fixed-guided segments, subject to tension and bending loads. A more detailed model can be developed by treating them as fixed-guided segments within the Pseudo-Rigid-Body Model. The resulting model, presented in Fig. 4-10, is now a six-link double-slider. The tensural pivots are modeled with Pseudo-Rigid-Body segments of length γL , pinned at both ends, and appropriate torsional springs. This mechanism has three degrees of freedom, as may be shown by Gruebler's Equation

$$DOF = 3(n - 1) - 2f_1 = 3(6 - 1) - 2(6) = 3 \quad (4.18)$$

as there are n represents the number of links (6 links for this model) and f_1 represents the number of kinematic pairs (4 pin joints and 2 sliders).

The link lengths, and spring constants for this model may be calculated using the parameters that are used to generate the geometry of the SRFBM (see APPENDIX C) as follows:

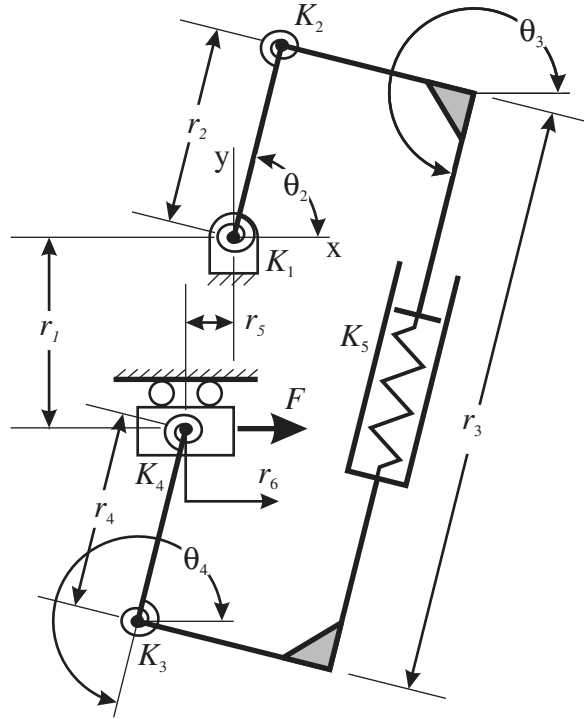


Figure 4-10 Pseudo-Rigid-Body Model for the three degree of freedom analysis of SRFBM

$$\theta_{1o} = \pi + \text{atan}\left(\frac{y_{off}}{x_{off}}\right) \quad (4.19)$$

$$r_1 = y_{off} - \left(\left(\frac{1-\gamma}{2}\right)(L_1 + L_2)\right) \sin\theta_{1o} \quad (4.20)$$

$$r_2 = \gamma L_1 \quad (4.21)$$

$$r_4 = \gamma L_2 \quad (4.22)$$

$$r_5 = x_{off} - \left(\left(\frac{1-\gamma}{2}\right)(L_1 + L_2)\right) \cos\theta_{1o} \quad (4.23)$$

$$r_{3o} = r_2 + r_4 + \sqrt{r_1^2 + r_5^2} \quad (4.24)$$

$$\theta_{2o} = \theta_{1o} - \pi \quad (4.25)$$

$$\theta_{3o} = \theta_{4o} = \theta_{1o} \quad (4.26)$$

$$K_1 = K_2 = 2\gamma K_{\Theta} \frac{EI_{TP}}{L_1} \quad (4.27)$$

$$K_3 = K_4 = 2\gamma K_{\Theta} \left(\frac{EI_{TP}}{L_2} \right) \quad (4.28)$$

K_5 is the same as K_3 used in the one degree of freedom PRBM as calculated with Equation (4.10).

The next step in the evaluation of the SRFBM modeled in this manner is to define a vector loop for the PRBM.

$$\vec{z}_2 + \vec{z}_3 = \vec{z}_1 + \vec{z}_4 + \vec{z}_5 + \vec{z}_6 \quad (4.29)$$

The origin is defined as shown in Fig. 4-10. These vectors may also be represented by the Cartesian vectors:

$$\vec{X} \Rightarrow r_2 \cos \theta_2 + r_3 \cos \theta_3 = -r_5 + r_6 + r_4 \cos \theta_4 \quad (4.30)$$

$$\vec{Y} \Rightarrow r_2 \sin \theta_2 + r_3 \sin \theta_3 = -r_1 + r_4 \sin \theta_4 \quad (4.31)$$

The steps of the Principle of Virtual Work are then followed. (The results of Steps 4, 7 and 8 are found in Table 4-2):

Step 1. Express the applied forces in vector form.

$$\vec{F} \quad (4.32)$$

Step 2. For each force identified in Step 1, express its placement (with respect to the origin) in vector form.

$$\dot{\vec{z}} = (r_6 - r_5)\dot{i} - r_1\dot{j} \quad (4.33)$$

Step 3. Choose the generalized (or Lagrangian) coordinate(s), q .

$$\begin{aligned} q_1 &= \theta_2 \\ q_2 &= \theta_3 \\ q_3 &= \theta_4 \end{aligned} \quad (4.34)$$

Step 4. Determine the virtual displacements of the applied forces by differentiating the position vectors (from Step 2) with respect to the generalized coordinate(s) (see Table 4-2).

Table 4-2 Partial derivatives of coordinates

Coordinate	$d\Theta_1 = \sum \frac{\partial \phi}{\partial q_1} dq_1$	$d\Theta_2 = \sum \frac{\partial \phi}{\partial q_2} dq_2$	$d\Theta_3 = \sum \frac{\partial \phi}{\partial q_3} dq_3$
$\vec{z} = (r_6 - r_5)\dot{i} - r_1\dot{j}$	$\frac{\partial \vec{z}}{\partial \theta_2} \delta \theta_2 = \frac{dr_6}{d\theta_2} \delta \theta_2$	$\frac{\partial \vec{z}}{\partial \theta_3} \delta \theta_3 = \frac{dr_6}{d\theta_3} \delta \theta_3$	$\frac{\partial \vec{z}}{\partial \theta_4} \delta \theta_4 = \frac{dr_6}{d\theta_4} \delta \theta_4$
$\phi_1 = (\theta_2 - \theta_{2o})$	$\frac{\partial \phi_1}{\partial \theta_2} \delta \theta_2 = \delta \theta_2$	$\frac{\partial \phi_1}{\partial \theta_3} \delta \theta_3 = 0$	$\frac{\partial \phi_1}{\partial \theta_4} \delta \theta_4 = 0$
$\phi_2 = [(\theta_2 - \theta_{2o}) - (\theta_3 - \theta_{3o})]$	$\frac{\partial \phi_2}{\partial \theta_2} \delta \theta_2 = \delta \theta_2$	$\frac{\partial \phi_2}{\partial \theta_3} \delta \theta_3 = -\delta \theta_3$	$\frac{\partial \phi_2}{\partial \theta_4} \delta \theta_4 = 0$
$\phi_3 = [(\theta_4 - \theta_{4o}) - (\theta_3 - \theta_{3o})]$	$\frac{\partial \phi_3}{\partial \theta_2} \delta \theta_2 = 0$	$\frac{\partial \phi_3}{\partial \theta_3} \delta \theta_3 = -\delta \theta_3$	$\frac{\partial \phi_3}{\partial \theta_4} \delta \theta_4 = \delta \theta_4$
$\phi_4 = (\theta_4 - \theta_{4o})$	$\frac{\partial \phi_4}{\partial \theta_2} \delta \theta_2 = 0$	$\frac{\partial \phi_4}{\partial \theta_3} \delta \theta_3 = 0$	$\frac{\partial \phi_4}{\partial \theta_4} \delta \theta_4 = \delta \theta_4$
$\phi_5 = (r_3 - r_{3o})$	$\frac{\partial \phi_5}{\partial \theta_2} \delta \theta_2 = \frac{dr_3}{d\theta_2} \delta \theta_2$	$\frac{\partial \phi_5}{\partial \theta_3} \delta \theta_3 = \frac{dr_3}{d\theta_3} \delta \theta_3$	$\frac{\partial \phi_5}{\partial \theta_4} \delta \theta_4 = \frac{dr_3}{d\theta_4} \delta \theta_4$

The partials performed at this point (and in Steps 8 and 11) result in the need to derive certain kinematic coefficients. The kinematic coefficients are based on the partials (with respect to the generalized coordinates) of the vector loop equations for the mechanism:

$$\frac{\partial \dot{X}}{\partial q} \Rightarrow -r_2 \sin \theta_2 \frac{\partial \theta_2}{\partial q} + \cos \theta_3 \frac{\partial r_3}{\partial q} - r_3 \sin \theta_3 \frac{\partial \theta_3}{\partial q} = \frac{\partial r_6}{\partial q} - r_4 \sin \theta_4 \frac{\partial \theta_4}{\partial q} \quad (4.35)$$

$$\frac{\partial \dot{Y}}{\partial q} \Rightarrow r_2 \cos \theta_2 \frac{\partial \theta_2}{\partial q} + \sin \theta_3 \frac{\partial r_3}{\partial q} + r_3 \cos \theta_3 \frac{\partial \theta_3}{\partial q} = r_4 \cos \theta_4 \frac{\partial \theta_4}{\partial q} \quad (4.36)$$

By definition the generalized coordinates are independent of each other, resulting in the following relations: $\frac{\partial q_m}{\partial q_n} \equiv 0$ for $m \neq n$ and $\frac{\partial q_m}{\partial q_n} \equiv 1$ for $m=n$. The resulting kinematic coefficients are found in Table 4-3.

Table 4-3 Kinematic coefficients

$\frac{\partial r_3}{\partial q}$	$\frac{\partial r_6}{\partial q}$
$\frac{\partial r_3}{\partial \theta_2} = -\frac{r_2 \cos \theta_2}{\sin \theta_3}$	$\frac{\partial r_6}{\partial \theta_2} = -\frac{r_2 \cos(\theta_2 - \theta_3)}{\sin \theta_3}$
$\frac{\partial r_3}{\partial \theta_3} = \frac{r_3 \cos \theta_3}{\sin \theta_3}$	$\frac{\partial r_6}{\partial \theta_3} = \frac{r_3}{\sin \theta_3}$
$\frac{\partial r_3}{\partial \theta_4} = \frac{r_4 \cos \theta_4}{\sin \theta_3}$	$\frac{\partial r_6}{\partial \theta_4} = \frac{r_4 \cos(\theta_3 - \theta_4)}{\sin \theta_3}$

Step 5. Calculate the virtual work, δW , due to the applied forces by taking the dot product of the force vector (Step 1) and the virtual displacement (Step 4).

$$\delta W = \vec{F} \cdot d\vec{z} = F \left(\frac{dr_6}{d\theta_2} \delta \theta_2 + \frac{dr_6}{d\theta_3} \delta \theta_3 + \frac{dr_6}{d\theta_4} \delta \theta_4 \right) \quad (4.37)$$

Step 6. Express the applied moments in vector form.

$$\begin{aligned}
\vec{T}_1 &= -K_1(\theta_2 - \theta_{2o})\vec{k} \\
\vec{T}_2 &= -K_2[(\theta_2 - \theta_{2o}) - (\theta_3 - \theta_{3o})]\vec{k} \\
\vec{T}_3 &= -K_3[(\theta_4 - \theta_{4o}) - (\theta_3 - \theta_{3o})]\vec{k} \\
\vec{T}_4 &= K_4(\theta_4 - \theta_{4o})\vec{k}
\end{aligned} \tag{4.38}$$

Step 7. Determine the angles the moments (from Step 6) act through, and express in vector form. See Table 4-2.

Step 8. Find the virtual angular displacements, $\delta\vec{\Theta}$, by differentiating the angular displacements (Step 7) with respect to the generalized coordinate(s). See Table 4-2.

Step 9. Calculate the virtual work, δW , due to moments by taking the dot product of the moment vector (Step 6) and the virtual angular displacement (Step 8).

Step 10. Find sources of potential energy that have not been accounted for in previous steps.

The C-Beam stores energy in a manner that can be modeled as a linear spring connecting the two links of the second slider (r_3). The spring force is calculated as

$$F_S = -K_5(r_3 - r_{3o}) \tag{4.39}$$

and the potential energy as

$$PE_S = \frac{1}{2}K_5(r_3 - r_{3o})^2 \tag{4.40}$$

Step 11. Find the virtual work from potential energy (Step 10) by differentiating the potential energy with respect to the generalized coordinate(s) and multiplying by $-\delta q$ (for each generalized coordinate)

$$\delta W_S = \sum \frac{\partial PE_S}{\partial q}(-\delta q) = F_S \left(\frac{dr_3}{d\theta_2} \delta\theta_2 + \frac{dr_3}{d\theta_3} \delta\theta_3 + \frac{dr_3}{d\theta_4} \delta\theta_4 \right) \quad (4.41)$$

Step 12. Calculate the total virtual work by summing the virtual work terms in Steps 5, 9, and 11.

$$\delta W = \vec{F} \cdot d\vec{z} + T_1 d\phi_1 + T_2 d\phi_2 + T_3 d\phi_3 + T_4 d\phi_4 + F_S d\phi_5 = 0 \quad (4.42)$$

By substituting in the partial derivatives from Table 4-2 and the kinematic coefficients from Table 4-3 and then grouping the equations with respect to the δq 's, the following set of equations can be obtained:

$$\delta W = \left(F \frac{\partial r_6}{\partial \theta_2} + T_1 + T_2 + F_S \frac{\partial r_3}{\partial \theta_2} \right) \delta\theta_2 = 0 \quad (4.43)$$

$$\delta W = \left(F \frac{dr_6}{d\theta_3} - T_2 - T_3 + F_S \frac{dr_3}{d\theta_3} \right) \delta\theta_3 = 0 \quad (4.44)$$

$$\delta W = \left(F \frac{dr_6}{d\theta_4} + T_3 + T_4 + F_S \frac{dr_3}{d\theta_4} \right) \delta\theta_4 = 0 \quad (4.45)$$

Step 13. Apply the principle of virtual work: if in equilibrium then the virtual work is equal to zero ($\delta W=0$)

The result of this step is three additional equations that can be used to solve for the motion of the system:

$$F \frac{\partial r_6}{\partial \theta_2} + T_1 + T_2 + F_S \frac{\partial r_3}{\partial \theta_2} = 0 \quad (4.46)$$

$$F \frac{dr_6}{d\theta_3} - T_2 - T_3 + F_S \frac{dr_3}{d\theta_3} = 0 \quad (4.47)$$

$$F \frac{dr_6}{d\theta_4} + T_3 + T_4 + F_s \frac{dr_3}{d\theta_4} = 0 \quad (4.48)$$

Step 14. Solve the equation(s) from step 13 for the unknown(s).

This step now involves the kinematic equations that would normally be used to evaluate a single degree of freedom mechanism. If the assumption is made that the input to the system is the displacement of the shuttle ($r_6 \dot{i}$), then the following equations may be developed:

for $(r_6 - r_5) < 0$

$$\theta_1 = \pi + \text{atan}\left(\frac{-r_1}{r_6 - r_5}\right) \quad (4.49)$$

for $(r_6 - r_5) > 0$

$$\theta_1 = 2\pi + \text{atan}\left(\frac{-r_1}{r_6 - r_5}\right) \quad (4.50)$$

and for $(r_6 - r_5) = 0$

$$\theta_1 = \frac{3\pi}{2} \quad (4.51)$$

The variable length of the “ground link” which is dependent on the shuttle displacement is calculated as

$$r_g = \sqrt{r_1^2 + (r_6 - r_5)^2} \quad (4.52)$$

and the following variables are defined for convenience:

$$\delta = (r_g^2 + r_2^2 - 2r_g r_2 \cos \theta_2') \quad (4.53)$$

$$\beta = \arccos\left(\frac{r_g^2 + \delta^2 - r_2^2}{2r_g\delta}\right) \quad (4.54)$$

$$\psi = \arccos\left(\frac{r_3^2 + \delta^2 - r_4^2}{2r_3\delta}\right) \quad (4.55)$$

$$\lambda = \arccos\left(\frac{r_4^2 + \delta^2 - r_3^2}{2r_4\delta}\right) \quad (4.56)$$

where relative angle (with respect to the variable θ_1) θ_2' is calculated by

$$\theta_2' = 2(\pi - \theta_1) + \theta_2 \quad (4.57)$$

The other angles can be calculated from these equations as follows:

$$\theta_3 = \theta_1 - (\beta + \psi) \quad (4.58)$$

$$\theta_4 = \theta_1 - \pi + (\lambda - \beta) \quad (4.59)$$

This complete set of equations can then be solved for the force-deflection behavior of the SRFBM. The solution to these equations is non-trivial, requiring non-linear techniques. The solutions for one SRFBM configuration are compared to other models in Fig. 4-14 and Fig. 4-15.

4.2.4 SRFBM FEA

To further refine the design of the SRFBM, two finite element models were developed: a simple beam element model and a detailed plane element model. All modeling was done in ANSYS, version 5.7. Displacement loading, broken up into a number of load steps, is used to deal with the non-linear behavior of a bistable mechanism. This allows the solver to deal with smaller displacements. Solutions based on force loading are difficult, due to the non-linear force-deflection behavior.⁴ At some point past the unstable equilibrium the displacement loading is removed, allowing the model to transition to the nearest equilib-

rium position. (Note: On occasion ANSYS converged on the unstable equilibrium position.) To investigate the behavior of the return stroke, the load steps were applied to return the system to the initial position.

4.2.4.1 Beam element model

The geometry for the beam element model was further simplified from that used in the PRBM. These simplifications included modeling the C-beam as a square bracket and ignoring some of the offsets that are present with the actual geometry. This model served two purposes: rapid verification of the preliminary results of the single degree of freedom PRBM, and investigation of thermal self-retraction. The batch file for this model is found in APPENDIX B.

During the development of the SRFBM, it was postulated that heating the tensural pivots would result in self-retraction. This phenomenon may be explained in two ways.

1. The heating of the tensural pivots results in axial elongation, relieving some of the compression in the C-beams. This alters the profile of the potential energy curve, resulting in the current position (the second stable position) no longer being in equilibrium. As the tensural pivots expand, the profile is eventually altered such that the mechanism is no longer bistable and it returns to the undeflected initial position
2. The expansion exerts an axial force, which due to the deflected shape of the tensural pivots, forms a couple (or moment) that acts to rotate the C-beams, retracting the mechanism.

The model predicted that heating the tensural pivots by 450°C was sufficient to retract the mechanism (fabricated in polysilicon). It should be noted that while heating is applied, the mechanism actually retracts beyond the initial position (negative displacement).

-
4. During the travel of a bistable mechanism, the actuation force increases until the critical force is achieved. This is prior to the unstable equilibrium. Past the position of the critical force, the actuation force decreases until at the unstable equilibrium it is zero. Beyond the unstable equilibrium the mechanism has negative actuation force, i.e., it is in transition to the second stable position. The same behavior is encountered, with a negative critical force (which must be overcome for the return stroke) up to the second stable equilibrium.

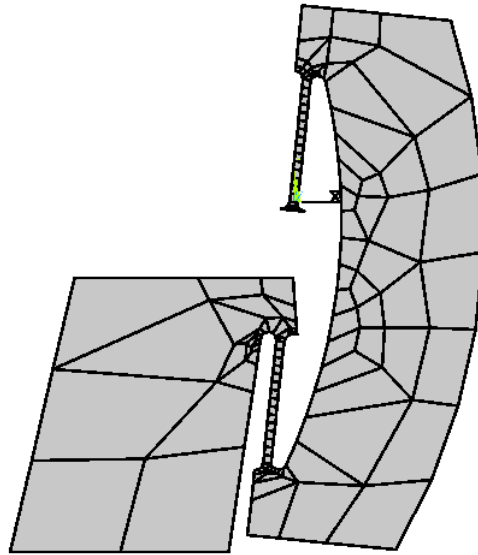


Figure 4-11 Geometry of plane element model.

4.2.4.2 Plane element model

The simplified models that have been used up to this point have greatly increased the speed of design, narrowing the scope of subsequent analysis. However, before finalizing the design it is important to evaluate the impact of the final geometry (as necessitated by the tensural pivots and fabrication design rules) on the behavior of the mechanism. Due to the planar nature of fabrication, plane elements can be used to perform this detailed analysis. This allows faster—but equally accurate—analysis than using three dimensional elements. At this point the geometry (as presented in Fig. 4-6) was parameterized and used to develop batch files for both ANSYS and AutoCAD (where the final layout would take place). In this way changes made to the analysis will be directly reflected in the production layout. These batch files and a description of their parameters can be found in APPENDIX C and APPENDIX D. Figure 4-11 shows the geometry used for this analysis meshed with 8 node plane elements.

A major difference between this and previous models is the inclusion of the slider support (see Fig. 4-6) which does significantly affect the behavior of the mechanism by reducing the effective spring constant of the C-beam.

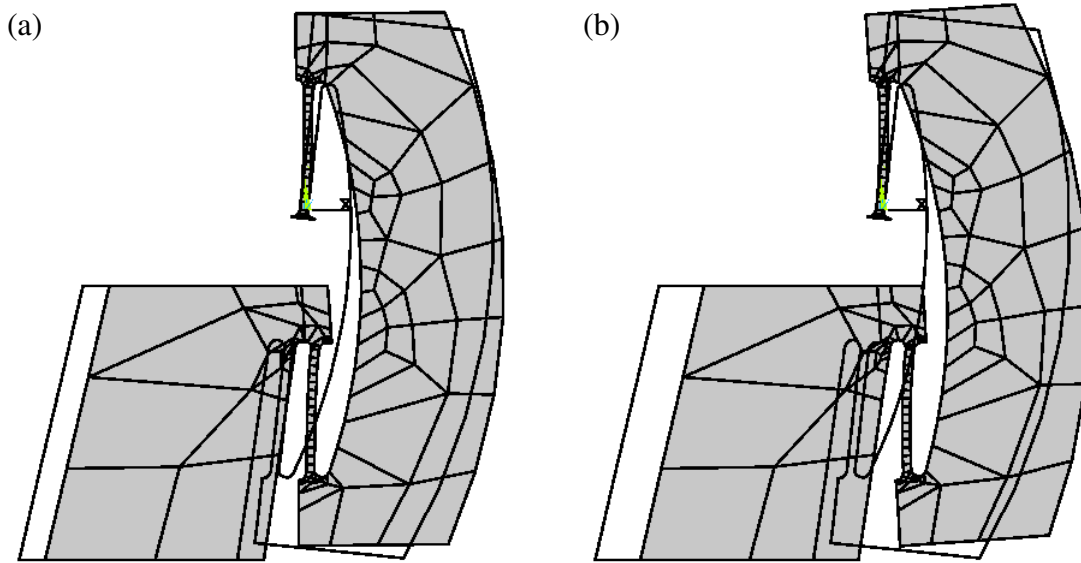


Figure 4-12 (a) Displaced SRFBM leg near the unstable equilibrium position (6.65 μm displacement) and (b) the second stable position (11.36 μm displacement).

The function of the SRFBM may be observed in Figures 4-11 and 4-12. As the shuttle slides to the right, the tensural pivots allow rotation of the C-beam. As it rotates, it is compressed, storing elastic strain energy (results from this analysis indicate that the total compression of the C-beam is approximately one-eighth μm over a span of approximately 100 μm). The tensural pivots also store strain energy. After the unstable equilibrium position (see Fig. 4-12), strain energy is released by the relaxation of the C-beam, resulting in a minimum energy, which is the second stable position (Fig. 4-12(b)).

Figure 4-13 summarizes the output of the FEA, including the strain energy⁵ ($\mu\text{N}\cdot\text{nm}$), Von Mises equivalent stress (MPa), and actuation force (μN) over the range of motion of the mechanism.

The calculated critical forces can also be observed in Fig. 4-13. The forward actuation requiring approximately 120 μN per leg and the return requiring approximately 33 μN per leg. Thus for a four-leg SRFBM with leg geometry corresponding to this model, a maxi-

5. For this conservative system the potential energy may be equated to the elastic strain energy.

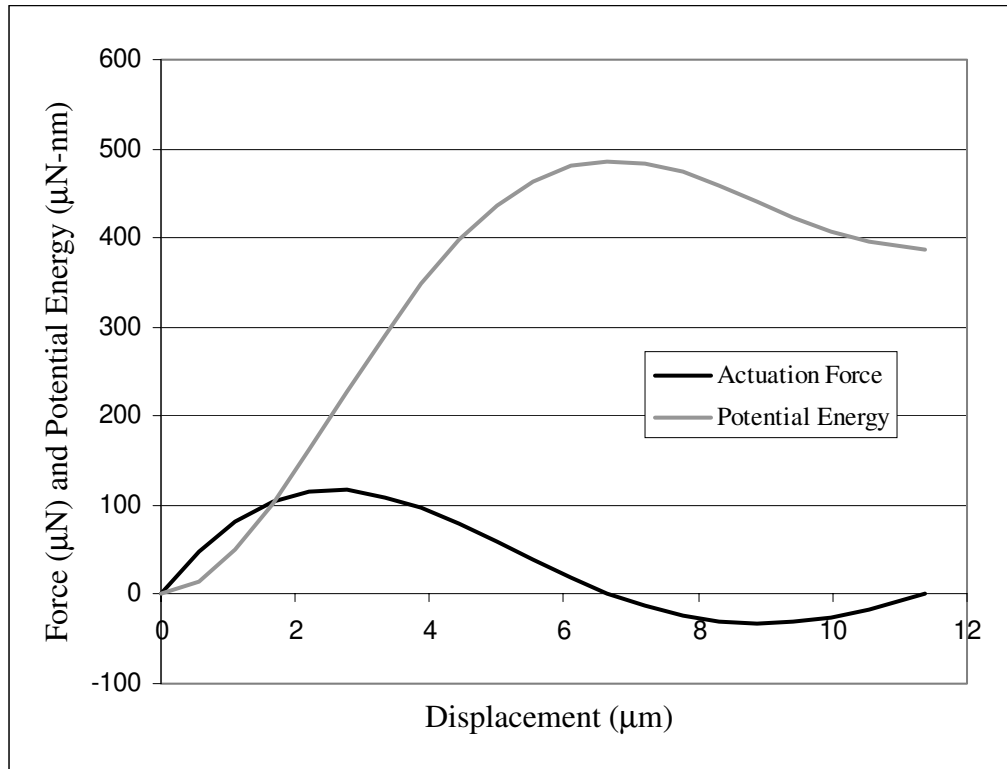


Figure 4-13 Results of finite element analysis including force-deflection and potential (strain) energy.

imum forward actuation force of approximately 480 μN is needed and a maximum contact (and return force) of 132 μN is available.

Based on the FEA analysis four configurations were chosen. They were all quite similar, as it was also desirable to minimize the overall size of the SRFBM. In particular the tensural pivots were kept relatively short, thus keeping them stiff out-of-plane to avoid stiction problems. Table 4-4 summarizes the results for the analyses for these mechanisms. The displacement to the unstable equilibrium and the contact position for all mechanisms is approximately 6.65 μm and 8.85 μm respectively⁶.

6. Model displacements are based on the x-offset of the tensural pivots, which is related to r_2 in the PRBM. All of these models used the same x-offset (3.9 μm), resulting in the same displacement load steps. Final layout varied slightly from this value.

Table 4-4 Summary of SRFBM selected for fabrication.

	SRFBM 1	SRFBM 2	SRFBM 3	SRFBM 4
Second Stable Position (μm)	11.28	11.23	11.24	11.37
Critical Force (μN)	125.06	123.28	121.41	116.57
Contact Force (μN)	37.54	36.06	34.98	33.21
Bistability Ratio (Equation (4.1))	0.22	0.21	0.21	0.20
Max. Stress (MPa)	1,753	1,737	1,721	1,678
Tensural Pivot Length (μm)	30	30	30	31

4.3 Comparison of SRFBM Models

Comparing the two Pseudo-Rigid-Body Models and the FEA plane element model⁷ reveals an interesting discrepancy. The location of equilibrium positions correlate well between the models. The magnitudes of the force-deflection and potential energy curves predicted by the two PRBM are approximately double those calculated by the FEA model (see Fig. 4-14). This may be a result of the unmodeled slider support or incompletely modeled tensural pivots. At this point the tensural pivots are treated like conventional PRBM fixed-fixed members, ignoring the effects of stress stiffening. Despite these differences, the Pseudo-Rigid-Body Models are still well suited to the initial phase of SRFBM design.

The PRBM were adjusted in an effort to improve agreement with FEA results. The first improvement was account for the compliance of the Slider Support. This segment is approximately twice as stiff as the C-beam, leading to a combined series spring constant of approximately two-thirds that of the C-beam alone (see Equation (4.10)). The actual ratio used for modeling is 0.65. The next modification involved selecting new values for γ and K_{Θ} to improve model agreement. This is essentially a curve fitting exercise, but the

7. The beam element model will not be included in this comparison as it was developed to quickly verify the concept of the mechanism and thermal self-retraction.

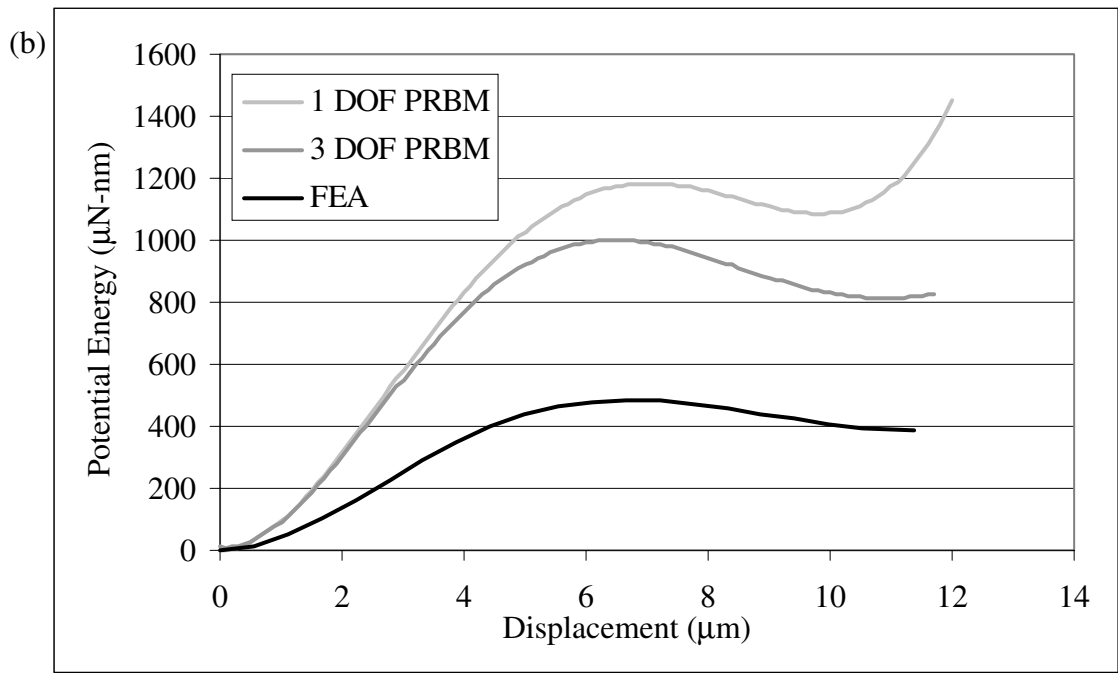
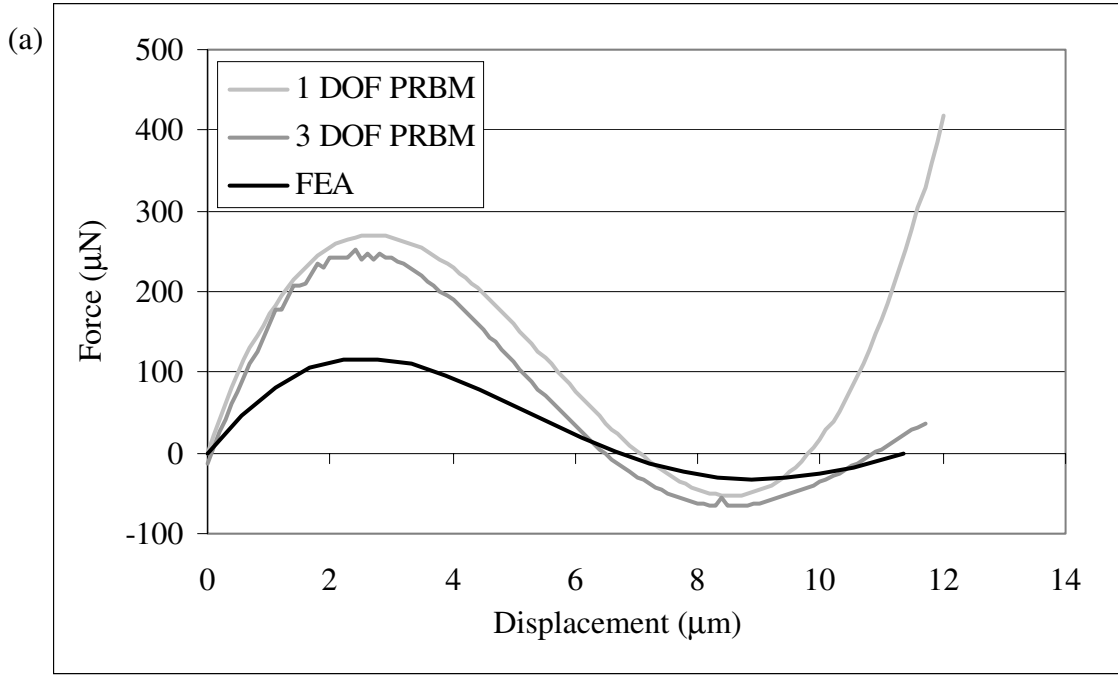


Figure 4-14 Comparison of SRFBM models: (a) force-deflection and (b) potential energy.

resulting values of $\gamma = 0.65$ and $K_{\Theta} = 1.45$ appear to be consistent with the loading experience by the tensural pivots considering that they fall somewhere in between the extremes of small length flexural pivots and vertically loaded cantilever beams, (and lean towards the SLFPs). (For small-length flexural pivots $\gamma = 0.5$ and $K_{\Theta} = 1.0$. For vertically loaded cantilever beams $\gamma = 0.85$ and $K_{\Theta} = 2.65$.)

The results of these modifications on the PRBMs can be seen in Figures 4-15 and show much better agreement. However, further work should be performed to fully characterize the PRBM of tensural pivots with the new approximate values of γ and K_{Θ} facilitating this effort. In any case, these improvements appear to make the Pseudo-Rigid-Body Models even more useful for initial design steps which can then be further refined with finite element analysis to determine the final geometry.

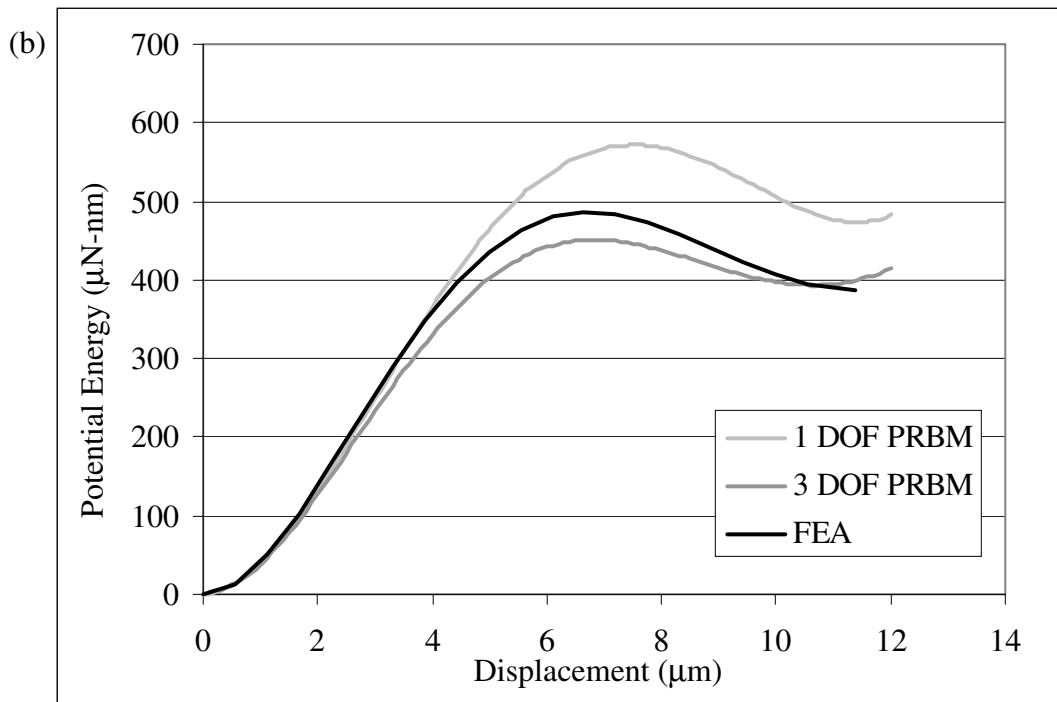
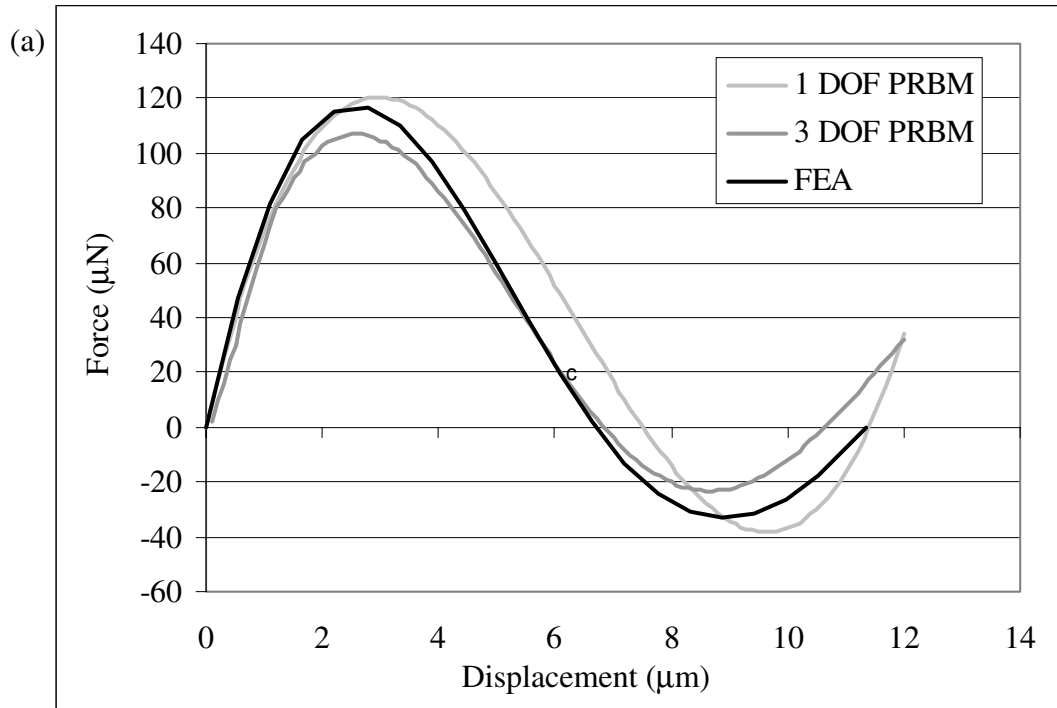


Figure 4-15 Comparison of SRFBM models: (a) force-deflection and (b) potential energy (using modified PRBM parameters $\gamma = 0.65$, $K_{\Theta} = 1.45$).

CHAPTER 5 *Fabrication and Testing*

This chapter discusses the fabrication and testing of SRFBM as fabricated in the Cronos MUMPs process. Actuators, electrical contacts, and other supporting structures are designed or selected to interface with the SRFBM configurations that were selected and refined using the models developed in Chapter 4. Testing evaluates the functionality and reliability of fabricated systems, including on-chip actuation, thermal self-retraction, critical forces, and high-cycle fatigue.

5.1 System Layout and Fabrication

The SRFBM was first fabricated in polysilicon in a form similar to Fig. 5-1, using the Cronos MUMPs process. This process provides three structural layers, two of which are mechanical, and a metal layer for electrical lines, contacts, and bond pads. The mechanical polysilicon layers, Poly1 and Poly2 are 2.0 μm and 1.5 μm thick, respectively, with 2.0 μm and 0.75 μm thick first and second sacrificial oxides. Dimples are nominally 0.75 μm deep. The SRFBMs uses the laminate of the two structural layers for a total thickness of 3.5 μm (nominal). Laminate layers are patterned with a single mask (Poly2 mask step). Minimum linewidth and linespacing rules are 2.0 μm , although 3.0 μm is recommended. Cronos does not guarantee that laminate structures of less than 3.0 μm width will survive the ultrasonic bath that is part of the lift-off process to pattern the metal layer. Due to the nature of the SRFBM, the tensural pivots should be as thin as possible. Despite rec-

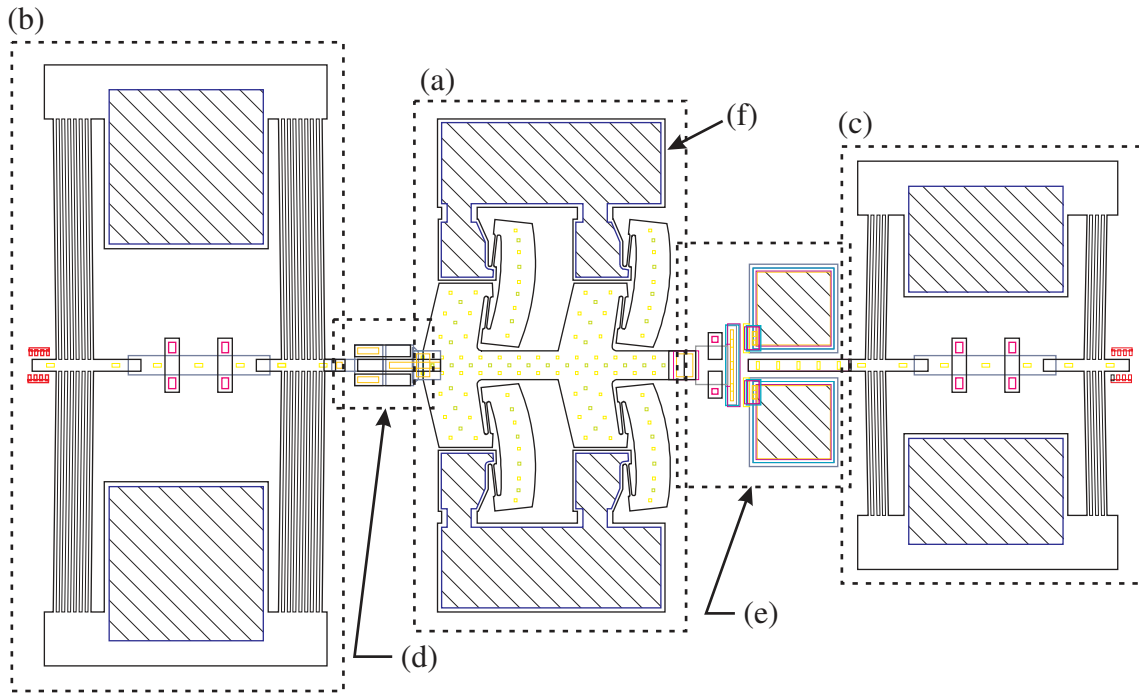


Figure 5-1 Layout of SRFBM system with (a) SRFBM, (b) forward and (c) return thermal actuators, (d) backlash reducing coupler, (e) electrical contacts, and (f) bond pads for self retraction.

ommendation for 3.0 μm linewidth, the decision was made based on past experience to use 2.0 μm wide tensural pivots.

Several variations were fabricated to evaluate minor differences in geometry and actuation and contact force. Displacements for all SRFBM systems are approximately 6.65 μm to the unstable equilibrium and 8.5 μm to the externally constrained stable equilibrium at the contact pads. Major differences between different configurations are (1) the clearance between the C-beam and the shuttle support, (2) C-beam width, and (3) length of the tensural pivots. Changes to the clearance affect the stiffness of the C-beam, which must be modified to balance the effect (usually larger clearance requires increased width to maintain stiffness). Tensural pivots 30 μm in length were used for three of the four SRFBM. The fourth used 31 μm long tensural pivots, resulting in reduced stress. Longer tensural pivots were not used at this time.

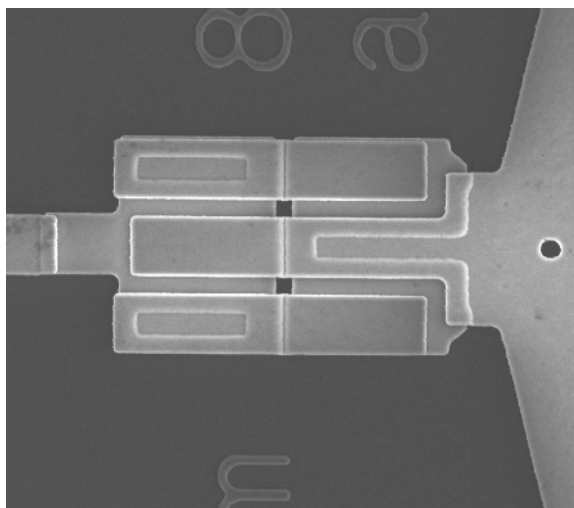


Figure 5-2 SEM of the interdigitated backlash reducing coupler. The forward actuator is out of the image at left.

Supporting structures include Thermal In-plane Microactuators (TIMs), electrical contacts, backlash reducing coupler, and bond pads for thermal self-retraction (see Fig. 5-1(a-f)). The overall dimensions of the SRFBM are less than 300 μm long (along the axis of travel) and 300 μm wide. Overall system dimensions, including all actuators and contacts are 1140 μm long by 625 μm wide.

5.1.1 On-chip actuation

Figure 5-1 presents the layout of a representative SRFBM system with actuators and supporting structures. Direct actuation via Thermal In-plane Microactuators (TIM) [13, 12] was possible due to the small linear displacement of the SRFBM. Eight-, fourteen-, and fifteen-leg TIMs with leg lengths of 200 μm , 200 μm , and 250 μm , respectively, were selected for forward actuation. The thermal actuators which best match the force-deflection characteristics of the SRFBM can then be identified. Eight-leg 150 μm TIMs were used for all return actuators.

The coupling between the forward actuator and the SRFBM is designed to reduce backlash and misalignment (see Figure 5-2). This improves the reliability of the system, especially in fabrication processes like MUMPs where the aspect ratio (layer thickness/minimum feature size) is close to unity (3.5/2 or 1.75). Processes with higher aspect ratios

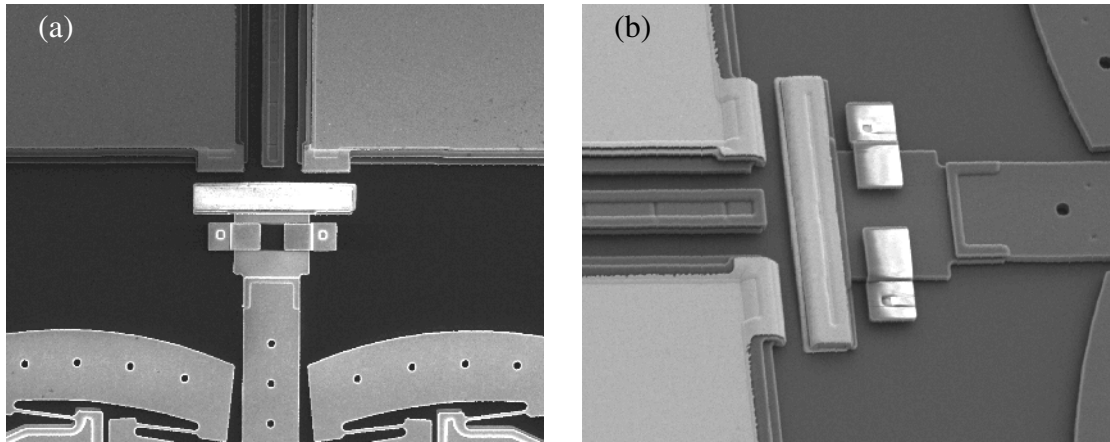


Figure 5-3 SEMs of SRFBM electrical contacts. Contacts use the interactions of the conformal layers to achieve some degree of gold sidewall coverage, useful for lateral contacts.

are more resistant to out-of-plane misalignment and can be much stiffer out-of-plane. This is one of the few system features that takes advantage of the separate mechanical layers. It would, however, be possible to fabricate the entire system from a single mechanical layer, greatly reducing fabrication complexity and cost.

5.1.2 Electrical contacts

Electrical contacts are integrated with the SRFBM to evaluate electrical switching (see Fig. 5-3). These contacts rely on the conformal nature of the polysilicon layers to provide gold-on-polysilicon (or perhaps gold-on-gold) contacts. Gomm [17] has documented additional testing of the SRFBM and electrical contact design.

5.1.3 Release

The dice returned to BYU from Cronos from the MUMPs 41 fabrication run were damaged. The damage appears to be a result of the lift-off process and is limited to Poly1/Poly2 Laminate structures. However, it was not limited only to structures with linewidths less than $3.0\ \mu\text{m}$. Damaged features include TIM legs and tensural pivots. Despite this damage, enough mechanisms remained intact on four dice to allow testing. Figure 5-4 illustrates the damage caused during the lift-off process.

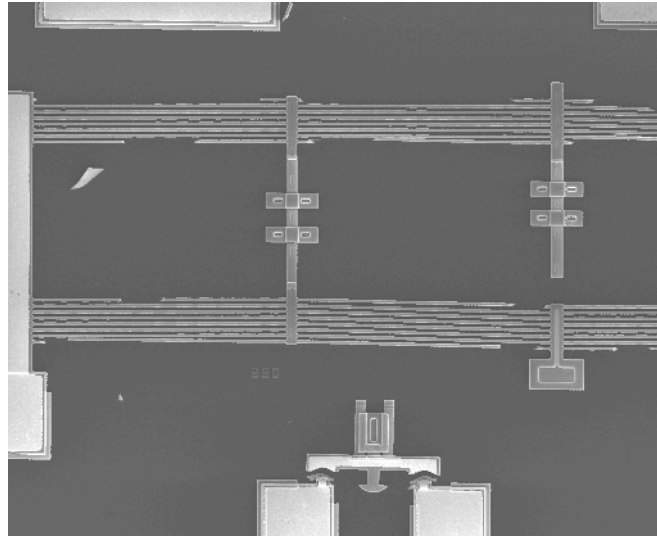


Figure 5-4 SEM of TIMs damaged by lift-off process.

All devices were released using an octadecyltrichlorosilane (ODTS) SAMS release [40] to reduce stiction. Release and testing was done in the BYU Integrated Microelectronics Laboratory (IML).

5.2 Testing

Following release, the SRFBM were tested for functionality and reliability. Functionality testing included bistability, on-chip actuation, critical force, and electrical switching characteristics. Reliability included fatigue testing and evaluation of the robustness of the the devices.

Figure 5-5 shows an SEM of a complete SRFBM system, as fabricated in MUMPs. To the right of the SRFBM is the forward actuator (an eight-leg 200 μm TIM is pictured). On the left are the electrical contacts and external return actuator.

5.2.1 Functionality

All correctly fabricated and released SRFBM were observed to be bistable. SEMs of an SRFBM in both stable equilibrium positions are found in Fig. 5-6. Minor out-of-plane deflections of the C-beams have been observed during transition. This deflection is mani-

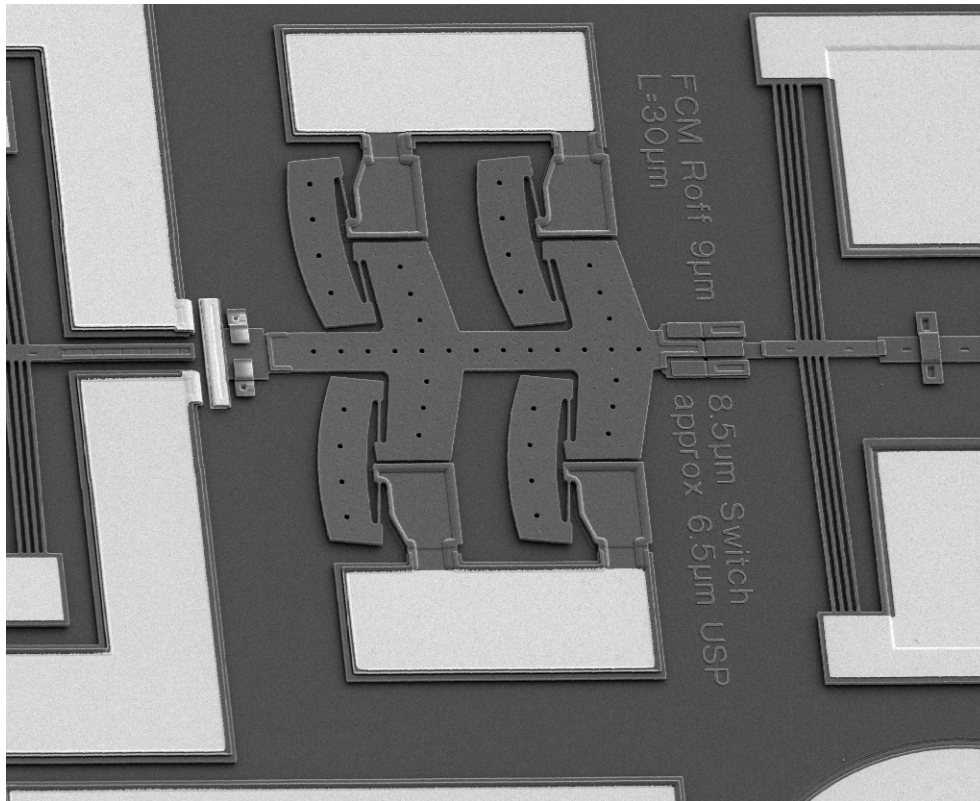


Figure 5-5 SEM of SRFBM system

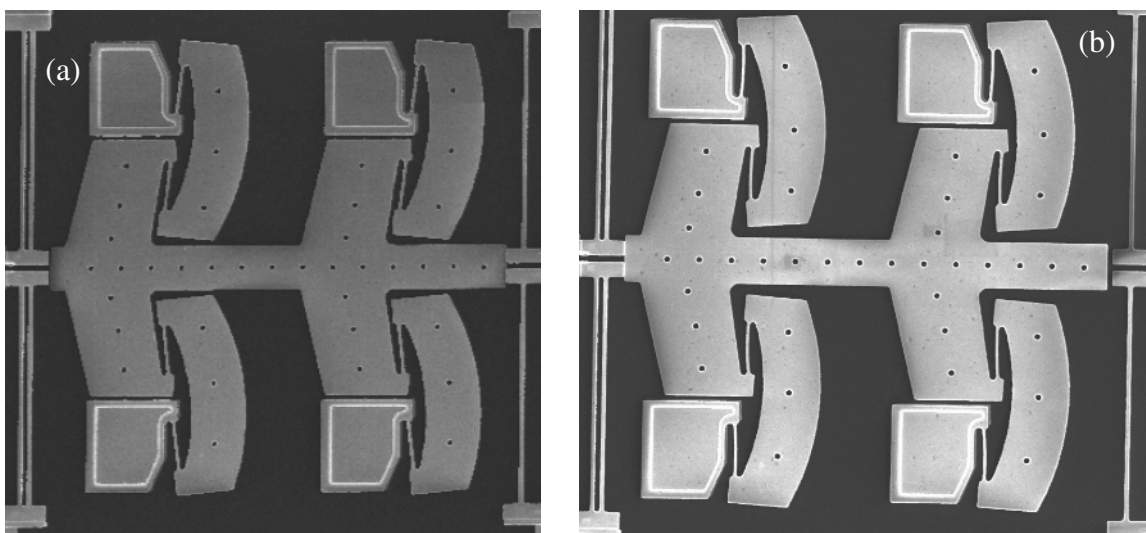


Figure 5-6 SEMs of SRFBM with force testers in (a) undeflected and (b) second stable positions. Compare deflected shape to Figure 4-12(b).

fest by a change in the intensity of light reflected off the C-beam as it changes angle with respect to the microscope objective. Although this behavior does not appear to affect on-chip actuation it will be discussed later as part of the discussion on force tester measurements.

On-chip actuation is a critical step in evaluating the bistability of the SRFBM. Electrical testing was done with an HP 4145A System Analyzer. Using this equipment actuation and electrical contact characteristics were measured by applying a current and measuring the voltage. In this manner actuator power consumption and electrical contact resistance can be evaluated. In the event that actuators suffered from stiction, manual probing was used to free up the system. In the case of damaged or insufficiently powerful actuators, some SRFBM were manually probed to verify bistability.

Testing revealed that only the larger—fourteen- and fifteen-leg—actuators are sufficiently powerful to switch the SRFBM. The fourteen-leg 200 μm TIMs were the most efficient, requiring approximately 150 mW (30 mA at 5 V) to switch the SRFBM. The fifteen-leg 250 μm TIMs needed approximately 400 mW (45mA at 9 V). Return actuation using the external eight-leg 150 μm TIMs is quite efficient, requiring approximately 70 mW (20 mA at 3.5 V). Self-retraction, which worked as predicted by the models, further reduces power needs—requiring approximately 28 mW (7 mA at 4 V). Despite the advantages, thermal damage may result from this type of actuation. Careful consideration should be given to the desired lifetime of the system if thermal self-retraction is to be used.

Force testers were used to further evaluate the nature of the SRFBM, in terms of bistability and critical force (see Fig. 5-7). The force testers consist of fully compliant parallel mechanisms (also referred to as folded beams) supported by a frame. The frame is constrained to slide in-line with the SRFBM. As the frame is displaced by microprobes, the beams apply a load to the SRFBM that can be calculated from the deflection of the beams (relative to the frame). Bistability can thus be verified and the motion of the system observed in detail. The measured critical forces are presented in Table 5-1. The measured forward critical forces correlate well with those predicted by the finite element model. Measured return forces are significantly higher than the model results. The discrepancy may be due to friction. SEM images (tilted approximately 74°) of SRFBM and force testers show some out-of-plane deflection of the shuttle (see Fig. 5-8). The shuttle is prob-

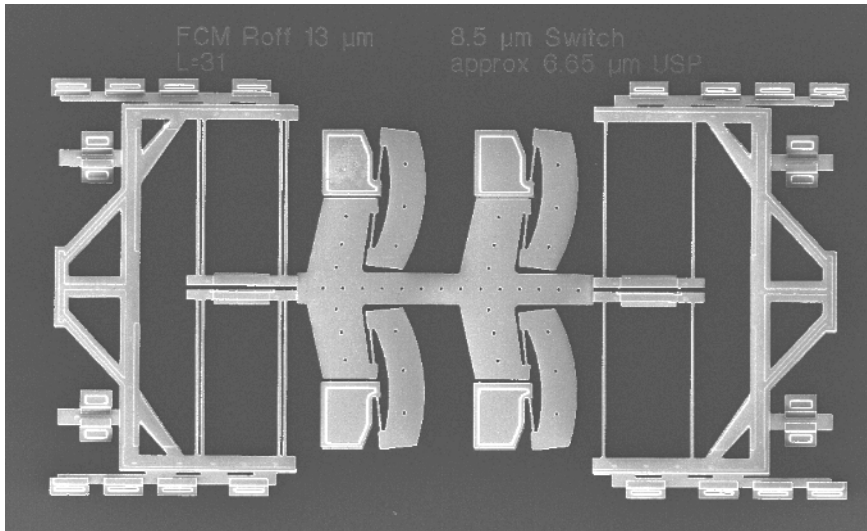


Figure 5-7 SEM of SRFBM and force testers.

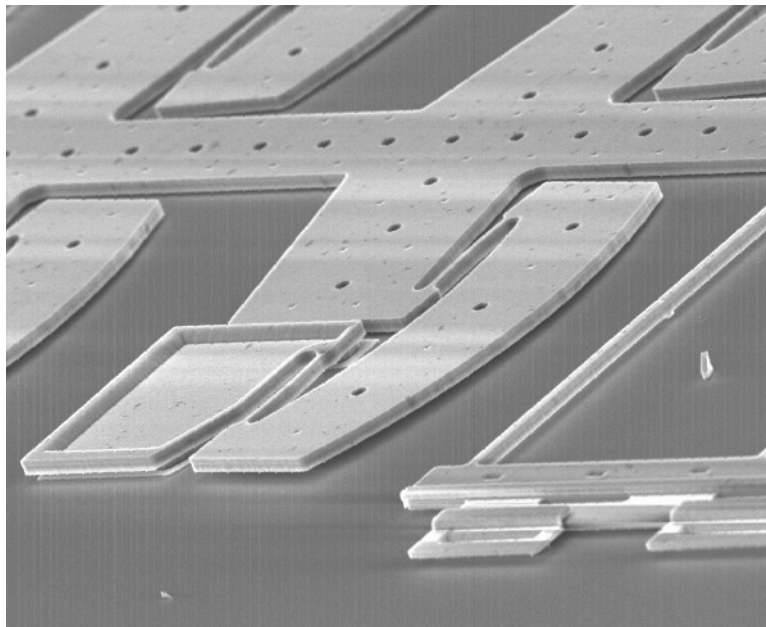


Figure 5-8 SEM of an SRFBM and force testers in the second stable equilibrium position. The shuttle and slider support can be observed to have deflected down to where they may be in contact with the substrate, resting on dimples.

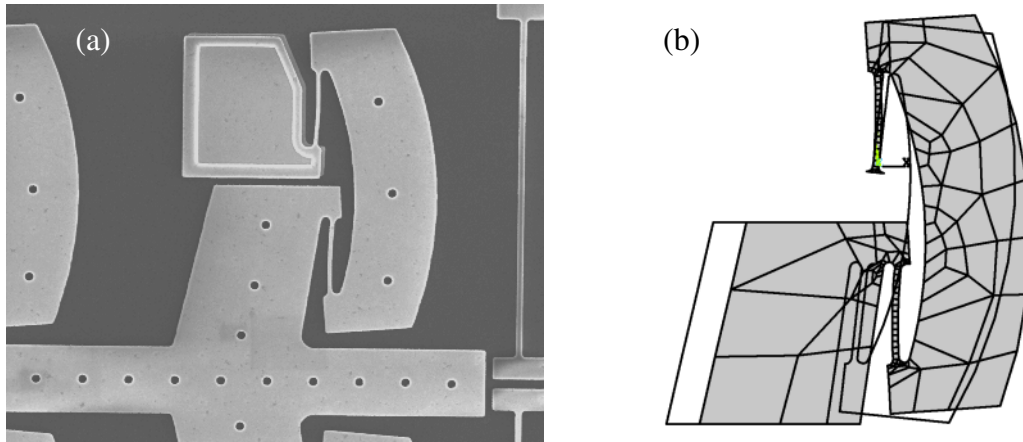


Figure 5-9 Comparison of (a) SRFBM to (b) FEA model

Table 5-1 Force tester results

Forces μN (Forward/ Return)	SRFBM 1	SRFBM 2	SRFBM 3	SRFBM 4
Predicted	512/152	492/144	484/140	464/132
Measured	557/317	396/254	594/341	396/240

ably resting on its dimples on the substrate. This may result in frictional forces that have not been accounted for in modeling. This did not result in any stiction effects that noticeably impaired on-chip actuation, as several SRFBM were left in the externally constrained second stable position at the electrical contacts for more than one month, and were still capable of on-chip return actuation. Higher aspect ratios would reduce this behavior but are not available in the MUMPs process. Other than this discrepancy, the FEA results agreed well with the observed behavior of the SRFBM. Figure 5-9 compares the deformed shape of one leg of a SRFBM with the FEA results.

Contact resistance was evaluated by passing a current, stepped from 1 to 15 mA, through the contacts and measuring the required driving voltages. The contact is then calculated (Ohm's law $R=V/I$). The first set of measurements for a set of contacts are often quite small, as low as 10 Ω . During testing the contacts seemed to suffer some damage at

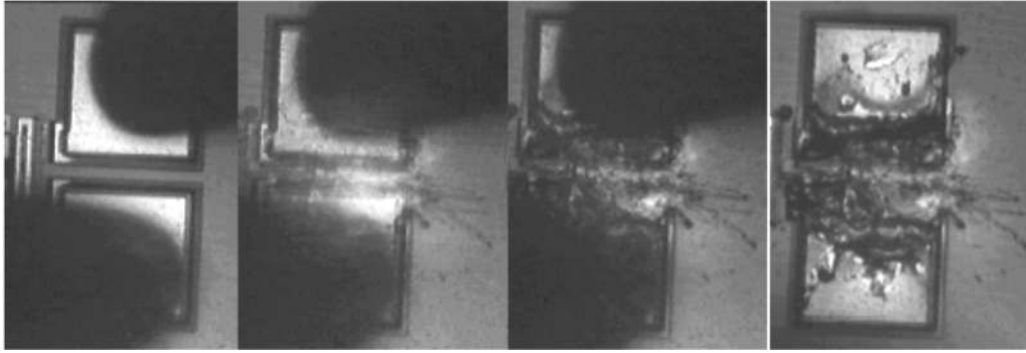


Figure 5-10 Images of high-voltage failure of electrical isolation of contacts and bond pads of a SRFBM [17].

currents above 7 mA. Subsequent resistance measurements were not as low, but were repeatable. The average repeatable contact resistance was approximately 35Ω . Contacts were also tested for electrical isolation. Leakage currents were very small, <0.01 mA, up to 350 V. Beyond this arcing resulted in catastrophic failure (see Fig. 5-10) [17].

Switching time was also measured and found to be limited by the speed of the actuators. 800 μ s switching times—measured from the application of actuation pulse to closure of the contacts—were repeatably measured. Switching time was reduced to 360 μ s by increasing the intensity of the actuation pulse, but resulted in damage to the thermal actuators.

5.2.2 Reliability

Fatigue testing was performed to explore the effects of the high stresses present in the tensural pivots. Timed pulses were sent to the forward and return actuators, with pauses to allow the mechanism to rest at the stable equilibria (See APPENDIX F for a detailed schematic of the system used for this testing). This resulted in a testing speed of 17.5 Hz. The test was run on a single SRFBM with a fourteen-leg 200 μ m TIM to approximately 2 million cycles, at which point the forward actuator failed.

The complete failure of the forward actuator at 2 million cycles was preceded by the fracture of a few legs at 400,000 cycles due to what appears to be a manufacturing defect. This resulted in uneven current paths and heating. At about 2 million cycles the accumu-

lated thermal fatigue resulted in the failure of the forward actuator. Future investigations should explore the effects of thermal fatigue on actuators.

Robustness is another aspect of reliability. A set of four legs was chosen for this implementation of the SRFBM as this is the minimum number of legs to insure the symmetry needed for correct sliding motion. Additional legs can be used, but would result in the need for additional actuation force which conflicts with the goal of low-power actuation.

During manufacturing some of the tensural pivots were damaged, resulting in SRFBM without their full complement of legs. Despite this damage, mechanisms with three intact legs still demonstrated bistability. The principle effect on the behavior of the mechanism is reduced actuation and contact force. However, for many applications the reduced forces may still be sufficient, thus providing increased reliability, due to the inherent redundancy of the system. For systems requiring high-reliability, super-redundant systems with additional legs can be used. Such systems would have to be tolerant of the variation in actuation and contact force that could result.

The SRFBM concept can be adapted to many different applications. The ability to fabricate SRFBM in a single mechanical layer provides great freedom for fabrication and integration with other systems. Several designs have already been completed but not fabricated at the time of this writing.

6.1 Low-Power Electrical Switches

The systems presented in Chapter 5 are intended to be used as microswitches (or microrelays). These systems are not currently compatible with the power available from microbatteries. In order to integrate the SRFBM with microbattery power it is necessary to reduce the actuation force and displacement. By so doing the SRFBM can be used with smaller thermal actuators.

A design has been completed to be fabricated in the MUMPs process. This design uses 40 μm long tensural pivots that are still 2.0 μm wide. The C-beam thickness has been increased to 38.0 μm . The X- and Y-offsets have been reduced to 3.0 μm and 32.5 μm , respectively (see APPENDIX C). Models predict that this SRFBM will require approximately 250 μN of forward actuation force. Return and contact force are approximately 55 μN . This is coupled with reduced displacement: 6.0 μm to the unstable equilibrium, 8.0 μm to the contacts, and 10 μm to the natural stable equilibrium. The Bistability Ratio of this configuration is only about 0.10 (see Equation (4.1)), but should operate reliably. This reduction in displacement and actuation force reduces the required power. Figure 6-1

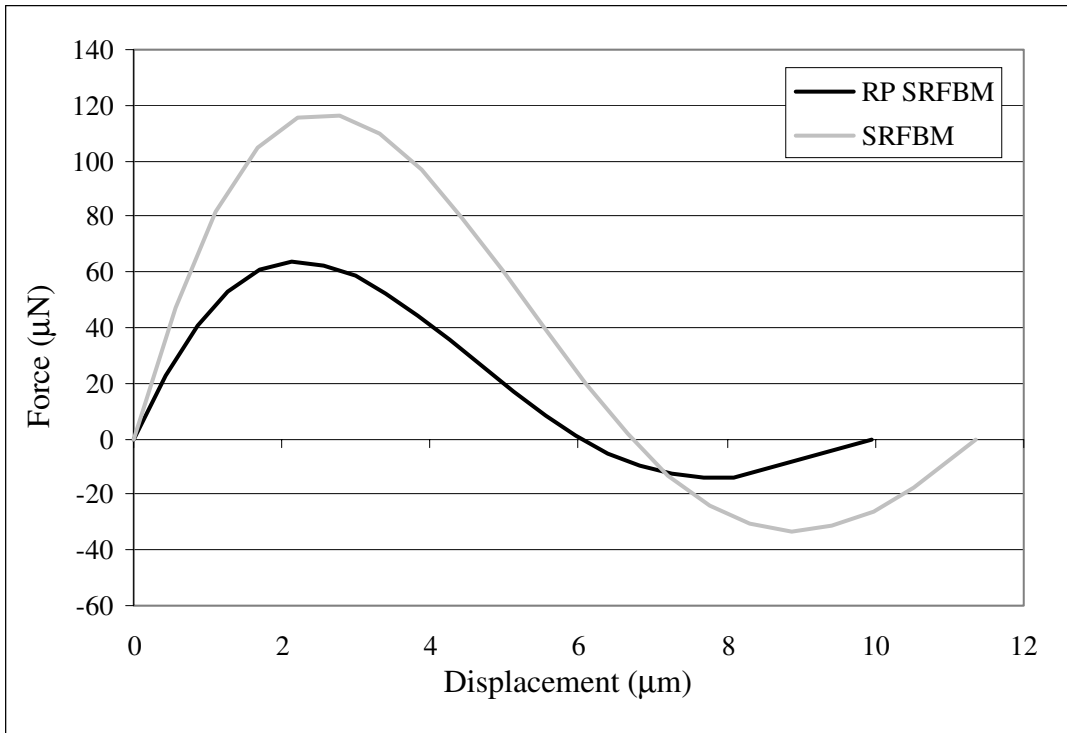


Figure 6-1 Comparison of force-deflection curves of reduced power (RP SRFBM) and current (SRFBM) devices.

compares the force-deflection curves for current and reduced power SRFBM, emphasizing the reduction in actuation force and displacement.

6.2 SUMMiT SRFBM

Sandia National Laboratories has developed the SUMMiT V MEMS prototyping process (Sandia Ultra-planar Multi-level MEMS Technology Five Layer). This process provides five structural layers, four of which are mechanical and two of which are planarized. There is also a specialized pin joint cut that reduces pin joint clearances to 0.6 µm. One of the great strengths of this process is smaller design rules: linewidth and linespacing of 1.0 µm. In addition, during mask fabrication all features are reduced by 0.15 µm on each side resulting in minimum features of 0.7 µm.

Thanks to these smaller design rules, SRFBM can be even smaller, with significantly smaller displacements. A design has been developed for SUMMiT V fabrication that has a Bistability Ratio of 0.40 (see Equation (4.1)) and will require less than 50 μN actuation force. Total displacement to the contacts is only 3.5 μm , with the unstable equilibrium located at 2.5 μm . Stresses are also reduced to slightly above 1 GPa.

The SUMMiT V process does not provide a metal layer that can be used for electrical contacts. This SRFBM will allow evaluation of future designs fabricated in similar processes as well as other applications of the bistable behavior. One such applications involves utilizing three of the mechanical layers (the first two mechanical layers are normally used as a laminate) to produce superimposed devices, i.e., identical SRFBM stacked on top of each other, but free to move independently of each other. Such a system (with larger displacement) could be used as a redundant shutter for a light signal, only allowing the signal to pass when all three devices are in the same position.

6.3 LIGA G-Switch

G-Switches are threshold accelerometers that are used to trigger an action when the inertial environment surpasses a threshold limit. The G-switch presented here is intended for defense applications but could also be used as a commercial threshold accelerometer. One possible commercial application would be to replace the current capacitive sensing MEMS accelerometers used as part of automotive airbag systems. The SRFBM has been designed to be fabricated in LIGA to be tested as a G-switch. This design has been submitted to Sandia National Laboratories-Livermore (California) for fabrication as a LIGA device. Figure 6-2 presents the layout for this device. There are only two components which require minimal, but precise, assembly. The SRFBM is completely surrounded by a skeletonized frame to facilitate assembly. The contact block is the only other component but should be located 75 μm \pm 10 μm from the end of the undeflected G-switch.

The LIGA process that will be used to fabricate this device uses Nickel as the plating material. The minimum feature size is 20 μm , with aspect ratios up to 30:1. Long slender features should be decorated with what Sandia designers refer to as “bulges” to facilitate the dissolution of the PMMA. Large structural areas should be skeletonized to allow for

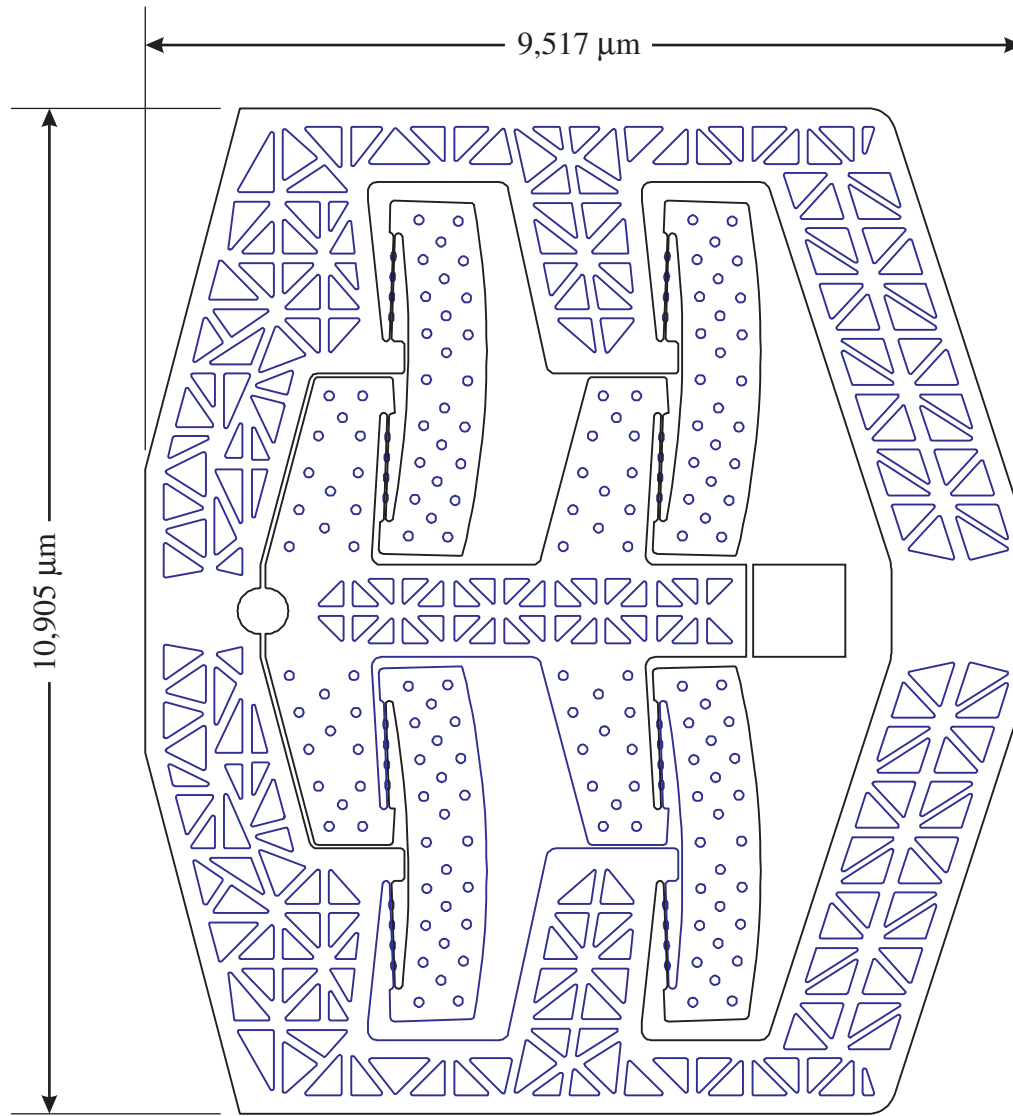


Figure 6-2 Layout for the LIGA G-switch.

more uniform dissolution and electroplating. These design rules all affected the design of the G-switch.

Figure 6-2 presents the geometry of the G-switch. Overall dimensions are as shown in Fig. 6-2 and material thickness will be approximately 600 μm. The G-switch is quite large in comparison to the surface micromachined SRFBM that have been presented, but is small for a LIGA device. Size will be an asset to the G-switch because it will facilitate assembly and make it more sensitive to moderate accelerations. Surface micromachined

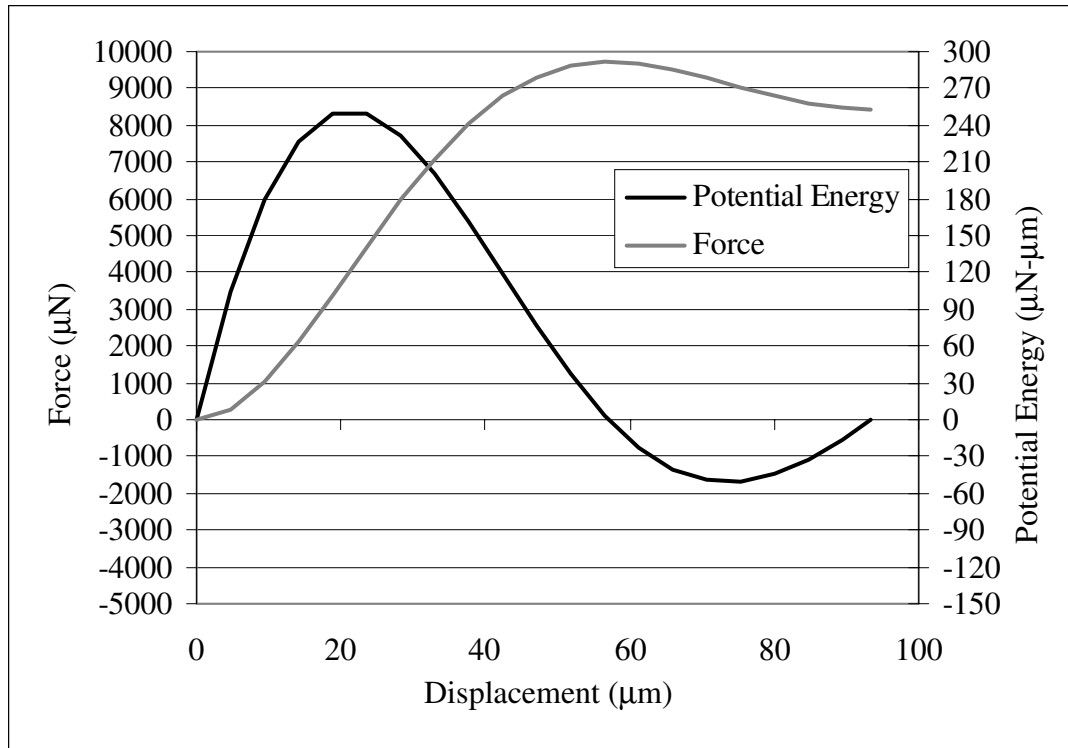


Figure 6-3 Finite element model results for LIGA G-switch.

SRFBM can be considered to be insensitive to inertial loads, requiring approximately 150,000g to switch states. The LIGA G-switch is sensitive to accelerative loads on the order of 50g, making it useful for much less severe inertial environments. If other actuation methods are used, the critical forces for the G-switch are approximately 8300 μN (forward) and 1700 μN (return) for single legs. Complete four-leg systems would require 33200 μN and 6800 μN respectively. See APPENDIX E for the ANSYS batch file for this device.

6.4 Amorphous Diamond

Amorphous diamond (aD) is a recent development in MEMS fabrication and has a number of advantages over silicon, including an inherently hydrophobic surface for improved resistance to stiction and higher modulus (800 GPa) and strength (8.5 GPa) [41]. The process being developed at Sandia National Laboratories is currently limited to single

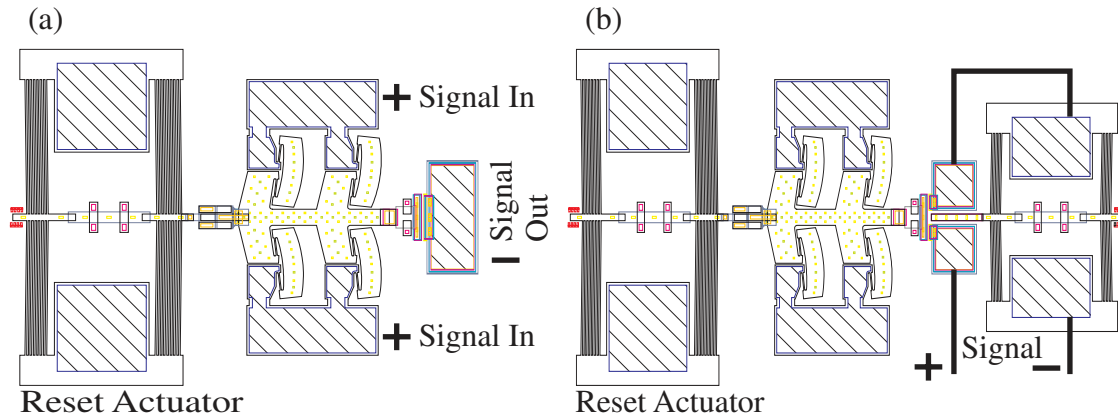


Figure 6-4 Circuit breaker schemes: (a) Current carrying tensural pivots and (b) external thermal return actuator. The reset actuator on the left side of the SRFBMs is common to both designs.

layer surface micromachining. At the request of Sandia National Laboratories (NM) an aD mechanism has been designed. Although aD is much stronger than polysilicon, the modulus is also higher. The ratio of the two, S/E is a good indicator of the suitability of a material for use in compliant mechanisms. The S/E for aD is actually slightly smaller than that of polysilicon (0.010 vs. 0.012). The result is that for similar designs in the two different materials, the ratio of the maximum stress to the strength of the material will be roughly the same. This would facilitate design, allowing existing polysilicon designs to be directly transferred to aD fabrication, except for the fact that actuation forces also are dependent on the modulus of elasticity. A design has been developed to keep the actuation forces at a manageable $550 \mu\text{N}$ (although the limited electrical conductivity of aD may make thermal actuators difficult to implement).

6.5 Circuit Breaker

The SRFBM is ideally suited for use as a micro-circuit breaker due to its integration with thermal actuators, and its ability to self retract. As a circuit breaker, the SRFBM would be set (or reset) to the second stable position by thermal actuation, closing electrical contacts. Either of the following actuation schemes may then be used to provide the circuit breaking action (see Fig. 6-4):

- The current path passes through the tensural pivots of the SRFBM and then through the electrical contacts. When the current surpasses a predetermined limit, the mechanism self-retracts, breaking the circuit.
- The current passes through an external return actuator. This has the benefit of reducing the possibility of thermal damage to the SRFBM.

6.6 Memory and Logic

A fundamental unit of computer logic and memory is a switch (usually a transistor). It is possible to reproduce the functionality of solid state systems with mechanical logic, though it would be very slow (17.5 Hz was the speed of the fatigue testing in Section 5.2.2). While this speed may be increased, it is unlikely to rival that of electrical systems. However, mechanical logic, and especially mechanical memory, do have inherent advantages: higher tolerance to harsh thermal and radiation environments than solid state devices, state retention and the possibility of power reduction in some applications.

6.7 Optical Switches

A system similar to that presented by Hoffmann, et al. [20], can be developed, using the SRFBM to carry and position an optical fiber. Actuating the SRFBM would then accurately reposition the optical fiber, redirecting the signal. Due to the size of optical fibers, such a system would be much larger than current surface micromachined devices, and require significantly larger displacement. As a result, suitable actuators will also need to be developed.

Other optical switches may be developed by using the SRFBM to position reflective elements to redirect light signals.

6.8 Microvalves

The freedom of fabrication provided by the fully compliant design of the SRFBM would allow it to be fabricated and used as a microvalve inside microfluidic channels. The

benefits of such a valve are similar to the benefits for an electrical system. Thermal, or other actuators can also be fabricated within the channels, providing a fully enclosed, actuable bistable microvalve.

Conclusions and Recommendations

The purpose of this thesis has been to present a class of Self-Retracting Fully-compliant Bistable Micromechanisms (SRFBM). The development and fabrication of the SRFBM have been presented, resulting in the demonstration of a fully compliant bistable micromechanism capable of on-chip actuation, thermal self-retraction and small displacements. This chapter briefly summarizes the work presented in this thesis and recommends areas of focus for future efforts.

7.1 Conclusions

The effects of the clearances in microfabricated pin joints have been identified as a major source of difficulties in the design and operation of bistable micromechanisms. *Tensural* pivots are proposed as a method to deal with compressive loading encountered in the fully compliant double-slider configuration selected as the basis for the SRFBM. Tensural pivots are integrated into the design of a compliant mechanism in such a way that they are subject to tension and bending. This allows reliable operation of compliant mechanisms subject to compressive loading. Further development of the SRFBM involved the creation of several models based on this basic topology.

Single and multiple degree of freedom Pseudo-Rigid-Body Models, developed for the SRFBM, have proven their usefulness in design, but are currently limited by their inability to accurately predict force-deflection relationships. These models allow rapid identifica-

tion of bistable configurations. Further refinement currently relies on finite element models that are based on the detailed geometry of the production-ready devices.

Using these models, devices have been designed and fabricated in the Cronos MUMPs process. The die containing these devices suffered from manufacturing defects, greatly reducing the yield of functional devices. Despite these problems, sufficient numbers were available for testing. Furthermore, damaged devices demonstrated their inherent robustness, as systems with damaged legs were still bistable.

On-chip actuation has been demonstrated and requires approximately 150 mW of power (in air). Fatigue testing of a single device was taken to 2 million duty cycles without failure. Testing ended when the forward actuator failed as a result of a manufacturing defect. Manual measurements of the critical force for forward switching correlate well with the finite element model calculations of approximately 500 μN . Return switching seems to be affected by frictional effects, resulting in higher than expected forces of approximately 250 μN . This phenomenon does not noticeably affect on-chip return actuation. Electrical contact resistance and switching times have also been evaluated.

7.2 Recommendations

The SRFBM has great commercial promise. As such it should be developed further and licensed for commercial applications. To facilitate this process, the models used in development should be improved.

7.2.1 Tensural pivots

The preliminary work on tensural pivots should be expanded to better characterize their behavior. Furthermore, design methodologies should be developed, specifying the size and orientation of tensural pivots in a system, and the modifications to the overall structure of the mechanism. These will be based on the function and loading of the mechanism.

Tensural pivots are also of value to macroscopic compliant mechanisms. Many compliant segments behave poorly or fail prematurely when subject to compressive loading. Developing techniques for tensural pivots can greatly improve the functionality and durability of many compliant mechanisms. This has already been shown by the author in an

unpublished effort to improve a macroscopic fully compliant light switch with tensural pivots.

7.2.2 Model improvement and design optimization

The method used to arrive at the designs presented in this thesis depended largely on engineering judgement. The models (especially the single degree of freedom PRBM) should be improved and implemented in a form that is amenable to optimization. Doing so allows the concept to be easily optimized for specific tasks or constraints. An additional benefit is the enhanced marketability of the SRFBM, as its design and implementation would be more accessible to those not intimately acquainted with the design of fully compliant mechanisms. This effort could also be directly applied to further reduction of power and displacement of the SRFBM. Better understanding of the nature of tensural pivots will contribute to the improvement of these models.

7.2.3 Investigation of critical return force

The unexpectedly large critical return force, apparently the result of contact with the substrate and the resulting friction, is a phenomenon that should be investigated. Failure due to stiction has not been observed in SRFBM left in the second position, but is possible if the shuttle is in fact resting on its dimples. To isolate any effects that may be due to other phenomena, SRFBM should be fabricated in processes (like SUMMiT V and LIGA) which allow higher aspect ratios and can be stiffer out-of-plane.

7.2.4 Additional applications

The SRFBM should be implemented and tested in the applications and processes described in Chapter 6. There are a number of these applications with considerable commercial promise. Production of low-power small-displacement bistable micromechanism for switching of microbattery power supplies should be a primary goal. Additional applications should also be developed based on the SRFBM concept.

7.2.5 Fully compliant mechanism design

Due to the poor performance of micro-pin joints, future work in MEMS should be almost exclusively fully compliant. With tools now available to the engineer (including the Pseudo-Rigid-Body Model and FEA) and the continued work to improve them, there is lit-

the reason to continue using rigid-body and partially compliant mechanisms that suffer from process limitations.

Work should continue to explore other classes of fully compliant mechanisms and the compliant segments of which they are constituted.

List of References

- [1] Ashurst, W.R., Yau, C., Carraro, C., Maboudian, R., and Dugger, M.T., 2001, "Dichlorodimethylsilane as an Anti-Stiction Monolayer for MEMS: A Comparison to the Octadecyltrichlorosilane Self-Assembled Monolayer," *Journal of Microelectromechanical Systems*, Vol. 10, No. 1, pp. 41-49.
- [2] Baker, M.S, Howell, L.L., 2001, "On-chip actuation of Young Mechanism", *Yet to be published*.
- [3] Baker, M.S., Lyon, S.M., and Howell, L.L., 2000, "A Linear Displacement Bistable Micromechanism," *Proceedings of the 2000 ASME Design Engineering Technical Conferences*, DETC2000/MECH-14117, pp. 1-7.
- [4] Bisshopp, K.E., and Drucker, D.C., 1945, "Large Deflection of Cantilever Beams," *Quarterly of Applied Mathematics*, Vol. 3, No. 3, pp. 272-275.
- [5] Cahners In-Stat Group, 2000, "Semiconductor Market to Reach Record Heights," available from <http://www.instat.com/insights/semi/2000/semii91900.htm>, Internet, accessed 12 July 2001.
- [6] Capanu, M., Boyd, J.G. IV, and Hesketh, P.J., 2000, "Design, Fabrication, and Testing of a Bistable Electromagnetically Actuated Microvalve," *Journal of Microelectromechanical Systems*, Vol. 9, No. 2, pp. 181-189.
- [7] Chalmers, P., 2001, "Relay Races," *Mechanical Engineering*, Vol. 123, No. 1, pp. 66-68.
- [8] Chiao, M., Lin, L., 2000, "Self-Buckling of Micromachined Beams Under Resistive Heating," *Journal of Microelectromechanical Systems*, Vol. 9, No. 1, pp.146-151.
- [9] Clements, D., 2000, "Implementing Compliant Mechanisms in Micro-Electro-Mechanical Systems (MEMS)," M.S. Thesis, Brigham Young University, Provo, Utah.
- [10] Clements, D., Howell, L.L., Masters, N., and Weight, B., 1999, "Floating Pin Joints Fabricated from Two Layers of Polysilicon at the Micro Level," *Proceedings of the Tenth World Congress on the Theory of Machines and Mechanisms*, Oulu, Finland, June 20-24, Vol. 2, pp. 874-879.

- [11] Comtois, J.H., Michalick, M.A., and Baron, C.C., 1997, "Characterization of Electrothermal Actuators and Arrays Fabricated in a Four-Level, Planarized Surface-Micromachined Polycrystalline Silicon Process," *1997 International Conference on Solid-State Sensors and Actuators*, Chicago, IL, June 16-19, Vol. 2, pp. 769-772.
- [12] Cragun, R., 1999, "Thermal microactuators for microelectromechanical systems," M.S. Thesis, Brigham Young University, Provo, Utah.
- [13] Cragun, R., and Howell, L.L., 1999, "Linear Thermomechanical Microactuators," *Microelectromechanical Systems (MEMS)*, at the 1999 ASME International Mechanical Engineering Congress and Exposition, pp. 181-188, November, 1999.
- [14] De Los Santos, H.J., 1999, *Introduction to Microelectromechanical (MEM) Microwave Systems*, Artech House, Boston.
- [15] Gere, J.M., Timoshenko, S.P., 1984, *Mechanics of Materials, third edition*, PWS-Kent Publishing Company, Boston, Massachusetts.
- [16] Goll, C., Bacher, W., Büstgens, B., Maas, D., Menz, W., and Schomburg, W.K., 1996, "Microvalves with bistable buckled polymer diaphragms," *Journal of Micromechanics and Microengineering*, Vol. 6, No. 1, pp. 77-79.
- [17] Gomm, T., 2001, "Development of In-Plane Compliant Bistable Microrelays," M.S. Thesis, Brigham Young University, Provo, Utah.
- [18] Hälg, B., 1990, "On a Nonvolatile Memory Cell Based on Micro-Electro-Mechanics," *Proceedings Micro Electro Mechanical Systems, 1990, An Investigation of Micro Structures, Sensors, Actuators, Machines and Robots, IEEE*, pp. 172 -176.
- [19] Hetherington, D.L., Sniegowski, J.J., 1998, "Improved Polysilicon Surface-micromachined Micromirror Devices using Chemical-mechanical Polishing," Presented at the International Symposium on Optical Science, Engineering, and Instrumentation, SPIE's 43rd Annual Meeting, San Diego, CA, July 22, 1998.
- [20] Hoffmann, M., Kopka, P., and Voges, E., 1999, "Bistable Micromechanical Fiber-Optic Switches on Silicon With Thermal Actuators," *Sensors and Actuators*, No. 78, pp. 28-35.
- [21] Hoffmann, M., Kopka, P., Groß, T., and Voges, E., 1999, "Optical fibre switches based on full wafer silicon micromachining," *Journal of Micromechanics and Microengineering*, Vol. 9, No. 2, pp. 151-155.
- [22] Howell, L.L., 2001, *Compliant Mechanisms*, Wiley, New York.

- [23] Howell, L.L., and Midha, A., 1994, "A Method for the Design of Compliant Mechanisms with Small-Length Flexural Pivots," *ASME Journal of Mechanical Design*, Vol. 116, No. 1, pp. 280-290.
- [24] Hruby, J., 2001, "LIGA Technologies and Applications," *MRS Bulletin April 2001*, pp. 1-4.
- [25] Jensen, B.D., 1998, "Identification of macro-and micro-compliant mechanism configurations resulting in bistable behavior," M.S. Thesis, Brigham Young University, Provo, Utah, 1998.
- [26] Jensen, B.D., Howell, L.L., and Salmon, L.G., 1998, "Introduction of Two-Link In-Plane, Bistable Compliant MEMS," *Proceeding of the 1998 ASME Design Engineering Technical Conferences*, DETC98/MECH-5837.
- [27] Jensen B.D., Howell, L.L., and Salmon, L.G., 1999, "Design of Two-Link In-Plane, Bistable Compliant Micro-Mechanisms," *Transactions of the ASME*, Vol. 121, pp. 416-423.
- [28] Kruglick, E.J.J., and Pister, K.S.J., 1998, "Bistable MEMS Relays and Contact Characterization," *IEEE Solid-State Sensor and Actuator Workshop*, Hilton Head Island, South Carolina, June 8-11, pp. 333-337, 1998.
- [29] Kruglick, E.J.J., and Pister, K.S.J., 1999, "Lateral MEMS Microcontact Considerations," *Journal of Microelectromechanical Systems*, Vol. 8, No. 3, pp. 264-271.
- [30] Maboudian R., Ashurst, W.R., Carraro, C., 2000, "Self-assembled monolayers as anti-stiction coatings for MEMS: characteristics and recent developments," *Sensors and Actuators A*, Vol. 82, Iss. 1-3, pp. 219-223.
- [31] Matoba H., Ishikawa, T., Kim, C.-J., Muller, R.S., 1994, "A bistable snapping micro-actuator," *Proc. IEEE Micro Electro-Mechanical Systems*, pp. 45-50, Jan. 1994, Oiso (Japan), pp. 45-50.
- [32] Parkinson, M.B., Jensen, B.D., Roach, G.M., 2000, "Optimization-Based Design of a Fully-Compliant Bistable Micromechanism," *Proceedings of the 2000 ASME Design Engineering Technical Conferences*, DETC2000/MECH-14119.
- [33] Paul, B., 1979, *Kinematics and Dynamics of Planar Machinery*, Prentice Hall, Upper Saddle River, New Jersey.
- [34] Ren, H., Gerhard, E., 1997, "Design and fabrication of a current-pulse-excited bistable magnetic microactuator," *Sensors and Actuators A*, Vol. 58, pp. 259-264.

- [35] Rodgers, M.S., Kota, S., Hetrick, J., Li, Z., Jensen, B.D., Krygowski, T.W., Miller, S.L., Barnes, S.M., Burg, S.M., 2000, "A New Class of High Force, Low-Voltage, Compliant Actuation Systems," *Solid-State Sensor and Actuator Workshop*, Hilton Head Island, South Carolina, June 4-8. Available at www.mdl.sandia.gov/micro-machine/biblog_summit.html
- [36] Rodgers, M.S., Sniegowski, J.J., 1998, "Designing Microelectromechanical Systems-on-a-Chip in a 5-Level Surface Micromachine Technology," *Second International Conference on Engineering Design and Automation*, Maui, Hawaii, August 9-12, 1998.
- [37] Sandia National Laboratories, "Comb Drive Close-Up—rs11622.jpg," available from <http://mems.sandia.gov/scripts/images.asp>, Internet, accessed 13 July 2001.
- [38] Sniegowski, J.J., Rodgers, M.S., 1998, "Manufacturing Micro-Systems-on-a-Chip with a 5-Level Surface Micromachining Technology," *Second International Conference on Engineering Design and Automation*, Maui, Hawaii, August 9-12, 1998.
- [39] Sniegowski, J.J., Smith, C., 1995, "An Application Of Mechanical Leverage To Microactuation," *Proceedings of the 8th International Conference on Solid-State Sensors and Actuators, and Eurosensors IX, Transducers '95 Eurosensors IX*, Stockholm, Sweden, June 25-29, 1995, Vol. 2, pp. 364-367.
- [40] Srinivasan, U., Houston, M.R., Howe, R.T., Maboudian, R., 1998, "Alkyltrichlorosilane-Based Self-Assembled Monolayer Films for Stiction Reduction in Silicon Micromachines," *Journal of Microelectromechanical Systems*, Vol. 7, No. 2, pp. 252-260.
- [41] Sullivan, J.P., Friedmann, T.A., de Boer, M.P., LaVan, D.A., Hohlfelder, R.J., Ashby, C.I.H., Dugger, M.T., Mitchell, M., Dunn, R.G., Magerkurth, A.J., 2000, "Developing a New Material for MEMS: Amorphous Diamond," *Materials Research Society Proceedings*, Vol. 657, M. de Boer, M. Judy, H. Kahn, and S. M. Spearing, Eds., pg. EE7.1.1, [SAND No. 2000-1753A].
- [42] Taher, M., Saif, A., 2000, "On a Tunable Bistable MEMS—Theory and Experiment," *Journal of Microelectromechanical Systems*, Vol. 9, No. 2, pp. 157-170.
- [43] Tanner, D.M., 2000, "Reliability of Surface Micromachined MicroElectroMechanical Actuators," *22nd International Conference in Microelectronics*, Nis, Yugoslavia, pp. 97-104.
- [44] Tanner, D.M., Peterson, K.A., Irwin, L.W., Tangyonyong, P., Miller, W.M., Eaton, W.P., Smith, N.F., and Rodgers, M.S., "Linkage Design Effect on the Reliability of Surface Micromachined Microengines Driving a Load," *SPIE, Micromachining and Microfabrication Symposium*, Vol. 3512, pp.215-226.

- [45] Tanner, D.M., Smith, N.F., Irwin, L.W., Eaton, W.P., Helgesen, H.S., Clement, J.J., Miller, W.M., Walraven, J.A., Peterson, K.A., Tangyunyong, P., Dugger, M.T., and Miller S.L., 2000, *MEMS Reliability: Infrastructure, Test Structures, Experiments, and Failure Modes*, Sandia Report SAND2000-0091, Sandia National Laboratories.
- [46] Texas Instruments Digital Light Processing, “DMD™ Architecture,” available from http://www.dlp.com/dlp/resources/pixels_micro.asp, Internet, accessed 13 July 2001.
- [47] Texas Instruments Digital Light Processing, “Two Mirrors,” available from <http://www.dlp.com/dlp/resources/dlpcinema.asp>, Internet, accessed 13 July 2001.
- [48] *Transistorized!* website of the PBS series, 1999, available from <http://www.pbs.org/transistor/>, Internet, accessed 12 July 2001.
- [49] University of Wisconsin-Madison, 1991, “wobble.jpg,” available from http://mems.engr.wisc.edu/images/misc_liga/wobble.jpg, Internet, accessed 13 July 2001.
- [50] Vangbo, M., 1998, “A lateral symmetrically bistable buckled beam,” *Journal of Micromechanics and Microengineering*, Vol. 8, No. 1, pp. 29-32.
- [51] Vangbo, M., 1998, “An Analytical Analysis of a Compressed Bistable Buckled Beam,” *Sensors and Actuators A*, Vol. 69, No. 3, pp. 212-216.
- [52] Ye, W., Mukherjee, S., and MacDonald, N.C., 1998, “Optimal Shape Design of an Electrostatic Comb Drive in Microelectromechanical Systems,” *Journal of Microelectromechanical Systems*, Vol. 7, No. 1, pp. 16-26.

Appendix

APPENDIX A *Gear Generation Program*

In the development of on-chip actuation for bistable micromechanisms a gear train was desired (see Section 2.3.2.4). In order to design the gears this program was written to automatically generate the gear with correct involute profile teeth based on user supplied parameters. The output can be either CIF or DXF format for use in L-Edit or AutoCAD respectively. This code was originally written for the Borland Turbo C++ compiler. This is a 160-bit DOS based compiler. I have used a number of not standard functions that are only available for this compiler. These are only used to format the text of the user interface. As such these non-standard functions can easily be replaced with standard i/o functions. The result will be the loss of colored text in the user interface. I have also adapted this code to a graphical user interface using an open source GUI toolkit called FLTK (pronounced “fulltick” and available at www.fltk.org). However, the code in this appendix contains all the algorithms and file formatting routines necessary to generate gears. As such the source code for the much more complex and larger GUI version will not be included.

```
/*
*****
/*  Title:  Gear Program  Version 0.8                               */
/*  Author: Nathan Masters      Date:  25 May 1999                 */
/*      Update: 09 Oct 2000 15:44:09                               */
/*  Description: This program generates involute profile gear teeth for */
/*              use in MCNC Technology MUMPS using CIF file export.  Open these */
/*              files in L-Edit (Tanner Research). The AutoCad DXF Export is still */
/*              under development.                                     */
/*  Copyright 1999 Brigham Young University CMEMS RESEARCH GROUP  */
*****
*/
```

```

#include <stdio.h>
#include <stdlib.h>
/*#include <fcntl.h>*/
/* #include <sys\stat.h>*/
/*#include <io.h>*/
#include <string.h>
#include <math.h>
#include <conio.h>

/*-----*/
/* Functions used in This file */
int cifHeader(FILE *fp);
/* This function generates the header for MUMPS technology CIF file */
int dxfHeader(FILE *fp);
/* This function generates the header for AutoCad DXF Files */
int gear(FILE *in, FILE *fp, FILE *info,int Ftype, char name[32]);
/* This functions generates the gear profiles */
int GearInput(FILE *in, double *PA, int *N, int *Nd, double *Bklsh, double *P,
              int *Lind,
              double *InitRot, double *DedRat);
int splash(void);
/*-----*/

int main(void)
{
    FILE *in, *out,*info;
    int fex,Ftype;
    char Temp[256]="",FName[32]="",Finfo[32],filetype[4];
    char *ptr,c='.',c2='\n',*suffc=".cif",*suffd=".dxf",*sufft=".txt";

    splash(); /* This calls splash to print use information */

    printf("Enter source filename (Enter for None): "); /* If a source file is
        used */
    fgets(Temp,32,stdin); /* Enter it here */
    ptr=strchr(Temp,c2);
    strncat (FName,Temp,strlen(Temp)-1);

    if ((in = fopen(FName, "rt")) /* Open Input File (if any) */
        == NULL)
    {
        fprintf(stderr, "No input file, run from prompt.\n");
        in=stdin;
    }

    strcpy(Temp,""); /* Reset string variables */
    strcpy(FName,"");
    strcpy(Finfo,"");
    printf("Enter output filename (Do not include suffix): ");
    /* Enter output file name */
    fgets (Temp,32,stdin);
    ptr=strchr(Temp,c2);
    strncat (FName,Temp,strlen(Temp)-1);
    strncat (Finfo,Temp,strlen(Temp)-1);
    fex=0; /* fex determines output (file/stdout)*/
    if(strlen(FName)==0) /* (fex=1=>stdout,fex=0=>file) */
    {

```

```

    fex=1;
    fprintf(stderr, "\nNo Output file. Output will be to screen.\n");
    out=stdout;
}

do /* This loop detemines the output file type */
{
    printf("\nOutput File Type ");
    textcolor(14);
    cprintf("C");
    textcolor(15);
    printf("IF/");
    textcolor(14);
    cprintf("D");
    textcolor(15);
    printf("XF (default is CIF): ");
    fgets(filetype,10,in);
    if (strlen(filetype)==1)
    {
        strcpy(filetype,"CIF");
    }

    if(!strncmp(filetype,"d",1)||!strncmp(filetype,"D",1))
        /*||!strncmp(filetype,"DXF",3)||!strncmp(filetype,"dxf",3)*/
    {

        Ftype=2; /* Ftype=2 => DXF file format */
    }
    else if(!strncmp(filetype,"c",1)||!strncmp(filetype,"C",1))
        /*||!strncmp(filetype,"CIF",3)||!strncmp(filetype,"cif",3)*/
    {

        Ftype=1; /* Ftype =1 => CIF file format */
    }
} while(abs(!strncmp(filetype,"c",1))&&abs(!strncmp(filetype,"C",1))
&&abs(!strncmp(filetype,"CIF",3))&&abs(!strncmp(filetype,"cif",3))
&&abs(!strncmp(filetype,"d",1))&&abs(!strncmp(filetype,"D",1))
&&abs(!strncmp(filetype,"DXF",3))&&abs(!strncmp(filetype,"dxf",3)));

/* Once the output filetype is determined the appropriate suffix is added */
/* ".cif" or ".dxf" if no suffix is specified by the user */
ptr = strchr(FName,c);
if(!ptr)
{
    if(Ftype==1)
    {
        strncat(FName,suffc,4);
    }
    else
    {
        strncat(FName,suffd,4);
    }
}
/* Open output file */
if (fex!=1)
{
    if ((out = fopen(FName, "wt"))
        == NULL||fex)
    {

```

```

        fprintf(stderr, "\nError opening output file. Output will be to
                screen.\n");
        out=stdout;
    }
    else
    {
        fprintf(stderr, "\nThe Output file will be saved in the current
                directory.\n");
    }
}
/* If output is to a file a text file containing relevant information is */
/* generated */
if(!fex)
{
    if(!ptr)
    {
        strncat(Finfo,sufft,4);
    }
    else
    {
        strcpy(Temp,"");
        strncpy(Temp,Finfo,ptr-FName);
        strncat(Temp,sufft,4);
        strcpy(Finfo,"");
        strcpy(Finfo,Temp);
    }
    if ((info = fopen(Finfo, "wt"))
        ==NULL)
    {
        fprintf(stderr, "\nCannot open information file.\n");
        return 1;
    }
}
else
{
    info=stdout;
}

/* The gear() function generates the gear profile, as well as calling */
/* other functions to prompt the user for more information */
gear(in,out,info,Ftype,Temp);
/* Close all opened files */
fclose(in);
fclose(out);
fclose(info);
return 0;
}

/*          This functions generates the gear profiles          */
int gear(FILE *in, FILE *fp, FILE *info,int Ftype, char name[32])
{
    double X,Y,t,scale,P,CP,PA,PAr,Dp,Rp,Rb,Add,Ded,DedRat,Rd,Rh;
    double Delta, Gamma, Lambda, Phi, Psi, Omega, Theta,THDiff;
    double Min,Max,ST;
    double Xl,Yl,Xu,Yu;

```



```

double RM11, RM12, RM21, RM22, CM11, CM12, CM21, CM22;
int i, j, N, Nd, NumP, Lind;
double Bklsh, InitRot;

/* GearInput() prompts the user for more information */
GearInput(in, &PA, &N, &Nd, &Bklsh, &P, &Lind, &InitRot, &DedRat);
/*GearInput(in, &PA, &N, &Nd, &Bklsh, &P, &Lind, &InitRot);*/
DedRat=1.35;
/* Calculated Values */
PAr=M_PI*PA/180.0; /* Convert Pressure Angle to Radians */
Dp=(double)N/P; /* Pitch Circle Diameter */
Rp=Dp/2.0; /* Pitch Circle Radius */
Rb=Rp*cos(PAr); /* Base Circle Radius */
Add=1.0/P; /* Addendum */
Ded=(double)(DedRat)/P; /* Dedendum */
Rd=Rp-Ded; /* Dedendum Circle Radius */

/* Output of Gear Parameters for assembly */
if(Ftype==1)
{
    fprintf(stdout, "\n\n CIF output for L-Edit");
    fprintf(info, "\n\n CIF output for L-Edit");
}
else /*if(Ftype==2)*/
{
    fprintf(stdout, "\n\n DXF output for AutoCad");
    fprintf(info, "\n\n DXF output for AutoCad");
}
fprintf(stdout, "\n The following values are needed for assembly");
fprintf(stdout, "\n Pitch Radius is %lf", Rp);
fprintf(stdout, "\n Dedendum Circle Radius is %lf", Rd);
fprintf(info, "\n The following values are needed for assembly");
fprintf(info, "\n Pitch Radius is %lf", Rp);
fprintf(info, "\n Dedendum Circle Radius is %lf", Rd);

Delta=M_PI/N; /* Angular (radians) thickness of Gear Tooth */
Gamma=Delta/2.0-Bklsh/Rp; /* Starting point of involute profile */
Psi=InitRot*M_PI/180.0; /* Takes care of any initial rotation */
Theta=Psi; /* Used to rotate each tooth, updated by THDiff */
THDiff=2.0*Delta; /* Used for angular placemet of each tooth */
NumP=50; /* Number of points in each tooth face profile */

if (Ftype==1)
{
    scale=2000.0;
    cifHeader(fp);
    fputs(name, fp); /* this is the Cell Name */
    fputs(";", fp);
    if(Lind==1)
    {
        fputs("\nL CPS;", fp);
    }
    else if(Lind==2)
    {
        fputs("\nL CPT;", fp);
    }
    fputs("\nP", fp);
}

```

```

else
{
    scale=1.0;
    dxfHeader(fp);
    if(Lind==1)
    {
        fprintf(fp, "\nPOLY_1");
    }
    else
    {
        fprintf(fp, "\nPOLY_2");
    }
    fprintf(fp, "\n100");
    fprintf(fp, "\nAcDbPolyline");
    fprintf(fp, "\n 90");
    if(Rd<Rb)
    {
        fprintf(fp, "\n          %d", (2*NumP+20+2)*Nd);
    }
    else
    {
        fprintf(fp, "\n          %d", (2*NumP+20)*Nd);
    }
    fprintf(fp, "\n 70");
    fprintf(fp, "\n      1");
    fprintf(fp, "\n 43");
    fprintf(fp, "\n0.0");
}

/* The functions here give the beginning and end points */
/*   for the involute functions                          */
/* This checks if the dedendum is below the base circle */
if (Rd<Rb)
{
    /* If dedendum is below the base circle, the curve starts at zero, */
    /* straight lines will later connect the involute to the dedendum circle */
    Min=0.0;
}
else
{
    /* If the base circle is below the dedendum calculate the starting point */
    Min=sqrt(pow((Rp-Ded)/Rb,2.0)-1.0);
}
Max=sqrt(pow((Rp+Add)/Rb,2.0)-1.0); /* Sets endpoint of Involute path */

t=(Max-Min)/(NumP); /* Incremental variable for generating involute curve */
/* t updates Phi */
ST=sqrt(pow((Rp/Rb),2.0)-1.0); /* There is some rotation if the */
/* Base circle is below the dedendum */
/* This adjusts for that */

X=Rb*(cos(ST)+ST*sin(ST));
Y=Rb*(sin(ST)-ST*cos(ST));
Omega=Gamma+atan(Y/X); /* Omega is the complete initial rotation of the */
/* first tooth */

```

```

Phi=Min; /* Parametric variable used to generate the involute */

for(j=0;j<Nd;j++)
{
  /* This sets up the Rotation Matrix for the Gear Teeth */
  RM11=cos(Theta); /* |RM11 RM12| |CM11 CM12| */
  RM12=-sin(Theta); /* |RM21 RM22| |CM21 CM22| */
  RM21=sin(Theta);
  RM22=cos(Theta);

  Phi=Min; /*0.0;*/
  /* This is the correction matrix that accounts for any initial
     rotations*/
  CM11=cos(-Omega);
  CM12=-sin(-Omega);
  CM21=sin(-Omega);
  CM22=cos(-Omega);
  if(Rd<Rb)
  {
    X=Rd;
    Y=0.0;
    X1=RM11*X+RM12*Y;
    Y1=RM21*X+RM22*Y;
    X=CM11*X1+CM12*Y1;
    Y=CM21*X1+CM22*Y1;
    if (Ftype==1)
    {
      fprintf(fp, "\n%.01f,%.01f", scale*X, scale*Y);
    }
    else
    {
      //fprintf(fp, "\n%lf,%lf", scale*X, scale*Y);
      fprintf(fp, "\n10");
      fprintf(fp, "\n%.4lf", scale*X);
      fprintf(fp, "\n20");
      fprintf(fp, "\n%.4lf", scale*Y);
    }
  }
}

for (i=0;i<NumP;i++)
{
  X=Rb*(cos(Phi)+Phi*sin(Phi));
  Y=Rb*(sin(Phi)-Phi*cos(Phi));
  X1=RM11*X+RM12*Y;
  Y1=RM21*X+RM22*Y;
  X=CM11*X1+CM12*Y1;
  Y=CM21*X1+CM22*Y1;
  Phi=Phi+t;
  if (Ftype==1)
  {
    fprintf(fp, "\n%.01f,%.01f", scale*X, scale*Y);
  }
  else
  {
    //fprintf(fp, "\n%lf,%lf", scale*X, scale*Y);
    fprintf(fp, "\n10");
    fprintf(fp, "\n%.4lf", scale*X);
    fprintf(fp, "\n20");
    fprintf(fp, "\n%.4lf", scale*Y);
  }
}

```

```

    }
}
Phi=Phi-t;
CM11=cos(Omega);
CM12=-sin(Omega);
CM21=sin(Omega);
CM22=cos(Omega);

for (i=NumP;i>0;i--)
{
    X=Rb*(cos(-(Phi))+(-Phi)*sin(-(Phi)));
    Y=Rb*(sin(-(Phi))-(-Phi)*cos(-(Phi)));
    Xu=RM11*X+RM12*Y;
    Yu=RM21*X+RM22*Y;
    X=CM11*Xu+CM12*Yu;
    Y=CM21*Xu+CM22*Yu;
    Phi=Phi-t;
    if (Ftype==1)
    {
        fprintf(fp,"\n%.01f,%.01f",scale*X,scale*Y);
    }
    else
    {
        //fprintf(fp,"\n%lf,%lf",scale*X,scale*Y);
        fprintf(fp,"\n10");
        fprintf(fp,"\n%.4lf",scale*X);
        fprintf(fp,"\n20");
        fprintf(fp,"\n%.4lf",scale*Y);
    }
}
ifb)
{
    X=Rd;
    Y=0.0;
    Xu=RM11*X+RM12*Y;
    Yu=RM21*X+RM22*Y;
    X=CM11*Xu+CM12*Yu;
    Y=CM21*Xu+CM22*Yu;

    if (Ftype==1)
    {
        fprintf(fp,"\n%.01f,%.01f",scale*X,scale*Y);
    }
    else
    {
        //fprintf(fp,"\n%lf,%lf",scale*X,scale*Y);
        fprintf(fp,"\n10");
        fprintf(fp,"\n%.4lf",scale*X);
        fprintf(fp,"\n20");
        fprintf(fp,"\n%.4lf",scale*Y);
    }
    }
    Theta=Theta+THDiff;
}

/* This makes the hub hollow */
if(Rd<Rb)
{
    Rh=Rd-4.0;

```

```

        }
        else
        {
                Rh=Rb-4.0;
        }
        t=Gamma-(N-Nd+1)*THDiff+InitRot*M_PI/180.0;
        for (j=0; j<Nd*20; j++)
        {
                X=Rh*cos(t);
                Y=Rh*sin(t);
                if (Ftype==1)
        {
                fprintf(fp, "\n%.01f,%.01f", scale*X, scale*Y);
        }
        else
        {
                //fprintf(fp, "\n%.1f,%.1f", scale*X, scale*Y);
                fprintf(fp, "\n10");
                fprintf(fp, "\n%.4lf", scale*X);
                fprintf(fp, "\n20");
                fprintf(fp, "\n%.4lf", scale*Y);
        }
                t=t-((Nd-1)*THDiff+2.0*Gamma)/(20.0*Nd);
        }
        if (Ftype==1)
        {
                fprintf(fp, "\nDF;\nE");
        }
        else
        {
                fprintf(fp, "\n0");
                fprintf(fp, "\nENDSEC");
                fprintf(fp, "\n0");
                fprintf(fp, "\nEOF\n");
        }
        return(1);
}

int GearInput(FILE *in, double *PA, int *N, int *Nd, double *Bklsh, double *P,
              int *Lind,
              double *InitRot, double *DedRat)
{
        char Layer[10], filetype[3], Temp[64], *endptr;

        printf("\nEnter Pressure Angle (20 degrees): ");
        fgets(Temp, 10, in);
        if (strlen(Temp)==1)
        {
                *PA=20.0;
        }
        else
        {
                *PA=strtod(Temp, &endptr);
        }
        printf("Enter Number of Teeth on Full Gear (18): ");
        fgets(Temp, 10, in);

```

```

if (strlen(Temp)==1)
{
    *N=18.0;
/*    printf("Yes");*/
}
else
{
    *N=strtod(Temp,&endptr);
}

    do{
        printf("Enter Desired Number of Teeth <=%d (%d):
                ",*N,*N);
        fgets(Temp,10,in);
        if (strlen(Temp)==1)
        {
            *Nd=*N;
        }
        else
        {
            *Nd=strtod(Temp,&endptr);
        }
        }while(*Nd>*N);
        printf("Enter Diametral Pitch (Teeth/micron) (.2): ");
fgets(Temp,10,in);
if (strlen(Temp)==1)
{
    *P=.2;
}
else
{
    *P=strtod(Temp,&endptr);
}
        printf("Enter Desired Tooth Clearance (2.5): ");
fgets(Temp,10,in);
if (strlen(Temp)==1)
{
    *Bklsh=2.5;
}
else
{
    *Bklsh=strtod(Temp,&endptr);
}
*Bklsh=*Bklsh/2.0;

        printf("Enter Dedendum Ratio (1.35 for 2um clearance): ");
fgets(Temp,10,in);
if (strlen(Temp)==1)
{
    *DedRat=1.35;
}
else
{
    *DedRat=strtod(Temp,&endptr);
}

    do{
        *Lind=0;
        printf("Select Layer Poly");
        textcolor(14);

```

```

        cprintf(                "1");
        textcolor(15);
        printf(                  "/ (Poly)");
        textcolor(14);
        cprintf(                  "2");
        textcolor(15);
        printf(                  "): ");
        fgets(Temp,6,in);
        if(strlen(Temp)==1)
        {
            *Lind=2;
            break;
        }
        strncpy(Layer, Temp,strlen(Temp)-1);
        if(!strcmp(Temp,"poly1",5) || !strcmp(Temp,"Poly1",5)
            || !strcmp(Temp,"POLY1",5) || !strcmp(Temp,"poly 1",6)
            || !strcmp(Temp,"Poly 1",6) || !strcmp(Temp,"POLY 1",6)
            || !strcmp(Temp,"p1",2) || !strcmp(Temp,"p 1",3)
            || !strcmp(Temp,"P1",2) || !strcmp(Temp,"P 1",3)
            || !strcmp(Temp,"1",1))
        {
            *Lind=1;
        }
        else
        {
            if(!strcmp(Temp,"poly2",5) || !strcmp(Temp,"Poly2",5)
                || !strcmp(Temp,"POLY2",5) || !strcmp(Temp,"poly 2",6)
                || !strcmp(Temp,"Poly 2",6) || !strcmp(Temp,"POLY 2",6)
                || !strcmp(Temp,"p2",2) || !strcmp(Temp,"p 2",3)
                || !strcmp(Temp,"P2",2) || !strcmp(Temp,"P 2",3)
                || !strcmp(Temp,"2",1))
            {
                *Lind=2;
            }
        }
        }while (*Lind==0);
        printf("Enter Initial Rotation (0.0 degrees): ");
        fgets(Temp,10,in);
        if (strlen(Temp)==1)
        {
            *InitRot=0.0;
        }
        else
        {
            *InitRot=strtod(Temp,&endptr);
        }
        return 1;
    }
}

```

```

/* This function generates the header for MUMPS technology CIF file */
int cifHeader(FILE *fp)
{
    fputs("CIF FILE",fp );
    fputs( "\n(CIF written by the Tanner Research layout editor, L-Edit);", fp);
    fputs( "\n(Version: 6.02);", fp);
    fputs( "\n(TECHNOLOGY: MUMPS~V1.00);", fp);
    fputs( "\n(DATE: 24 Feb 99);", fp);
}

```

```

fputs( "\n(FABCELL: NONE);", fp);
fputs( "\n(L-Edit Layer POLY0 = CIF Layer CPZ);", fp);
fputs( "\n(L-Edit Layer HOLE 0 = CIF Layer CHZ);", fp);
fputs( "\n(L-Edit Layer ANCHOR1 = CIF Layer COF);", fp);
fputs( "\n(L-Edit Layer DIMPLE = CIF Layer COS);", fp);
fputs( "\n(L-Edit Layer POLY1 = CIF Layer CPS);", fp);
fputs( "\n(L-Edit Layer HOLE1 = CIF Layer CHO);", fp);
fputs( "\n(L-Edit Layer POLY1_POLY2_VIA = CIF Layer COT);", fp);
fputs( "\n(L-Edit Layer ANCHOR2 = CIF Layer COL);", fp);
fputs( "\n(L-Edit Layer POLY2 = CIF Layer CPT);", fp);
fputs( "\n(L-Edit Layer HOLE2 = CIF Layer CHT);", fp);
fputs( "\n(L-Edit Layer METAL = CIF Layer CCM);", fp);
fputs( "\n(L-Edit Layer HOLE METAL = CIF Layer CHM);", fp);
fputs( "\n(L-Edit Layer METAL2 = CIF Layer CMB);", fp);
fputs( "\n(L-Edit Layer MPT = CIF Layer MPT);", fp);
fputs( "\n(L-Edit Layer New Layer 1 = CIF Layer LAY1);", fp);
fputs( "\n(L-Edit Layer New Layer 2 = CIF Layer LAY2);", fp);
fputs( "\n(L-Edit Layer New Layer 3 = CIF Layer LAY3);", fp);
fputs( "\n(L-Edit Layer New Layer 4 = CIF Layer LAY4);", fp);
fputs( "\n(L-Edit Layer New Layer 5 = CIF Layer LAY5);", fp);
fputs( "\n(L-Edit Layer New Layer 6 = CIF Layer LAY6);", fp);
fputs( "\n(L-Edit Layer New Layer 7 = CIF Layer LAY7);", fp);
fputs( "\n(L-Edit Layer New Layer 8 = CIF Layer LAY8);", fp);
fputs( "\n(L-Edit Layer New Layer 9 = CIF Layer LAY9);", fp);
fputs( "\n(L-Edit Layer New Layer 10 = CIF Layer LAY10);", fp);
fputs( "\n(L-Edit Layer CHO = CIF Layer CHO);", fp);
fputs( "\n(L-Edit Layer CHT = CIF Layer CHT);", fp);
fputs( "\n(L-Edit Layer Icon/Outline = CIF Layer XP);", fp);
fputs( "\n(SCALING: 1 CIF Unit = 1/2000 Lambda, 1 Lambda = 1/1 Microns);",
      fp);
fputs( "\nDS 1 2 40;", fp);
fputs( "\n9 ", fp);
/*   fprintf(fp, "\n0");   */           /* This Sets up for a PolyLine
      */
/*   fprintf(fp, "\nPOLYLINE");
  fprintf(fp, "\n8");
  fprintf(fp, "\nPOLY_2");
  fprintf(fp, "\n6");
  fprintf(fp, "\nCONTINUOUS");
  fprintf(fp, "\n70");
  fprintf(fp, "\n1"); */
return 1;
}

int dxfHeader(FILE *fp)
{
  /* This is the Header for an AutoCAD DXF file */

  fprintf(fp, "0");           /* Open New Section */
  fprintf(fp, "\nSECTION");

  fprintf(fp, "\n2");           /* Open Header Section */
  fprintf(fp, "\nHEADER");

  fprintf(fp, "\n 9");
  fprintf(fp, "\n$CLAYER");     /* Sets Current Layer */
  fprintf(fp, "\n 8");
  fprintf(fp, "\n0");

```



```

        fprintf(fp, "\n 9");          /* Sets Length Units */
        fprintf(fp, "\n$LUNITS");
        fprintf(fp, "\n 70");
        fprintf(fp, "\n2");

        fprintf(fp, "\n 9");          /* Sets Length Precision*/
        fprintf(fp, "\n$LUPREC");
        fprintf(fp, "\n 70");
        fprintf(fp, "\n4");

fprintf(fp, "\n 0");          /* Close Header Section */
fprintf(fp, "\nENDSEC");

fprintf(fp, "\n0");          /* Open New Section */
fprintf(fp, "\nSECTION");

        fprintf(fp, "\n 2");          /* Open Table Section */
        fprintf(fp, "\nTABLES");
        fprintf(fp, "\n 0");
        fprintf(fp, "\nTABLE");      /* Opens New Table */
        fprintf(fp, "\n 2");
        fprintf(fp, "\nLAYER");
        fprintf(fp, "\n 5");
        fprintf(fp, "\n2");
        fprintf(fp, "\n100");
        fprintf(fp, "\nAcDbSymbolTable");
        fprintf(fp, "\n 70");
        fprintf(fp, "\n 3");
        fprintf(fp, "\n 0");
        fprintf(fp, "\nLAYER");
        fprintf(fp, "\n 5");
        fprintf(fp, "\nF");
        fprintf(fp, "\n100");
        fprintf(fp, "\nAcDbSymbolTableRecord");
        fprintf(fp, "\n100");
        fprintf(fp, "\nAcDbLayerTableRecord");
        fprintf(fp, "\n 2");
        fprintf(fp, "\n0");
        fprintf(fp, "\n 70");
        fprintf(fp, "\n 0");
        fprintf(fp, "\n 62");
        fprintf(fp, "\n 7");
        fprintf(fp, "\n 6");
        fprintf(fp, "\nCONTINUOUS");
        fprintf(fp, "\n 0");
        fprintf(fp, "\nLAYER");
        fprintf(fp, "\n 5");
        fprintf(fp, "\n4F");
        fprintf(fp, "\n100");
        fprintf(fp, "\nAcDbSymbolTableRecord");
        fprintf(fp, "\n100");
        fprintf(fp, "\nAcDbLayerTableRecord");
        fprintf(fp, "\n 2");
        fprintf(fp, "\nPOLY_1");
        fprintf(fp, "\n 70");
        fprintf(fp, "\n 0");
        fprintf(fp, "\n 62");
        fprintf(fp, "\n 173");
        fprintf(fp, "\n 6");

```

```

    fprintf(fp, "\nCONTINUOUS");
    fprintf(fp, "\n 0");
    fprintf(fp, "\nLAYER");
    fprintf(fp, "\n 5");
    fprintf(fp, "\n50");
    fprintf(fp, "\n100");
    fprintf(fp, "\nAcDbSymbolTableRecord");
    fprintf(fp, "\n100");
    fprintf(fp, "\nAcDbLayerTableRecord");
    fprintf(fp, "\n 2");
    fprintf(fp, "\nPOLY_2");
    fprintf(fp, "\n 70");
    fprintf(fp, "\n 0");
    fprintf(fp, "\n 62");
    fprintf(fp, "\n 1");
    fprintf(fp, "\n 6");
    fprintf(fp, "\nCONTINUOUS");
    fprintf(fp, "\n 0");
    fprintf(fp, "\nENDTAB");

fprintf(fp, "\n0");          /* End Section          */
fprintf(fp, "\nENDSEC");

fprintf(fp, "\n0");          /* Opens new section    */
fprintf(fp, "\nSECTION");

    fprintf(fp, "\n2");          /* Opens New Entities   */
    fprintf(fp, "\nENTITIES");
        /* This is to be used in the generation of poylines      */

    fprintf(fp, "\n0");          /* PolyLine             */
    fprintf(fp, "\nLWPOLYLINE");
    fprintf(fp, "\n 5");
    fprintf(fp, "\n51");
    fprintf(fp, "\n 100");
    fprintf(fp, "\nAcDbEntity");
    fprintf(fp, "\n 8");
return 1;
}

int splash(void)
{
    printf("\n

    _____");
    printf("\n | Gear
    printf("\n | This program will generate involute profile gears for
    printf("\n | use in MEMS applications
    printf("\n |
    printf("\n |
    printf("\n | Copyright 1999 Compliant Mechanisms/MEMS Research Group
    printf("\n |
    printf("\n | "); /*Brigham Young University
    printf("\n | "); */
    textcolor(14);

```

```

cprintf(          "Brigham Young University");
textcolor(15);
printf(          "
cprintf("\r\n |");
cprintf("\r\n |   Written by Nathan Masters
cprintf("\r\n |");
cprintf("\r\n |   Gear Layouts may be output in CIF for Tanner L-Edit/
MEMS-Pro |");
cprintf("\r\n |   or AutoCad DXF for Sandia National Labs SUMMiT
Process |");
cprintf("\r\n |");
cprintf("\r\n |");
cprintf("\r\n |   See GearUse.pdf for further instructions
cprintf("\r\n |");
cprintf("\r\n |   or visit");
textcolor(14);
cprintf(          " www.et.byu.edu/~llhwww");
printf(          " for more MEMS/Compliant
|");
printf("\n |   Mechanisms information
|");
printf("\n |
|_____|\n\n\n");

textcolor(15);
return 1;
}

```

APPENDIX B *Beam Element Model for
Thermal Self-Retraktion*

This batch file was used for finite element analysis, using beam analysis to investigate thermal self-retraction.

```
/BATCH
! /COM,ANSYS RELEASE 5.5.3 UP19990405      11:45:47    12/07/2000
/input,start55,ans      ,/ansys55/docu/,,,,,,,,,,,,,1
!*
/NOPR
/PMETH,OFF
/PREP7

*set,pi,acos(-1)

/COM, INPUT *****
*set,l1,19e-4
*set,l2,19e-4
*set,l3,10e-4
*set,l5,10e-4

*set,h1,2e-4
*set,h2,2e-4
*set,h3,25e-4
*set,h4,9e-4

*set,w1,3.5e-4
*set,w2,3.5e-4
*set,w3,3.5e-4

*set,xoff,3.6e-4
*set,yoff,32e-4

*set,theta1,atan(yoff/xoff)
*set,theta2,theta1+pi
*set,theta2,theta1+pi

*set,ldiv1,20
*set,ldiv2,20
*set,ldiv3,10
*set,ldiv4,30

*set,LSDMax,20
*set,LSPause,10
*set,LSTMax,30
*set,PDisp,2.15
*set,BeamTemp,650
```

/COM, END OF INPUT *****

ET,1,BEAM3

R,1,w1*h1,w1*h1*h1*h1/12,h1,1.2, , ,
R,2,w2*h2,w2*h2*h2*h2/12,h2,1.2, , ,
R,3,w3*h3,w3*h3*h3*h3/12,h3,1.2, , ,
R,4,w3*h4,w3*h4*h4*h4/12,h4,1.2, , ,

UIMP,1,EX, , ,1.69e12,
UIMP,1,DENS, , , ,
UIMP,1,ALPX, , ,2.7e-6,
UIMP,1,REFT, , , ,
UIMP,1,NUXY, , , ,
UIMP,1,PRXY, , , ,
UIMP,1,GXY, , , ,
UIMP,1,MU, , , ,
UIMP,1,DAMP, , , ,
UIMP,1,KXX, , , ,
UIMP,1,C, , , ,
UIMP,1,ENTH, , , ,
UIMP,1,HF, , , ,
UIMP,1,EMIS, , , ,
UIMP,1,QRATE, , , ,
UIMP,1,RSVX, , , ,

k,1,0,0
k,2,11*cos(theta1),11*sin(theta1)
k,3,11*cos(theta1)+13*sin(theta1),11*sin(theta1)-13*cos(theta1)
k,4,-xoff+12*cos(theta2)+15*sin(theta1),-yoff+12*sin(theta2)-13*cos(theta1)
k,5,-xoff+12*cos(theta2),-yoff+12*sin(theta2)
k,6,-xoff,-yoff

l,1,2,ldiv1
l,2,3,ldiv3
l,3,4,ldiv4
l,4,5,ldiv3
l,5,6,ldiv2

type,1
mat,1

real,1
lmesh,1

real,4
lmesh,2

real,3
lmesh,3

real,4
lmesh,4

real,2
lmesh,5
/shrink,.5
FINISH

/SOLU

```

nlgeom,1
NROPT,AUTO, ,
LUMPM,0
EQSLV, , ,0,
PREC,0
PIVCHECK,1
SSTIF
PSTRES
TOFFST,0,

dk,1,ux,0
dk,1,uy,0
dk,1,rotz,0
dk,6,uy,0
dk,6,rotz,0

*SET,ii,0
*do,ii,1,LSDMax,1
dk,6,ux,ii*PDisp*xoff/(LSDMax-1)
lswrite,ii
*enddo

dkdel,6,ux
lswrite,LSDMax

*set,kk,0
*do,kk,1,LSPause+1,1
lswrite,LSDMax+kk
*enddo

/COM,FLST,2,2,4,ORDE,2
/COM,FITEM,2,1
/COM,FITEM,2,5

*set,jj,0

*do,jj,1,LSTMax,1
BFL,1,TEMP,jj*BeamTemp/(LSTMax-1)
BFL,5,TEMP,jj*BeamTemp/(LSTMax-1)
lswrite,LSDMax+LSPause+jj
*enddo

BFLDELE,1,TEMP
BFLDELE,2,TEMP
lswrite,LSDMax+LSPause+LSTMax

lssolve,1,LSDMax+LSPause+LSTMax,1
FINISH

/POST26
ksel,s,kp,,6
nslk,s
*get,nkp6,node,0,num,max
nsel,all
ksel,all
nsol,2,nkp6,u,x,ux
rforce,3,nkp6,f,x,fx
/output,ThermalRes_T650.txt

```

prvar, 2, 3
/output

SRFBM ANSYS Model Batch File

C.1 Geometry

The batch file included in this appendix and APPENDIX D generate the same geometry. Figure C-1 presents the user specified parameters and the geometry of the SRFBM. Radii of curvature, for use with the Pseudo-Rigid-Body Models are also included. To correctly generate this geometry keypoints are used, and then connected with lines and arcs (see Fig. C-2).

C.2 ANSYS Plane Element Batch File

A consistent set of units was selected for this and other modeling based on μm - μN -MPa.

Lengths, areas and volumes are all in terms of μm (or μm^2 or μm^3). Force is in terms of μN . Young's Modulus (and Stress) are in MPa (so for polysilicon use 165e3 for the modulus of elasticity). Strain energy (which is used as potential energy for these models is in $\mu\text{N}\cdot\text{nm}$). Mass is in mg and density in $\text{mg}/\mu\text{m}^3$. The units selected for mass and density allow the units of acceleration to remain m/s^2 . (Do not forget to divide by 9.81 $\text{g}/(\text{m}/\text{s}^2)$ if you want g's.)

```
/BATCH
! /COM,ANSYS RELEASE 5.5.3 UP19990405      11:22:12      01/29/2001
/input,start57,ans      ,/ansys55/docu/,,,,,,,,,,,,,1

/NOPR
/PMETH,OFF
```

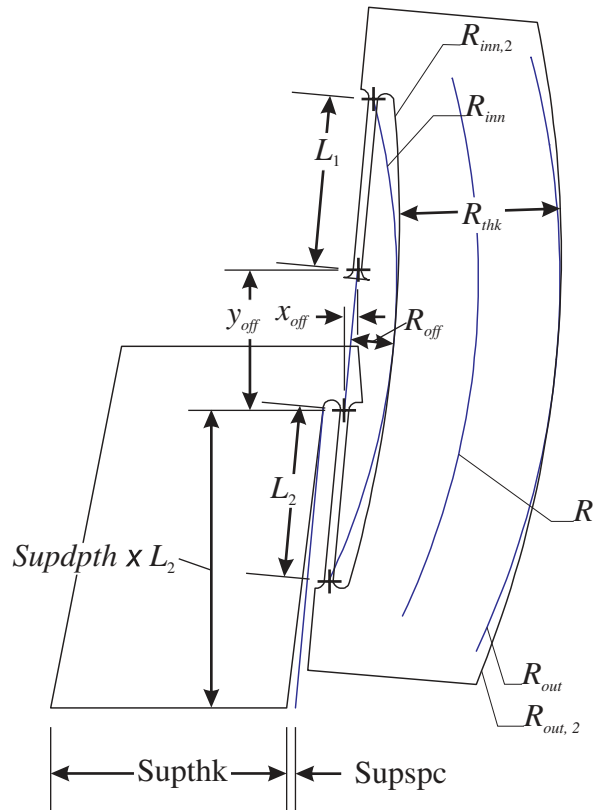


Figure C-1 Geometry of SRFBM for batch files. Only user specified parameters (and the radii of curvature for use in the PRBMs) are presented.

```

!KEYW,PR_SET,1
!KEYW,PR_STRUC,1
!KEYW,PR_THERM,0
!KEYW,PR_FLUID,0
!KEYW,PR_ELMAG,0
!KEYW,MAGNOD,0
!KEYW,MAGEDG,0
!KEYW,MAGHFE,0
!KEYW,MAGELC,0
!KEYW,PR_MULTII,0
!KEYW,PR_CFD,0
/GO

```

! User supplied Parameters

```

*SET,xoff,3.9
*SET,yoff,35
*set,smsize,0

```

```

*SET,h1,2
*SET,h2,2
!*SET,h3,18

```

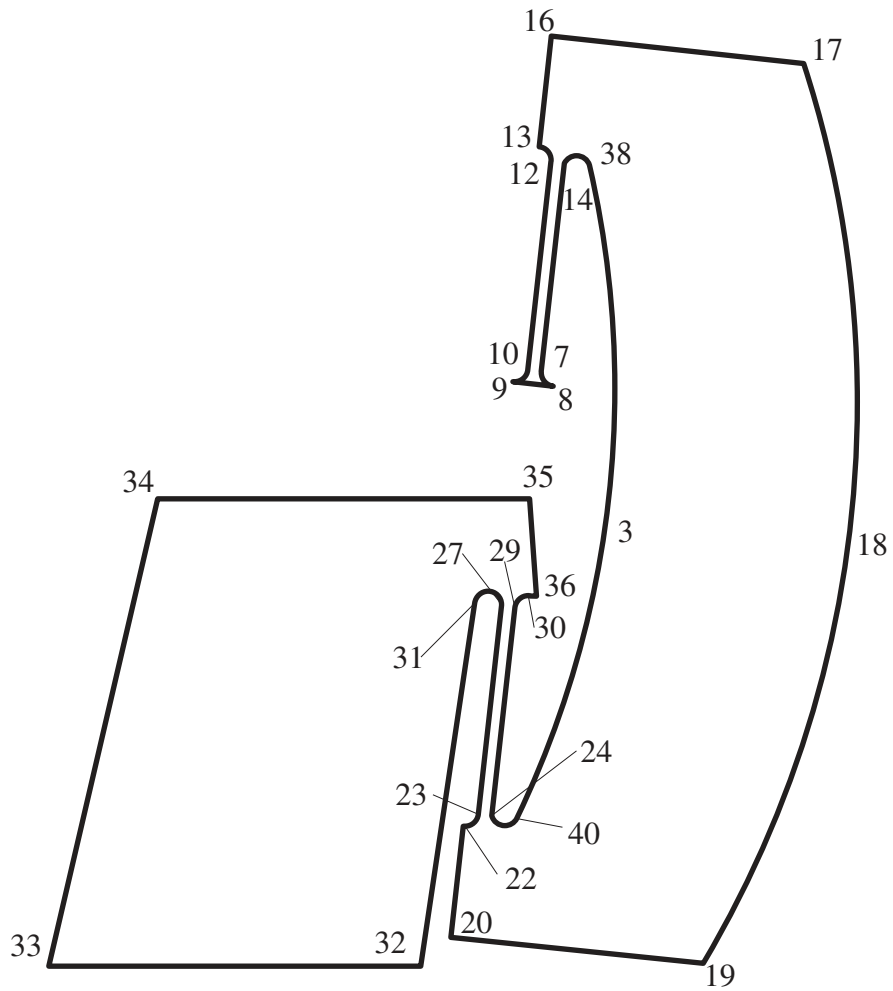


Figure C-2 SRFBM keypoint numbers and locations

```

!*SET,h4,35
*set,Roff,13
*set,Rthk,36

*SET,11,31
*SET,12,31
!*SET,13,6
!*SET,14,13

*set,LSDMax,20
*set,LSPause,1
*set,RetMax,10

*set,PDisp,2.7

*set,Rcut,.83

```

```

*set,supdpth,1.8
*set,supspc,2.0
*set,supthk,55

*SET,theta1,atan(yoff/xoff)
*SET,pi,acos(-1)
*SET,theta2,theta1+pi/2
*SET,filrad,2
*set,horgn,sqrt((xoff/2)*(xoff/2)+(yoff/2)*(yoff/2))
!*set,hRinn,sqrt((xoff/2)*(xoff/2)+(yoff/2)*(yoff/2))+filrad+(l1+l2)/2
*set,hRinn,sqrt((xoff/2)*(xoff/2)+(yoff/2)*(yoff/2))+(l1+l2)/2
*set,Rinn,(Roff*Roff+hRinn*hRinn)/(2*Roff)
*set,Rout,Rinn+Rthk
!*set,Rtheta2,acos((Rinn-Roff+filrad+h1/2+Rcut*Rthk)/(Rout))
*set,Rtheta2,acos((Rinn-Roff+h1/2+Rcut*Rthk)/(Rout))
*set,hRout,Rout*sin(Rtheta2)

! /COM,Preferences for GUI filtering have been set to display:
! /COM, Structural

/PREP7
! These are user supplied material properties
ET,1,PLANE82

KEYOPT,1,3,3
KEYOPT,1,5,0
KEYOPT,1,6,0

! Young's Modulus (MPa)
! By Using MPa a consistent system of units based on microns can be used.

UIMP,1,EX,, , ,165e3,
UIMP,1,DENS,, , , ,
UIMP,1,ALPX,, , , ,
UIMP,1,REFT,, , , ,
UIMP,1,NUXY,, , , ,
! Poisson's Ratio
UIMP,1,PRXY,, , ,.23,
UIMP,1,GXY,, , , ,
UIMP,1,MU,, , , ,
UIMP,1,DAMP,, , , ,

! This is the out-of-plane thickness of the material
R,1,3.5,

!/BATCH

k,1,0,0
k,2,l1*cos(theta1),l1*sin(theta1)
k,3,-xoff/2-Roff*cos(theta2),-yoff/2-Roff*sin(theta2)
k,4,-xoff-l2*cos(theta1),-yoff-l2*sin(theta1)
k,5,-xoff,-yoff

```

```

k,6,-filrad*cos(theta1),-filrad*sin(theta1)
k,7,-h1/2*cos(theta2),-h1/2*sin(theta2)
k,8,-filrad*cos(theta1)-(h1/2+filrad)*cos(theta2),-filrad*sin(theta1)-(h1/
2+filrad)*sin(theta2)
k,9,-filrad*cos(theta1)+(h1/2+filrad)*cos(theta2),-filrad*sin(theta1)+(h1/
2+filrad)*sin(theta2)
k,10,h1/2*cos(theta2),h1/2*sin(theta2)
k,11,(l1+filrad)*cos(theta1),(l1+filrad)*sin(theta1)
k,12,l1*cos(theta1)+h1/2*cos(theta2),l1*sin(theta1)+h1/2*sin(theta2)
k,13,(l1+filrad)*cos(theta1)+(h1/
2+filrad)*cos(theta2),(l1+filrad)*sin(theta1)+(h1/
2+filrad)*sin(theta2)
k,14,l1*cos(theta1)-h1/2*cos(theta2),l1*sin(theta1)-h1/2*sin(theta2)
k,15,(l1+filrad)*cos(theta1)-(h1/2+filrad)*cos(theta2),(l1+filrad)*sin(theta1)-
(h1/2+filrad)*sin(theta2)
k,16,-xoff/2+(hRout)*cos(theta1)+(h1/2+filrad)*cos(theta2),-yoff/
2+(hRout)*sin(theta1)+(h1/2+filrad)*sin(theta2)
*set,temp1,h1/2+filrad+filrad*cos(Rtheta2)+Rthk*Rcut
*set,temp2,h1/2+filrad+filrad*sin(Rtheta2)+Rthk*Rcut
k,17,(hRout-horgn)*cos(theta1)-temp1*cos(theta2),(hRout-horgn)*sin(theta1)-
temp2*sin(theta2)
k,18,-xoff/2-(Roff+Rthk)*cos(theta2),-yoff/2-(Roff+Rthk)*sin(theta2)
*set,temp1,h2/2+filrad+filrad*cos(-Rtheta2)+Rthk*Rcut
*set,temp2,h2/2+filrad+filrad*sin(-Rtheta2)+Rthk*Rcut
k,19,-(hRout+horgn)*cos(theta1)-temp1*cos(theta2),-(hRout+horgn)*sin(theta1)-
temp2*sin(theta2)
k,20,-(hRout+horgn)*cos(theta1)+(h2/2+filrad)*cos(theta2),-
(hRout+horgn)*sin(theta1)+(h2/2+filrad)*sin(theta2)
k,21,-xoff-(l2+filrad)*cos(theta1),-yoff-(l2+filrad)*sin(theta1)
k,22,-xoff-(l2+filrad)*cos(theta1)+(h2/2+filrad)*cos(theta2),-yoff-
(l2+filrad)*sin(theta1)+(h2/2+filrad)*sin(theta2)
k,23,-xoff-l2*cos(theta1)+h2/2*cos(theta2),-yoff-l2*sin(theta1)+h2/2*sin(theta2)
k,24,-xoff-l2*cos(theta1)-h2/2*cos(theta2),-yoff-l2*sin(theta1)-h2/2*sin(theta2)
k,25,-xoff-(l2+filrad)*cos(theta1)-(h2/2+filrad)*cos(theta2),-yoff-
(l2+filrad)*sin(theta1)-(h2/2+filrad)*sin(theta2)
k,26,-xoff+filrad*cos(theta1),-yoff+filrad*sin(theta1)
k,27,-xoff+h2/2*cos(theta2),-yoff+h2/2*sin(theta2)
k,28,-xoff+filrad*cos(theta1)+(h2/2+filrad)*cos(theta2),-
yoff+filrad*sin(theta1)+(h2/2+filrad)*sin(theta2)
k,29,-xoff-h2/2*cos(theta2),-yoff-h2/2*sin(theta2)
k,30,-xoff+filrad*cos(theta1)-(h2/2+filrad)*cos(theta2),-
yoff+filrad*sin(theta1)-(h2/2+filrad)*sin(theta2)
k,31,-xoff+(h2/2+2*filrad)*cos(theta2),-yoff+(h2/2+2*filrad)*sin(theta2)
!k,31,-xoff+filrad*cos(theta1)+(h2/2+2*filrad)*cos(theta2)-1,-
yoff+filrad*sin(theta1)+(h2/2+2*filrad)*sin(theta2)
*set,temp1,-xoff+(filrad-supdpth*l2)*cos(theta1)+(h2/2+filrad)*cos(theta2)-
supspc*filrad
*set,temp2,-yoff+(filrad-supdpth*l2)*sin(theta1)+(h2/2+filrad)*sin(theta2)
k,32,temp1,temp2
*set,temp1,-xoff+(filrad-supdpth*l2)*cos(theta1)+(h2/2+filrad)*cos(theta2)-
supspc*filrad-supthk
*set,temp2,-yoff+(filrad-supdpth*l2)*sin(theta1)+(h2/2+filrad)*sin(theta2)
k,33,temp1,temp2
k,34,-xoff+filrad*cos(theta1)-(h2/2+filrad)*cos(theta2)-supthk,-(yoff/2+1.5)
k,35,-xoff+filrad*cos(theta1)-(h2/2+filrad)*cos(theta2),-(yoff/2+1.5)
k,36,-xoff+filrad*cos(theta1)-(h2/2+filrad)*cos(theta2)+1,-
yoff+filrad*sin(theta1)-(h2/2+filrad)*sin(theta2)
k,37,(l1)*cos(theta1)-(h1/2+filrad)*cos(theta2),(l1)*sin(theta1)-(h1/
2+filrad)*sin(theta2)

```

```

k,38,(l1)*cos(theta1)-(h1/
      2+filrad+filrad*cos(Rtheta2))*cos(theta2),(l1)*sin(theta1)-
      (h1/2+filrad+filrad*sin(Rtheta2))*sin(theta2)

k,39,-xoff-12*cos(theta1)-(h2/2+filrad)*cos(theta2),-yoff-12*sin(theta1)-(h2/
      2+filrad)*sin(theta2)
k,40,-xoff-12*cos(theta1)-(h2/2+filrad+filrad*cos(-Rtheta2))*cos(theta2),-yoff-
      12*sin(theta1)-(h2/2+filrad+filrad*cos(-
      Rtheta2))*sin(theta2)

l,8,9
larc,9,10,13,filrad
l,10,12
larc,12,13,9,filrad
l,13,16
l,16,17
larc,17,19,18
l,19,20
l,20,22
larc,22,23,28,filrad
l,23,27
larc,27,28,23,filrad
larc,28,31,23,filrad
!l,28,31
l,31,32
l,32,33
l,33,34
l,34,35
l,35,36
l,36,30
larc,30,29,25,filrad
l,29,24
larc,24,40,30,filrad
larc,40,38,3
larc,38,14,8,filrad
l,14,7
larc,7,8,15,filrad

AL,all
*if,smsize,eq,0,:nossiz
SMRTSIZE,smsize
:nossiz
AMESH,1

fini
/SOLU

nlgeom,1
NROPT,AUTO, ,
LUMP,0
EQSLV, , ,0,
PREC,0
PIVCHECK,1
SSTIF
PSTRES
TOFFST,0,

```

```

dl,1,,ux,0
dl,1,,uy,0
!dl,15,,uy,0
dl,15,,SYMM

*SET,ii,0
*do,ii,1,LSDMax,1
!dldele,15,ux
!dldele,17,ux
!dl,15,,ux,ii*PDisp*xoff/(LSDMax-1)
dk,33,ux,ii*PDisp*xoff/(LSDMax-1)
lswrite,ii
*enddo

!dldele,15,ux
dkdele,33,ux
lswrite,LSDMax

*set,kk,0
*do,kk,1,LSPause+1,1
lswrite,LSDMax+kk
*enddo

*set,jj,0

*do,jj,1,RetMax,1
!dldele,15,ux
!dldele,17,ux
!dl,15,,ux,PDisp*xoff*(1-jj/(RetMax-1))
dk,33,ux,PDisp*xoff*(1-jj/(RetMax-1))
lswrite,LSDMax+LSPause+jj
*enddo
!dldele,15,ux
dkdele,33,ux
lswrite,LSDMax+LSPause+RetMax
*set,LSTMax,RetMax

lssolve,1,LSDMax+LSPause+LSTMax,1
FINISH

/post1
!set,24
!pldisp,1

*set,mm,0
*DIM,te,ARRAY,LSDMax+LSPause+LSTMax,4,
mm=1
set,mm
ETABLE,engry,SENE,
AVPRIN,0,0,
ssum
*GET,tot,SSUM,,ITEM,ENRGY

nset,all
NSORT,S,EQV,0,0,,
*get,MaxStrs,SORT,0,MAX

```

```

*get,MaxStNd,SORT,0,IMAX

ksel,s,kp,,33
nslk,s
*get,nkp33,node,0,num,max
*get,dux,node,nkp33,u,x
te(mm,1)=dux
te(mm,2)=tot
te(mm,3)=MaxStrs
te(mm,4)=MaxStNd

*do,mm,2,LSDMax+LSPause+LSTMax,1
set,mm
ETABLE,refl

ssum
*GET,tot,SSUM, ,ITEM,ENRGY

nset,all
NSORT,S,EQV,0,0,,
*set,MaxStrs,0
*set,MaxStNd,0
*get,MaxStrs,SORT,0,MAX
*get,MaxStNd,SORT,0,IMAX

ksel,s,kp,,33
nslk,s
*get,nkp33,node,0,num,max
*get,dux,node,nkp33,u,x

te(mm,1)=dux
te(mm,2)=tot
te(mm,3)=MaxStrs
te(mm,4)=MaxStNd

*enddo

/POST26
ksel,s,kp,,33
nslk,s
*get,nkp33,node,0,num,max
ksel,s,kp,,10
nslk,s
*get,nkp10,node,0,num,max
nset,all
ksel,all
nsol,2,nkp33,u,x,ux
rforce,3,nkp33,f,x,fx

ksel,all
nset,all
ksel,s,kp,,13
nslk,s
*get,nkp13,node,0,num,max

```



```

nsol,4,nkp13,u,x,ux13
nsol,5,nkp13,u,y,uy13

ksel,all
nsel,all
ksel,s,kp,,22
nslk,s
*get,nkp22,node,0,num,max
nsol,6,nkp22,u,x,ux22
nsol,7,nkp22,u,y,uy22

ksel,all
nsel,all
ksel,s,kp,,35
nslk,s
*get,nkp35,node,0,num,max
nsol,8,nkp35,u,x,ux35
nsol,9,nkp35,u,y,uy35
ksel,all
nsel,all

/output,AMout.txt
*stat
*stat,te
*stat,sts
prvar,2,3
!The following values are the nodal locations of several points on the
! C-beam and Slider Support. This allows evaluation of the total deflection
! of the C-beam.
prvar,4,5,6,7,8,9
/prep7
!These are the initial positions for the points on the C-beam and Slider Support.
! These are used with the deflections found above to calculate the deflections
klist,13
klist,22
klist,35

/output

```


D.1 Geometry

For a description of the geometry generated by this AutoLISP batch file see APPENDIX C. The keypoints all correspond, as do the user supplied parameters.

D.2 AutoLISP batch File

```

;Function definitions (these are not part of the LISP language)
(defun asin (ang) (atan (/ ang (sqrt (- 1 (* ang ang))))))
(defun acos (ang) (- (/ pi 2) (asin ang)))

;;-----
;; User Supplied Parameters
(setq xoff 3.0)      ;X-offset
(setq yoff 32.5)    ;Yoffset

(setq h1 2.0)       ;Tensural Pivot No.1 Width
(setq l1 40)        ;Tensural Pivot No.1 Length
(setq h2 2.0)       ;Tensural Pivot No.2 Width
(setq l2 40)        ;Tensural Pivot No.2 Length

(setq filrad 2.0)   ;Fillet radius

(setq Roff 10.0)    ;Offset of the Inner C-beam radius from line connecting TP
(setq Rthk 38.0)    ;Width of the C-beam
(setq Rcut 0.83)    ;Parameter to shorten the C-beam

(setq supdpth 1.8) ;Parameter determining the height of the shuttle support
(setq supspc 2)     ;Spacing of the Shuttle Support from the C-beam
(setq supthk 55)    ;Thickness of the Shuttle Support

;;End of User Supplied Parameters
;;-----
;;Calculated Parameters
(setq theta1 (atan (/ yoff xoff)))
(setq theta2 (+ theta1 (/ pi 2.0)))
(setq horgn (/ (sqrt (+ (* xoff xoff) (* yoff yoff))) 2.0))
(setq hRinn (+ horgn (/ (+ l1 l2) 2.0)))
(setq Rinn (/ (+ (* Roff Roff) (* hRinn hRinn)) (* 2.0 Roff)))
(setq Rout (+ Rinn Rthk))
(setq Rtheta2 (acos (/ (+ (- Rinn Roff) (/ h1 2.0) (* Rcut Rthk)) Rout)))
(setq hRout (* Rout (sin Rtheta2)))

```

```

;Keypoints--correspond to those used in the Ansys batch file
(setq k1 (list 0 0))
(setq k2 (list (* l1 (cos theta1)) (* l1 (sin theta1))))
(setq k3 (list (- 0 (/ xoff 2) (* Roff (cos theta2))) (- 0 (/ yoff 2) (* Roff
(sin theta2))))))
(setq k4 (list (- 0 xoff (* l2 (cos theta1))) (- 0 yoff (* l2 (sin theta1))))))
(setq k5 (list (- xoff) (- yoff)))
(setq k6 (list (- (* filrad (cos theta1))) (- (* filrad (sin theta1))))))
(setq k7 (list (- (* (/ h1 2) (cos theta2))) (- (* (/ h1 2) (sin theta2))) ) )
(setq k8 (list (- 0 (* filrad (cos theta1)) (* (+ (/ h1 2) filrad) (cos
theta2))) (- 0 (* filrad (sin theta1)) (* (+ (/ h1 2)
filrad) (sin theta2))))))
(setq k9 (list (- (* (+ (/ h1 2) filrad) (cos theta2)) (* filrad (cos theta1)))
(- (* (+ (/ h1 2) filrad) (sin theta2)) (* filrad (sin
theta1))))))
(setq k10 (list (* (/ h1 2) (cos theta2)) (* (/ h1 2) (sin theta2))))
(setq k11 (list (* (+ l1 filrad) (cos theta1)) (* (+ l1 filrad) (sin theta1))))
(setq k12 (list (+ (* l1 (cos theta1)) (* (/ h1 2) (cos theta2))) (+ (* l1 (sin
theta1)) (* (/ h1 2) (sin theta2))))))
(setq k13 (list (+ (* (+ l1 filrad) (cos theta1)) (* (+ (/ h1 2) filrad) (cos
theta2))) (+ (* (+ l1 filrad) (sin theta1)) (* (+ (/ h1 2)
filrad) (sin theta2))))))
(setq k14 (list (- (* l1 (cos theta1)) (* (/ h1 2) (cos theta2))) (- (* l1 (sin
theta1)) (* (/ h1 2) (sin theta2))))))
(setq k15 (list (- (* (+ l1 filrad) (cos theta1)) (* (+ (/ h1 2) filrad) (cos
theta2))) (- (* (+ l1 filrad) (sin theta1)) (* (+ (/ h1 2)
filrad) (sin theta2))))))
(setq k16 (list (- (+ (* hRout (cos theta1)) (* (+ (/ h1 2) filrad) (cos
theta2))) (/ xoff 2)) (- (+ (* hRout (sin theta1)) (* (+ (/
h1 2) filrad) (sin theta2))) (/ yoff 2))))
(setq temp1 (+ (/ h1 2) filrad (* filrad (cos Rtheta2)) (* Rthk Rcut)))
(setq temp2 (+ (/ h1 2) filrad (* filrad (sin Rtheta2)) (* Rthk Rcut)))
(setq k17 (list (- (* (- hRout horgn) (cos theta1)) (* temp1 (cos theta2))) (-
(* (- hRout horgn) (sin theta1)) (* temp2 (sin theta2))))))
(setq k18 (list (- 0 (/ xoff 2) (* (+ Roff Rthk) (cos theta2))) (- 0 (/ yoff 2)
(* (+ Roff Rthk) (sin theta2))))))
(setq temp1 (+ (/ h2 2) filrad (* filrad (cos (- Rtheta2))) (* Rthk Rcut)))
(setq temp2 (+ (/ h2 2) filrad (* filrad (sin (- Rtheta2))) (* Rthk Rcut)))
(setq k19 (list (- 0 (* (+ hRout horgn) (cos theta1)) (* temp1 (cos theta2))) (-
0 (* (+ hRout horgn) (sin theta1)) (* temp2 (sin theta2))))))
(setq k20 (list (- (* (+ (/ h2 2) filrad) (cos theta2)) (* (+ hRout horgn) (cos
theta1))) (- (* (+ (/ h2 2) filrad) (sin theta2)) (* (+
hRout horgn) (sin theta1))))))
(setq k21 (list (- 0 xoff (* (+ l2 filrad) (cos theta1))) (- 0 yoff (* (+ l2
filrad) (sin theta1))))))
(setq k22 (list (- (* (+ (/ h2 2) filrad) (cos theta2)) xoff (* (+ l2 filrad)
(cos theta1))) (- (* (+ (/ h2 2) filrad) (sin theta2)) yoff
(* (+ l2 filrad) (sin theta1))))))
(setq k23 (list (- (* (/ h2 2) (cos theta2)) xoff (* l2 (cos theta1))) (- (* (/
h2 2) (sin theta2)) yoff (* l2 (sin theta1))))))
(setq k24 (list (- 0 xoff (* l2 (cos theta1)) (* (/ h2 2) (cos theta2))) (- 0
yoff (* l2 (sin theta1)) (* (/ h2 2) (sin theta2))))))
(setq k25 (list (- 0 xoff (* (+ l2 filrad) (cos theta1)) (* (+ (/ h2 2) filrad)
(cos theta2))) (- 0 yoff (* (+ l2 filrad) (sin theta1)) (*
(+ (/ h2 2) filrad) (sin theta2))))))
(setq k26 (list (- (* filrad (cos theta1)) xoff) (- (* filrad (sin theta1))
yoff)))
(setq k27 (list (- (* (/ h2 2) (cos theta2)) xoff) (- (* (/ h2 2) (sin theta2))
yoff)))

```

```

(setq k28 (list (- (+ (* (+ (/ h2 2) filrad) (cos theta2)) (* filrad (cos
theta1))) xoff) (- (+ (* filrad (sin theta1)) (* (+ (/ h2 2)
filrad) (sin theta2)))) yoff)))
(setq k29 (list (- 0 xoff (* (/ h2 2) (cos theta2))) (- 0 yoff (* (/ h2 2) (sin
theta2)))))
(setq k30 (list (- (* filrad (cos theta1)) xoff (* (+ (/ h2 2) filrad) (cos
theta2))) (- (* filrad (sin theta1)) yoff (* (+ (/ h2 2)
filrad) (sin theta2)))))
(setq k31 (list (- (* (+ (/ h2 2) (* 2 filrad)) (cos theta2)) xoff) (- (* (+ (/
h2 2) (* 2 filrad)) (sin theta2)) yoff)))
(setq k32 (list (- (+ (* (- filrad (* supdpth l2)) (cos theta1)) (* (+ (/ h2 2)
(* 1 filrad)) (cos theta2))) xoff (* supspc filrad)) (- (+
(* (- filrad (* supdpth l2)) (sin theta1)) (* (+ (/ h2 2) (*
1 filrad)) (sin theta2))) yoff)))
(setq k33 (list (- (+ (* (- filrad (* supdpth l2)) (cos theta1)) (* (+ (/ h2 2)
(* 1 filrad)) (cos theta2))) xoff (* supspc filrad) supthk)
(- (+ (* (- filrad (* supdpth l2)) (sin theta1)) (* (+ (/ h2
2) (* 1 filrad)) (sin theta2))) yoff)))
(setq k34 (list (- (* filrad (cos theta1)) xoff (* (+ (/ h2 2) filrad) (cos
theta2)) supthk) (- 0 (/ yoff 2) 1.5)))
(setq k35 (list (- (* filrad (cos theta1)) xoff (* (+ (/ h2 2) filrad) (cos
theta2))) (- 0 (/ yoff 2) 1.5)))
(setq k36 (list (- (+ (* filrad (cos theta1)) (/ filrad 2)) xoff (* (+ (/ h2 2)
filrad) (cos theta2))) (- (* filrad (sin theta1)) yoff (* (+
(/ h2 2) filrad) (sin theta2)))))
(setq k37 (list (- (* l1 (cos theta1)) (* (+ (/ h1 2) filrad) (cos theta2))) (-
(* l1 (sin theta1)) (* (+ (/ h1 2) filrad) (sin theta2)))))
(setq k38 (list (- (* l1 (cos theta1)) (* (+ (/ h1 2) filrad (* filrad (cos
Rtheta2))) (cos theta2))) (- (* l1 (sin theta1)) (* (+ (/ h1
2) filrad (* filrad (sin Rtheta2))) (sin theta2)))))
(setq k39 (list (- 0 xoff (* l2 (cos theta1)) (* (+ (/ h2 2) filrad) (cos
theta2))) (- 0 yoff (* l2 (sin theta1)) (* (+ (/ h2 2)
filrad) (sin theta2)))))
(setq k40 (list (- 0 xoff (* l2 (cos theta1)) (* (+ (/ h2 2) filrad (* filrad
(cos (- Rtheta2)))) (cos theta2))) (- 0 yoff (* l2 (sin
theta1)) (* (+ (/ h2 2) filrad (* filrad (cos (- Rtheta2))))
(sin theta2)))))

```

```

;Geometry creation

```

```

(command "line" k8 k9 "")
(command "arc" k9 "R" filrad k10)
(command "line" k10 k12 "")
(command "arc" k12 "R" filrad k13)
(command "line" k13 k16 k17 "")
(command "arc" k17 k18 k19)
(command "line" k19 k20 k22 "")
(command "arc" k22 "R" filrad k23)
(command "line" k23 k27 "")
(command "arc" k27 "R" filrad k31)

(command "line" k31 k32 k33 k34 k35 k36 k30 "")
(command "arc" k30 "R" filrad k29)
(command "line" k29 k24 "")
(command "arc" k24 "R" filrad k40)
(command "arc" k40 k3 k38)
(command "arc" k38 "R" filrad k14)
(command "line" k14 k7 "")
(command "arc" k7 "R" filrad k8)

```

APPENDIX E *LIGA G-Switch ANSYS Batch File*

Due to the modifications to the geometry of the SRFBM necessitated by the design rules for the Sandia LIGA process, it was necessary to modify the ANSYS batch file to include the new geometry. Also additional loading conditions are needed to evaluate the behavior of the mechanism subject to inertial loads.

E.1 Displacement Loaded batch File

```
/BATCH
! /COM,ANSYS RELEASE 5.5.3 UP19990405      11:22:12      01/29/2001
/input,start57,ans      ,/ansys_inc/ansys57/docu/,,,,,,,,,,,,,1

/NOPR
/PMETH,OFF
!KEYW,PR_SET,1
!KEYW,PR_STRUC,1
!KEYW,PR_THERM,0
!KEYW,PR_FLUID,0
!KEYW,PR_ELMAG,0
!KEYW,MAGNOD,0
!KEYW,MAGEDG,0
!KEYW,MAGHFE,0
!KEYW,MAGELC,0
!KEYW,PR_MULTI,0
!KEYW,PR_CFD,0
/GO

*SET,xoff,28
*SET,yoff,860
*set,smsize,5

*SET,h1,20
*SET,h2,20
!*SET,h3,18
```

```

!*SET,h4,35
*set,Roff,200
*set,Rthk,850

*SET,11,1100
*SET,12,1100
!*SET,13,6
!*SET,14,13

*set,LSDMax,20
*set,LSPause,1
*set,RetMax,10

*set,PDisp,3.2

*set,Rcut,.9
*SET,theta1,atan(yoff/xoff)
*SET,pi,acos(-1)
*SET,theta2,theta1+pi/2
*SET,filrad,40
*set,horgn,sqrt((xoff/2)*(xoff/2)+(yoff/2)*(yoff/2))
!*set,hRinn,sqrt((xoff/2)*(xoff/2)+(yoff/2)*(yoff/2))+filrad+(11+12)/2
*set,hRinn,sqrt((xoff/2)*(xoff/2)+(yoff/2)*(yoff/2))+filrad+(11+12)/2
*set,Rinn,(Roff*Roff+hRinn*hRinn)/(2*Roff)
*set,Rout,Rinn+Rthk
!*set,Rtheta2,acos((Rinn-Roff+filrad+h1/2+Rcut*Rthk)/(Rout))
*set,Rtheta2,acos((Rinn-Roff+h1/2+Rcut*Rthk)/(Rout))
*set,hRout,Rout*sin(Rtheta2)
*set,supdpth,1.5
*set,supspc,2.0
*set,supthk,850

! /COM,Preferences for GUI filtering have been set to display:
! /COM, Structural

/PREP7

ET,1,PLANE82

KEYOPT,1,3,3
KEYOPT,1,5,0
KEYOPT,1,6,0

UIMP,1,EX,,207e3,
UIMP,1,DENS,,,,
UIMP,1,ALPX,,,,
UIMP,1,REFT,,,,
UIMP,1,NUXY,,,,
UIMP,1,PRXY,,,,.3,
UIMP,1,GXY,,,,
UIMP,1,MU,,,,
UIMP,1,DAMP,,,,

R,1,1000,

!/BATCH

```



```

k,1,0,0
k,2,l1*cos(theta1),l1*sin(theta1)
k,3,-xoff/2-Roff*cos(theta2),-yoff/2-Roff*sin(theta2)
k,4,-xoff-l2*cos(theta1),-yoff-l2*sin(theta1)
k,5,-xoff,-yoff

k,6,-filrad*cos(theta1),-filrad*sin(theta1)
k,7,-h1/2*cos(theta2),-h1/2*sin(theta2)
k,8,-filrad*cos(theta1)-(h1/2+filrad)*cos(theta2),-filrad*sin(theta1)-(h1/
2+filrad)*sin(theta2)
k,9,-filrad*cos(theta1)+(h1/2+filrad)*cos(theta2),-filrad*sin(theta1)+(h1/
2+filrad)*sin(theta2)
k,10,h1/2*cos(theta2),h1/2*sin(theta2)
k,11,(l1+filrad)*cos(theta1),(l1+filrad)*sin(theta1)
k,12,l1*cos(theta1)+h1/2*cos(theta2),l1*sin(theta1)+h1/2*sin(theta2)
k,13,(l1+filrad)*cos(theta1)+(h1/
2+filrad)*cos(theta2),(l1+filrad)*sin(theta1)+(h1/
2+filrad)*sin(theta2)
k,14,l1*cos(theta1)-h1/2*cos(theta2),l1*sin(theta1)-h1/2*sin(theta2)
k,15,(l1+filrad)*cos(theta1)-(h1/2+filrad)*cos(theta2),(l1+filrad)*sin(theta1)-
(h1/2+filrad)*sin(theta2)
k,16,-xoff/2+(hRout)*cos(theta1)+(h1/2+filrad)*cos(theta2),-yoff/
2+(hRout)*sin(theta1)+(h1/2+filrad)*sin(theta2)
*set,temp1,h1/2+filrad+filrad*cos(Rtheta2)+Rthk*Rcut
*set,temp2,h1/2+filrad+filrad*sin(Rtheta2)+Rthk*Rcut
k,17,(hRout-horgn)*cos(theta1)-temp1*cos(theta2),(hRout-horgn)*sin(theta1)-
temp2*sin(theta2)
k,18,-xoff/2-(Roff+Rthk)*cos(theta2),-yoff/2-(Roff+Rthk)*sin(theta2)
*set,temp1,h2/2+filrad+filrad*cos(-Rtheta2)+Rthk*Rcut
*set,temp2,h2/2+filrad+filrad*sin(-Rtheta2)+Rthk*Rcut
k,19,-(hRout+horgn)*cos(theta1)-temp1*cos(theta2),-(hRout+horgn)*sin(theta1)-
temp2*sin(theta2)
k,20,-(hRout+horgn)*cos(theta1)+(h2/2+filrad)*cos(theta2),-
(hRout+horgn)*sin(theta1)+(h2/2+filrad)*sin(theta2)
k,21,-xoff-(l2+filrad)*cos(theta1),-yoff-(l2+filrad)*sin(theta1)
k,22,-xoff-(l2+filrad)*cos(theta1)+(h2/2+filrad)*cos(theta2),-yoff-
(l2+filrad)*sin(theta1)+(h2/2+filrad)*sin(theta2)
k,23,-xoff-l2*cos(theta1)+h2/2*cos(theta2),-yoff-l2*sin(theta1)+h2/2*sin(theta2)
k,24,-xoff-l2*cos(theta1)-h2/2*cos(theta2),-yoff-l2*sin(theta1)-h2/2*sin(theta2)
k,25,-xoff-(l2+filrad)*cos(theta1)-(h2/2+filrad)*cos(theta2),-yoff-
(l2+filrad)*sin(theta1)-(h2/2+filrad)*sin(theta2)
k,26,-xoff+filrad*cos(theta1),-yoff+filrad*sin(theta1)
k,27,-xoff+h2/2*cos(theta2),-yoff+h2/2*sin(theta2)
k,28,-xoff+filrad*cos(theta1)+(h2/2+filrad)*cos(theta2),-
yoff+filrad*sin(theta1)+(h2/2+filrad)*sin(theta2)
k,29,-xoff-h2/2*cos(theta2),-yoff-h2/2*sin(theta2)
k,30,-xoff+filrad*cos(theta1)-(h2/2+filrad)*cos(theta2),-
yoff+filrad*sin(theta1)-(h2/2+filrad)*sin(theta2)
k,31,-xoff+(h2/2+2*filrad)*cos(theta2),-yoff+(h2/2+2*filrad)*sin(theta2)
!k,31,-xoff+filrad*cos(theta1)+(h2/2+2*filrad)*cos(theta2)-1,-
yoff+filrad*sin(theta1)+(h2/2+2*filrad)*sin(theta2)
*set,temp1,-xoff+(filrad-supdpth*l2)*cos(theta1)+(h2/2+filrad)*cos(theta2)-
supspc*filrad
*set,temp2,-yoff+(filrad-supdpth*l2)*sin(theta1)+(h2/2+filrad)*sin(theta2)
k,32,temp1,temp2
*set,temp1,-xoff+(filrad-supdpth*l2)*cos(theta1)+(h2/2+filrad)*cos(theta2)-
supspc*filrad-supthk

```

```

*set,temp2,-yoff+(filrad-supdpth*12)*sin(theta1)+(h2/2+filrad)*sin(theta2)
k,33,temp1,temp2
k,34,-xoff+filrad*cos(theta1)-(h2/2+filrad)*cos(theta2)-supthk,-(yoff/2+1.5)
k,35,-xoff+filrad*cos(theta1)-(h2/2+filrad)*cos(theta2),-(yoff/2+1.5)
k,36,-xoff+filrad*cos(theta1)-(h2/2+filrad)*cos(theta2)+filrad/2,-
      yoff+filrad*sin(theta1)-(h2/2+filrad)*sin(theta2)
k,37,(l1)*cos(theta1)-(h1/2+filrad)*cos(theta2),(l1)*sin(theta1)-(h1/
      2+filrad)*sin(theta2)
k,38,(l1)*cos(theta1)-(h1/
      2+filrad+filrad*cos(Rtheta2))*cos(theta2),(l1)*sin(theta1)-
      (h1/2+filrad+filrad*sin(Rtheta2))*sin(theta2)

k,39,-xoff-12*cos(theta1)-(h2/2+filrad)*cos(theta2),-yoff-12*sin(theta1)-(h2/
      2+filrad)*sin(theta2)
*set,temp1,-xoff-12*cos(theta1)-(h2/2+filrad+filrad*cos(-Rtheta2))*cos(theta2)
*set,temp2,-yoff-12*sin(theta1)-(h2/2+filrad+filrad*cos(-Rtheta2))*sin(theta2)
k,40,temp1,temp2

l,8,9
larc,9,10,13,filrad
l,10,12
larc,12,13,9,filrad
l,13,16
l,16,17
larc,17,19,18
l,19,20
l,20,22
larc,22,23,28,filrad
l,23,27
larc,27,28,23,filrad
larc,28,31,23,filrad
!l,28,31
l,31,32
l,32,33
l,33,34
l,34,35
l,35,36
l,36,30
larc,30,29,25,filrad
l,29,24
larc,24,40,30,filrad
larc,40,38,3
larc,38,14,8,filrad
l,14,7
larc,7,8,15,filrad
AL,all
CYL4,330.3,986.9,100
CYL4,700.3,986.9,100

CYL4,700.3,673.3,100
CYL4,330.3,673.3,100

CYL4,370.5,319.5,100
CYL4,732.45,319.5,100

CYL4,732.45,-34.3,100
CYL4,370.5,-34.3,100

CYL4,354.45,-420.25,100

```

```

CYL4,708.35,-420.25,100

CYL4,708.35,-838.4,100
CYL4,354.45,-838.4,100

CYL4,298.15,-1160.05,100
CYL4,619.85,-1160.05,100

CYL4,619.85,-1538,100
CYL4,298.15,-1438,100

CYL4,233.8,-1747.05,100

CYL4,-337.25,-605.2,100
CYL4,-691.15,-918.8,100
CYL4,-417.7,-1312.85,100
CYL4,-747.45,-1626.45,100
ASBA, 1,2,,delete,delete
asba, 23,3,,delete,delete
asba,1,4,,delete,delete
asba,2,5,,delete,delete
asba,1,6,,delete,delete
asba,2,7,,delete,delete
asba,1,8,,delete,delete
asba,2,9,,delete,delete
asba,1,10,,delete,delete
asba,2,11,,delete,delete
asba,1,12,,delete,delete
asba,2,13,,delete,delete
asba,1,14,,delete,delete
asba,2,15,,delete,delete
asba,1,16,,delete,delete
asba,2,17,,delete,delete
asba,1,18,,delete,delete
asba,2,19,,delete,delete
asba,1,20,,delete,delete
asba,2,21,,delete,delete
asba,1,22,,delete,delete
!asel,s,AREA,1

CYL4,L1*cos(theta1)/4,L1*sin(theta1)/4,50
CYL4,L1*cos(theta1)/2,L1*sin(theta1)/2,50
CYL4,3*L1*cos(theta1)/4,3*L1*sin(theta1)/4,50
CYL4,-xoff-L2*cos(theta1)/4,-yoff-L2*sin(theta1)/4,50
CYL4,-xoff-L2*cos(theta1)/2,-yoff-L2*sin(theta1)/2,50
CYL4,-xoff-3*L2*cos(theta1)/4,-yoff-3*L2*sin(theta1)/4,50
add,all

/prep7
!asel,s,AREA,27
!*set,smsize,1
SMRTSIZE,smsize
:nossiz
asel,all
AMESH,all

```

```

fini
/SOLU

nlgeom,1
NROPT,AUTO, ,
LUMPM,0
EQSLV, , ,0,
PREC,0
PIVCHECK,1
SSTIF
PSTRES
TOFFST,0,

dl,1,,ux,0
dl,1,,uy,0
!dl,15,,uy,0
dl,15,,SYMM

*SET,ii,0
*do,ii,1,LSDMax,1
!dldele,15,ux
!dldele,17,ux
!dl,15,,ux,ii*PDisp*xoff/(LSDMax-1)
dk,33,ux,ii*PDisp*xoff/(LSDMax-1)
lswrite,ii
*enddo

!dldele,15,ux
dkdele,33,ux
lswrite,LSDMax

*set,kk,0
*do,kk,1,LSPause+1,1
lswrite,LSDMax+kk
*enddo

*set,jj,0

*do,jj,1,RetMax,1
!dldele,15,ux
!dldele,17,ux
!dl,15,,ux,PDisp*xoff*(1-jj/(RetMax-1))
dk,33,ux,PDisp*xoff*(1-jj/(RetMax-1))
lswrite,LSDMax+LSPause+jj
*enddo
!ldel,15,ux
dkdel,33,ux
lswrite,LSDMax+LSPause+RetMax
*set,LSTMax,RetMax

lssolve,1,LSDMax+LSPause+LSTMax,1
FINISH

/post1

```

```

!set,24
!pldisp,1

*set,mm,0
*DIM,te,ARRAY,LSDMax+LSPause+LSTMax,4,
mm=1
set,mm
ETABLE,engry,SENE,
AVPRIN,0,0,
ssum
*GET,tot,SSUM, ,ITEM,ENRGY

nselect,all
NSORT,S,EQV,0,0,,
*get,MaxStrs,SORT,0,MAX
*get,MaxStNd,SORT,0,IMAX

kselect,s,kp,,33
nslk,s
*get,nkp33,node,0,num,max
*get,dux,node,nkp33,u,x
te(mm,1)=dux
te(mm,2)=tot
te(mm,3)=MaxStrs
te(mm,4)=MaxStNd

*do,mm,2,LSDMax+LSPause+LSTMax,1
set,mm
ETABLE,refl

ssum
*GET,tot,SSUM, ,ITEM,ENRGY

nselect,all
NSORT,S,EQV,0,0,,
*set,MaxStrs,0
*set,MaxStNd,0
*get,MaxStrs,SORT,0,MAX
*get,MaxStNd,SORT,0,IMAX

kselect,s,kp,,33
nslk,s
*get,nkp33,node,0,num,max
*get,dux,node,nkp33,u,x

te(mm,1)=dux
te(mm,2)=tot
te(mm,3)=MaxStrs
te(mm,4)=MaxStNd

*enddo

```

```

/POST26
ksel,s,kp,,33
nslk,s
*get,nkp33,node,0,num,max
ksel,s,kp,,10
nslk,s
*get,nkp10,node,0,num,max
nset,all
ksel,all
nsol,2,nkp33,u,x,ux
rforce,3,nkp33,f,x,fx

/output,AMout.txt
*stat
*stat,te
*stat,sts
prvar,2,3
/output

```

E.2 Inertial Loading

This batch file adds density to the set of material properties. Load steps consist of increasingly negative accelerations. Accelerations have units of m/s^2 , consistent with the units system chosen for the analysis.

```

/BATCH
! /COM,ANSYS RELEASE 5.5.3 UP19990405 11:22:12 01/29/2001
/input,start57,ans ,/ansys_inc/ansys57/docu/,,,,,,,,,,,,,1

/NOPR
/PMETH,OFF
!KEYW,PR_SET,1
!KEYW,PR_STRUC,1
!KEYW,PR_THERM,0
!KEYW,PR_FLUID,0
!KEYW,PR_ELMAG,0
!KEYW,MAGNOD,0
!KEYW,MAGEDG,0
!KEYW,MAGHFE,0
!KEYW,MAGELC,0
!KEYW,PR_MULTII,0
!KEYW,PR_CFD,0
/GO

*SET,xoff,28
*SET,yoff,860
*set,smsize,5

*SET,h1,20
*SET,h2,20
!*SET,h3,18
!*SET,h4,35
*set,Roff,200

```

```

*set,Rthk,850

*SET,11,1100
*SET,12,1100
!*SET,13,6
!*SET,14,13

*set,LSDMax,20
*set,LSPause,1
*set,RetMax,10

*set,PDisp,3.2

*set,Rcut,.9
*SET,theta1,atan(yoff/xoff)
*SET,pi,acos(-1)
*SET,theta2,theta1+pi/2
*SET,filrad,40
*set,horgn,sqrt((xoff/2)*(xoff/2)+(yoff/2)*(yoff/2))
!*set,hRinn,sqrt((xoff/2)*(xoff/2)+(yoff/2)*(yoff/2))+filrad+(l1+l2)/2
*set,hRinn,sqrt((xoff/2)*(xoff/2)+(yoff/2)*(yoff/2))+filrad/2
*set,Rinn,(Roff*Roff+hRinn*hRinn)/(2*Roff)
*set,Rout,Rinn+Rthk
!*set,Rtheta2,acos((Rinn-Roff+filrad+h1/2+Rcut*Rthk)/(Rout))
*set,Rtheta2,acos((Rinn-Roff+h1/2+Rcut*Rthk)/(Rout))
*set,hRout,Rout*sin(Rtheta2)
*set,supdpth,1.5
*set,supspc,2.0
*set,supthk,850

! /COM,Preferences for GUI filtering have been set to display:
! /COM, Structural

/PREP7

ET,1,PLANE82

KEYOPT,1,3,3
KEYOPT,1,5,0
KEYOPT,1,6,0

UIMP,1,EX,,207e3,
UIMP,1,DENS,,8.3e-9,
UIMP,1,ALPX,,,,
UIMP,1,REFT,,,,
UIMP,1,NUXY,,,,
UIMP,1,PRXY,,.3,
UIMP,1,GXY,,,,
UIMP,1,MU,,,,
UIMP,1,DAMP,,,,

R,1,600,

!/BATCH

```

```

k,1,0,0
k,2,l1*cos(theta1),l1*sin(theta1)
k,3,-xoff/2-Roff*cos(theta2),-yoff/2-Roff*sin(theta2)
k,4,-xoff-l2*cos(theta1),-yoff-l2*sin(theta1)
k,5,-xoff,-yoff

k,6,-filrad*cos(theta1),-filrad*sin(theta1)
k,7,-h1/2*cos(theta2),-h1/2*sin(theta2)
k,8,-filrad*cos(theta1)-(h1/2+filrad)*cos(theta2),-filrad*sin(theta1)-(h1/
    2+filrad)*sin(theta2)
k,9,-filrad*cos(theta1)+(h1/2+filrad)*cos(theta2),-filrad*sin(theta1)+(h1/
    2+filrad)*sin(theta2)
k,10,h1/2*cos(theta2),h1/2*sin(theta2)
k,11,(l1+filrad)*cos(theta1),(l1+filrad)*sin(theta1)
k,12,l1*cos(theta1)+h1/2*cos(theta2),l1*sin(theta1)+h1/2*sin(theta2)
k,13,(l1+filrad)*cos(theta1)+(h1/
    2+filrad)*cos(theta2),(l1+filrad)*sin(theta1)+(h1/
    2+filrad)*sin(theta2)
k,14,l1*cos(theta1)-h1/2*cos(theta2),l1*sin(theta1)-h1/2*sin(theta2)
k,15,(l1+filrad)*cos(theta1)-(h1/2+filrad)*cos(theta2),(l1+filrad)*sin(theta1)-
    (h1/2+filrad)*sin(theta2)
k,16,-xoff/2+(hRout)*cos(theta1)+(h1/2+filrad)*cos(theta2),-yoff/
    2+(hRout)*sin(theta1)+(h1/2+filrad)*sin(theta2)
*set,temp1,h1/2+filrad+filrad*cos(Rtheta2)+Rthk*Rcut
*set,temp2,h1/2+filrad+filrad*sin(Rtheta2)+Rthk*Rcut
k,17,(hRout-horgn)*cos(theta1)-temp1*cos(theta2),(hRout-horgn)*sin(theta1)-
    temp2*sin(theta2)
k,18,-xoff/2-(Roff+Rthk)*cos(theta2),-yoff/2-(Roff+Rthk)*sin(theta2)
*set,temp1,h2/2+filrad+filrad*cos(-Rtheta2)+Rthk*Rcut
*set,temp2,h2/2+filrad+filrad*sin(-Rtheta2)+Rthk*Rcut
k,19,-(hRout+horgn)*cos(theta1)-temp1*cos(theta2),-(hRout+horgn)*sin(theta1)-
    temp2*sin(theta2)
k,20,-(hRout+horgn)*cos(theta1)+(h2/2+filrad)*cos(theta2),-
    (hRout+horgn)*sin(theta1)+(h2/2+filrad)*sin(theta2)
k,21,-xoff-(l2+filrad)*cos(theta1),-yoff-(l2+filrad)*sin(theta1)
k,22,-xoff-(l2+filrad)*cos(theta1)+(h2/2+filrad)*cos(theta2),-yoff-
    (l2+filrad)*sin(theta1)+(h2/2+filrad)*sin(theta2)
k,23,-xoff-l2*cos(theta1)+h2/2*cos(theta2),-yoff-l2*sin(theta1)+h2/2*sin(theta2)
k,24,-xoff-l2*cos(theta1)-h2/2*cos(theta2),-yoff-l2*sin(theta1)-h2/2*sin(theta2)
k,25,-xoff-(l2+filrad)*cos(theta1)-(h2/2+filrad)*cos(theta2),-yoff-
    (l2+filrad)*sin(theta1)-(h2/2+filrad)*sin(theta2)
k,26,-xoff+filrad*cos(theta1),-yoff+filrad*sin(theta1)
k,27,-xoff+h2/2*cos(theta2),-yoff+h2/2*sin(theta2)
k,28,-xoff+filrad*cos(theta1)+(h2/2+filrad)*cos(theta2),-
    yoff+filrad*sin(theta1)+(h2/2+filrad)*sin(theta2)
k,29,-xoff-h2/2*cos(theta2),-yoff-h2/2*sin(theta2)
k,30,-xoff+filrad*cos(theta1)-(h2/2+filrad)*cos(theta2),-
    yoff+filrad*sin(theta1)-(h2/2+filrad)*sin(theta2)
k,31,-xoff+(h2/2+2*filrad)*cos(theta2),-yoff+(h2/2+2*filrad)*sin(theta2)
!k,31,-xoff+filrad*cos(theta1)+(h2/2+2*filrad)*cos(theta2)-1,-
    yoff+filrad*sin(theta1)+(h2/2+2*filrad)*sin(theta2)
*set,temp1,-xoff+(filrad-supdpth*l2)*cos(theta1)+(h2/2+filrad)*cos(theta2)-
    supspc*filrad
*set,temp2,-yoff+(filrad-supdpth*l2)*sin(theta1)+(h2/2+filrad)*sin(theta2)
k,32,temp1,temp2
*set,temp1,-xoff+(filrad-supdpth*l2)*cos(theta1)+(h2/2+filrad)*cos(theta2)-
    supspc*filrad-supthk
*set,temp2,-yoff+(filrad-supdpth*l2)*sin(theta1)+(h2/2+filrad)*sin(theta2)
k,33,temp1,temp2

```



```

k,34,-xoff+filrad*cos(theta1)-(h2/2+filrad)*cos(theta2)-supthk,-(yoff/2+1.5)
k,35,-xoff+filrad*cos(theta1)-(h2/2+filrad)*cos(theta2),-(yoff/2+1.5)
k,36,-xoff+filrad*cos(theta1)-(h2/2+filrad)*cos(theta2)+filrad/2,-
      yoff+filrad*sin(theta1)-(h2/2+filrad)*sin(theta2)
k,37,(l1)*cos(theta1)-(h1/2+filrad)*cos(theta2),(l1)*sin(theta1)-(h1/
      2+filrad)*sin(theta2)
k,38,(l1)*cos(theta1)-(h1/
      2+filrad+filrad*cos(Rtheta2))*cos(theta2),(l1)*sin(theta1)-
      (h1/2+filrad+filrad*sin(Rtheta2))*sin(theta2)

k,39,-xoff-12*cos(theta1)-(h2/2+filrad)*cos(theta2),-yoff-12*sin(theta1)-(h2/
      2+filrad)*sin(theta2)
*set, temp1, -xoff-12*cos(theta1)-(h2/2+filrad+filrad*cos(-Rtheta2))*cos(theta2)
*set, temp2, -yoff-12*sin(theta1)-(h2/2+filrad+filrad*cos(-Rtheta2))*sin(theta2)
k,40,temp1,temp2

l,8,9
larc,9,10,13,filrad
l,10,12
larc,12,13,9,filrad
l,13,16
l,16,17
larc,17,19,18
l,19,20
l,20,22
larc,22,23,28,filrad
l,23,27
larc,27,28,23,filrad
larc,28,31,23,filrad
!l,28,31
l,31,32
l,32,33
l,33,34
l,34,35
l,35,36
l,36,30
larc,30,29,25,filrad
l,29,24
larc,24,40,30,filrad
larc,40,38,3
larc,38,14,8,filrad
l,14,7
larc,7,8,15,filrad
AL,all
CYL4,330.3,986.9,100
CYL4,700.3,986.9,100

CYL4,700.3,673.3,100
CYL4,330.3,673.3,100

CYL4,370.5,319.5,100
CYL4,732.45,319.5,100

CYL4,732.45,-34.3,100
CYL4,370.5,-34.3,100

CYL4,354.45,-420.25,100
CYL4,708.35,-420.25,100

```

```

CYL4,708.35,-838.4,100
CYL4,354.45,-838.4,100

CYL4,298.15,-1160.05,100
CYL4,619.85,-1160.05,100

CYL4,619.85,-1538,100
CYL4,298.15,-1438,100

CYL4,233.8,-1747.05,100

CYL4,-337.25,-605.2,100
CYL4,-691.15,-918.8,100
CYL4,-417.7,-1312.85,100
CYL4,-747.45,-1626.45,100
ASBA, 1,2,,delete,delete
asba, 23,3,,delete,delete
asba,1,4,,delete,delete
asba,2,5,,delete,delete
asba,1,6,,delete,delete
asba,2,7,,delete,delete
asba,1,8,,delete,delete
asba,2,9,,delete,delete
asba,1,10,,delete,delete
asba,2,11,,delete,delete
asba,1,12,,delete,delete
asba,2,13,,delete,delete
asba,1,14,,delete,delete
asba,2,15,,delete,delete
asba,1,16,,delete,delete
asba,2,17,,delete,delete
asba,1,18,,delete,delete
asba,2,19,,delete,delete
asba,1,20,,delete,delete
asba,2,21,,delete,delete
asba,1,22,,delete,delete
!asel,s,AREA,1

CYL4,L1*cos(thetal)/4,L1*sin(thetal)/4,50
CYL4,L1*cos(thetal)/2,L1*sin(thetal)/2,50
CYL4,3*L1*cos(thetal)/4,3*L1*sin(thetal)/4,50
CYL4,-xoff-L2*cos(thetal)/4,-yoff-L2*sin(thetal)/4,50
CYL4,-xoff-L2*cos(thetal)/2,-yoff-L2*sin(thetal)/2,50
CYL4,-xoff-3*L2*cos(thetal)/4,-yoff-3*L2*sin(thetal)/4,50
aadd,all

/prep7
!asel,s,AREA,27
!*set,smsize,1
SMRTSIZE,smsize
:nossiz
asel,all
AMESH,all

fini
/SOLU

```

```
nlgeom,1
NROPT,AUTO, ,
LUMPM,0
EQSLV, , ,0,
PREC,0
PIVCHECK,1
SSTIF
PSTRES
TOFFST,0,
```

```
dl,1,,ux,0
dl,1,,uy,0
!dl,15,,uy,0
dl,15,,SYMM
```

```
ACEL,-500,0,0
lswrite,1
ACEL,-525,0,0
lswrite,2
ACEL,-530,0,0
lswrite,3
ACEL,-535,0,0
lswrite,4
ACEL,-540,0,0
lswrite,5
ACEL,-545,0,0
lswrite,6
ACEL,-550,0,0
lswrite,7
ACEL,-555,0,0
lswrite,8
ACEL,-556,0,0
lswrite,9
ACEL,-557,0,0
lswrite,10
ACEL,-558,0,0
lswrite,11
ACEL,-559,0,0
lswrite,12
ACEL,-560,0,0
lswrite,13
ACEL,-561,0,0
lswrite,14
ACEL,-562,0,0
lswrite,15
ACEL,-563,0,0
lswrite,16
ACEL,-564,0,0
lswrite,17
ACEL,-565,0,0
lswrite,18
ACEL,-566,0,0
lswrite,19
ACEL,-567,0,0
lswrite,20
ACEL,-568,0,0
lswrite,21
```

```
ACEL,-569,0,0
lswrite,22
ACEL,-570,0,0
lswrite,23
ACEL,-571,0,0
lswrite,24
ACEL,-572,0,0
lswrite,25
ACEL,-573,0,0
lswrite,26
ACEL,-574,0,0
lswrite,27
ACEL,-575,0,0
lswrite,28

lssolve,1,28,1

/POST26
ksel,s,kp,,33
nslk,s
*get,nkp33,node,0,num,max
ksel,s,kp,,10
nslk,s
*get,nkp10,node,0,num,max
nsel,all
ksel,all
nsol,2,nkp33,u,x,ux
rforce,3,nkp33,f,x,fx

/output,AMout.txt
*stat
prvar,2
/output
```

APPENDIX F *Fatigue Testing Circuit*

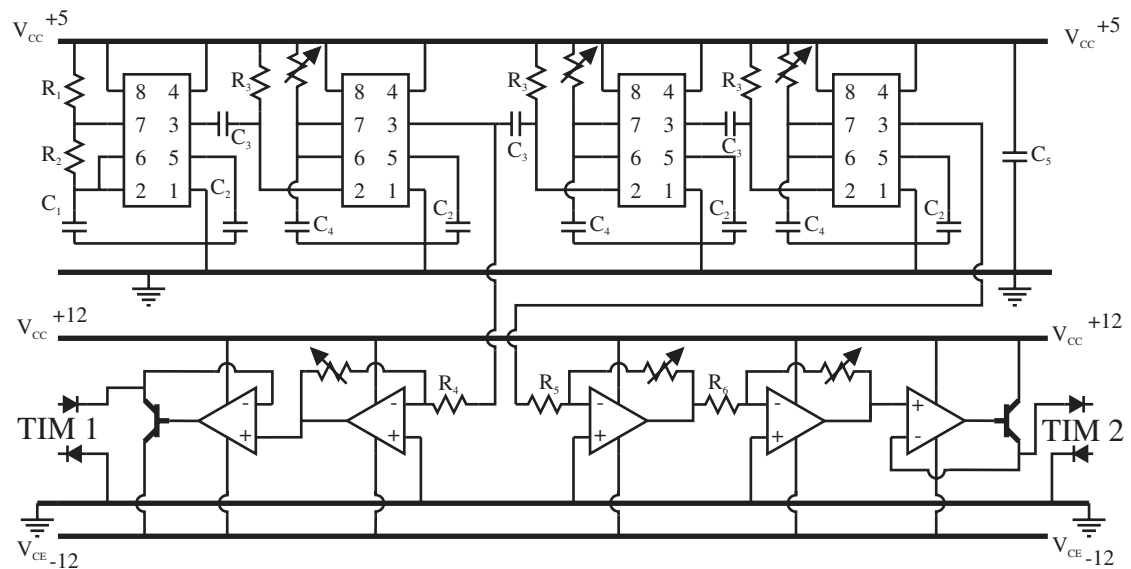


Figure F-1 Schematic of test circuit used for fatigue testing. TIM 1 and TIM 2 correspond to the forward and reverse actuators.

This circuit uses 555 times to generate the signal for fatigue testing. Operational amplifiers are used to set the voltage output of the signals. The signal is then amplified again by transistors to provide the necessary current.

F.1 Component List

Table F-1 Resistors

Resistor	Value
R ₁	100 kΩ
R ₂	100 kΩ
R ₃	33 kΩ
R ₄	220 kΩ
R ₅	51 kΩ
R ₆	51 kΩ
R ₇	15 kΩ

The Potentiometers are 200 kΩ for first and third timer circuits and 50 kΩ for the second Timer Circuit.

Table F-2 Capacitors

Capacitor	Value
C ₁	0.1 μF
C ₂	0.1 μF
C ₃	0.01 μF
C ₄	10 nF
C ₅	10 μF

F.1.1 Other components

Standard size components were used for diodes, transistors and operational amplifiers.